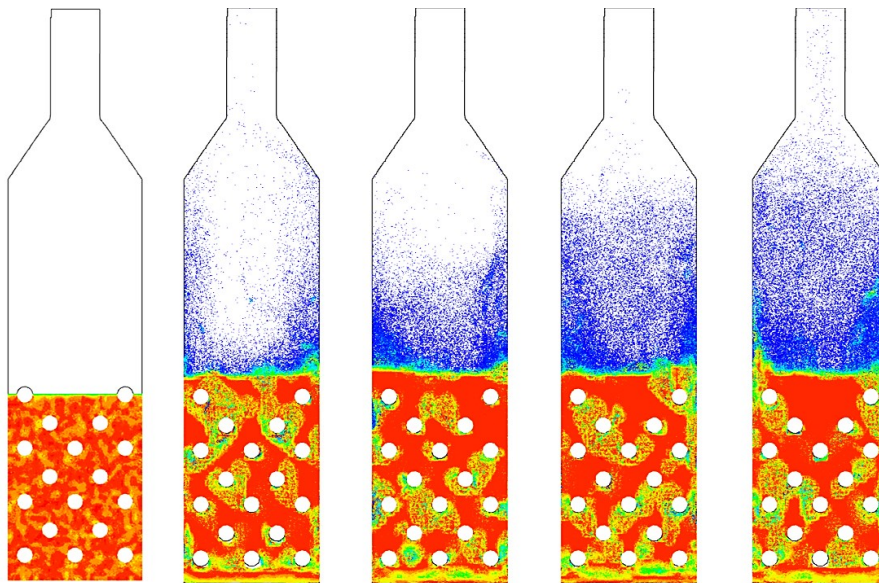


FMH606 Master's Thesis 2024

Process Technology

Design of Electrified Calciner for Direct Capture of CO₂ from Cement Raw Meal



Ladan Samaei

Faculty of Technology, Natural Sciences and Maritime Sciences
Campus Porsgrunn

Course: FMH606 Master's Thesis, 2024

Title: Design of Electrified Calciner for Direct Capture of CO₂ from Cement Raw Meal

Number of pages: 85

Keywords: Carbon Capture, Electrification, Binary fluidized bed, Calciner

Student: Ladan Samaei
Supervisor: **Main supervisor:** Lars-André Tokheim,
External partner: Heidelberg Materials
External Supervisor: Christoffer Moen
Availability: Open

Summary:

The main focus in this thesis is on designing an electrified calciner for direct CO₂ capture from cement raw meal, investigating various operating conditions using CPFD simulations. The calciner, a binary fluidized bed reactor with several immersed electrically heated cylinders, includes the raw meal (fine powder <200µm) and coarse lime particles (400µm-800µm). The electrically heated cylinders immersed in the bed provide energy both for heating up the raw meal to calcination temperature and for the endothermic calcination reaction. The design has been made using mass and energy balance as well as fluidized bed calculations. The reactor performance is deeply investigated in different operating conditions using CPFD simulations. Key findings show that efficient spreading the raw meal over the heat source (hot cylinders) and preheating the meal can improve the calcination degree in the reactor. Also, the hotter the cylinders (up to 1150°C) the higher the calcination degree. The designed reactor showed a performance of 90% calcination degree for a preheated meal to 720°C and a hot cylinder temperature of 1150°C. Also, for a 20°C cold meal, having 1150°C wall temperature of hot cylinders can lead to almost 70% calcination in the reactor. It should be noted that the more calcination the more gas production and higher particle entrainment. Another investigated factor was the fluidization velocity which has been calculated between 0.2 m/s-0.8 m/s. Simulation results showed that 0.3 m/s works best in terms of mixing and fluidization efficiency and 0.8m/s shall be avoided as it makes even coarse particles escape the bed very quickly. The results of this study also showed that the fluidization velocity has the most effect on the residence time of particles. Having 0.2 m/s fluidization velocity leads to almost 30 s average residence time of fine particles, for the case with 0.3 m/s it is decreased to 24 s while for the case with 0.8 m/s fluidization velocity, the average residence time is only 5 seconds!

The University of South-Eastern Norway takes no responsibility for the results and conclusions in this student report.

Preface

This study was done to support the project “Electrification of High Temperature and Flexible Technologies for Transforming Cement, Lime and Pulp Industry” (ELECTRA). University of South-Eastern Norway and Heidelberg Materials are two of the participants in the ELECTRA project, which has received funding from the European Union’s Horizon Europe research and innovation program under Grant Agreement No 101138392.

This report was written on the topic of "Design of Electrified Calciner for Direct Capture of CO₂ from Cement Raw Meal " to fulfill the partial requirement for the Master's study program in Process Technology at the University of South-Eastern Norway, Faculty of Technology, Natural Science and Maritime Sciences, Department of Process, Energy and Environmental Technology.

The goal of the work was to design a lab scale electrified calciner to directly capture CO₂ from the cement raw material and use CFPD simulation as a tool for investigating different operating conditions.

I would like to take this opportunity to express my deep appreciation and gratitude to my supervisors, professor Lars-André Tokheim from University of South-Eastern Norway and Christoffer Moen from Heidelberg Materials, for their invaluable support, guidance, and expertise throughout the completion of this thesis.

In addition, I would like to extend my heartfelt thanks to my beloved husband and my dear family for their unwavering help and support.

Porsgrunn, 29.05.2024

Ladan Samaei

Contents

Preface	3
Contents.....	4
Nomenclature	6
1 Introduction	9
1.1 Scope of work	9
1.2 Report outline.....	10
2 Theory and literature review	11
2.1 Carbon capture	11
2.1.1 <i>Carbon capture technologies in the cement industry</i>	11
2.1.2 <i>Combination of electrified calciner and CO₂ capture</i>	14
2.2 Theory of fluidized bed.....	16
2.2.1 <i>Fluidization regimes</i>	17
2.2.2 <i>Minimum fluidization</i>	18
2.2.3 <i>Settling velocity</i>	19
2.3 Fluidization conditions of fine particles	19
2.3.1 <i>Binary particle Fluidized bed</i>	20
3 Reactor design	24
3.1 Design basis values.....	25
3.2 Step 1, mass and energy balance:	26
3.3 Step 2, fluidized bed calculations:	28
3.4 Reactor specifications and working principles	31
4 CPFD Simulation.....	33
4.1 Theory and governing equations	33
4.1.1 <i>Flow governing equations</i>	33
4.1.2 <i>Particle governing equations</i>	34
4.1.3 <i>Heat transfer governing equations</i>	36
4.1.4 <i>Reaction kinetics</i>	36
4.2 Simulation specifications	37
4.2.1 <i>Geometry and grid</i>	37
4.2.2 <i>Specifications of the particles and the fluid</i>	38
4.2.3 <i>Mass balance check</i>	40
5 Result and discussion	43
5.1 The effect of fluid temperature on the fluidization	44
5.2 The effect of heat transfer on particle entrainment (without considering the reaction).....	46
5.3 The effect of raw meal spreading on the reactor performance	47
5.4 The effect of temperature on the reactor performance.....	54
5.4.1 <i>The effect of increasing the temperature of hot cylinders on the reactor performance</i>	54
5.4.2 <i>The effect of the raw meal temperature on the reactor performance</i>	57
5.4.3 <i>The effect of increasing hot cylinders' temperature on the calcination of cold injected raw meal</i>	59
5.4.4 <i>Investigation of the reactor performance in a more practical operating condition</i>	63
5.5 The effect of fluidization velocity on the reactor performance	67

5.5.1 *The effect of fluidization velocity on the residence time of raw material in the reactor*
.....74

5.6 Overview of the results75

6 Conclusion and Further Work.....78

6.1 Suggestion for future studies.....79

References80

Appendix A: Task Description84

Nomenclature

Abbreviation	Description
A_{bottom}	Bottom cross section area of the reactor
A_{cal}	Heat transfer area required for calcination
A_{eff}	Excess area fraction
$A_{sensible}$	Heat transfer area required for heating up the raw meal
A_{sp}	Particle surface area
A_w	Wall area
C_{rm}	Specific heat capacity of raw meal
CPFD	Computational Particle Fluid Dynamics
D_{cyl}	Cylinders' diameter
D_h	Hydraulic diameter
d_p	Particle diameter
D_p	Drag function
d_p^*	Dimensionless particle diameter
D_{top}	Top cross section diameter
\dot{E}	Available energy (electricity)
ELECTRA	Electrification of High Temperature and Flexible Technologies for Transforming Cement, Lime, and Pulp Industry
F	Particle force per volume of the fluid
F_{wp}	Wall particle view factor
g	Gravity acceleration
H_{bed}	Height of bed before expansion
H_{cal}	Enthalpy of calcination
h_d	Dense particle phase heat transfer coefficient
H_{Exp}	Height of expanded bed
h_{fw}	Heat transfer coefficient between fluid and wall
h_l	Lean gas phase heat transfer coefficient
H_p	Enthalpy of the particle
H_{total}	Total height of the reactor
k_D	Rate kinetics of calcination reaction
k_f	Fluids conduction coefficient

L_1	One side of bottom cross section of the reactor, Cylinder length
L_2	Other side of the bottom cross section of the reactor
LES	Large Eddy Simulation
\dot{m}_{CaCO_3}	Mass flow rate of calcium carbonate
M_{CaCO_3}	Molecular mass of calcium carbonate
\dot{m}_{CaO}	Mass flow rate of calcium oxide
M_{CaO}	Molecular weight of calcium oxide
\dot{m}_{CO_2}	Mass flow rate of carbon dioxide
M_{CO_2}	Molecular weight of carbon dioxide
M_j	Molecular mass of component j
m_p	Particle mass
\dot{m}_{rm}	Mass flow rate of raw meal
\dot{n}_{CaCO_3}	Molar flow rate of calcium carbonate
\dot{n}_{CaO}	Molar flow rate of calcium oxide
\dot{n}_{CO_2}	Molar flow rate of carbon dioxide
N_{cyl}	Number of hot cylinders
Nu_{f-p}	Nusselt number of heat transfer between particle and fluid
P_{CO_2}	Partial pressure of CO ₂
P_{eq}	Equilibrium pressure
Pr	Prandtl number
\ddot{q}_f	Fluid heat flux
Q_{cal}	Heat transfer related to calcination
$Q_{sensible}$	Sensible heat transfer
R	Ideal gas constant
Re	Reynolds number
S_h	Energy exchange between fluid and particles
$T_{in,rm}$	Inlet temperature of the raw meal
T_{cal}	Calcination temperature
T_{cyl}	Cylinders' wall temperature
T_f	Temperature of fluid
T_{in}	Inlet temperature

T_p	Temperature of particle
T_w	Wall temperature
U	Overall heat transfer coefficient
$u_{CO_2,out}$	Minimum entrainment velocity of gas
u_F	Fluidization velocity
U_{mf}	Minimum fluidization velocity
u_p	Particle velocity
U_t	Terminal settling velocity
u_t^*	Dimensionless terminal settling velocity
USN	University of South-Eastern Norway
$\dot{V}_{CO_2,prod}$	Volume flow rate of carbon dioxide production
$\dot{V}_{CO_2,rec}$	Volume flow rate of carbon dioxide recycled
w_{CaCO_3}	Weight fraction of calcite in the raw meal
x_p	Spatial location of particles
ΔT_{LMTD}	LMTD temperature difference
∇p	Pressure gradient
ε_{mf}	Void fraction at minimum fluidization condition
ε_{wp}	Particle emissivity
η	Degree of calcination
θ_f	Fluid volume fraction
θ_p	Particle volume fraction
θ_{cp}	Close pack value fraction
λ_f	Fluid thermal conductivity
μ	Dynamic viscosity
ρ	Density
ρ_{CaCO_3}	Density of limestone
ρ_{coarse}	Density of lime coarse particle
σ	Stefan-Boltzmann constant
ϕ	Viscous dissipation rate
φ_s	Sphericity

1 Introduction

In this chapter a background of the problem and the outline of this thesis is described.

The use of cement is growing significantly due to urbanization, while the cement industry is the second largest industrial CO₂ emission source and contributes with almost 27% of the industrial emissions and about 7 % of the overall global emissions [1]. Thus, it is important to reduce the carbon emissions of this industry. There are two processes in the cement industry which emits most CO₂. One of them is the calcination process in which limestone (CaCO₃) converts to lime (CaO) and carbon dioxide (CO₂), the other one is using fossil fuels to provide heat for the process. About two thirds of the CO₂ emissions from the cement industry are from calcination of limestone, whereas one third comes from the burning of fuels [2]. Having said that, using green electricity to calcine the raw materials and combining this with storage of the pure CO₂ generated in the calcination process can significantly reduce CO₂ emissions in the cement industry [3]. It is noteworthy that in this case, CO₂ is the only gaseous phase produced in the calciner which makes the capture process much easier.

But which type of reactor is the best for designing an electrified calciner? This has been investigated in previous studies and the fluidized bed calciner selected due to providing good mixing and high heat and mass transfer. However, as the raw meal particles are too small and difficult to fluidize, a binary particle fluidized bed is a better selection for the calcination process. [4]

1.1 Scope of work

This thesis is subjected to design a fluidized bed lab-scale electrified calciner and support the design with some CFPD simulations. The reactor includes several hot cylinders which are electrically heated to provide energy both for heating up the raw meal, which contains 77% calcium carbonate (CaCO₃), up to the calcination temperature and for the endothermic calcination reaction ($\text{CaCO}_3 \rightarrow \text{CaO} + \text{CO}_2$).

In this thesis, the main aim is to:

1. Make design calculations of a binary particle fluidized bed reactor for electrically heated calciner.
2. Investigating the reactor performance in different operating conditions that varies in fluidization velocity, raw meal temperature and hot cylinders temperature using a CFPD tool:
 - a. Visualize the gas/particle flow pattern in the reactor with the arrangement of hot cylinders and heat transfer in the reactor
 - b. Investigate the mixing efficiency and heat transfer rate in the reactor
 - c. Determine the separation efficiency of the unit
 - d. Determine the calculation degree by postprocessing of simulation data
 - e. Determine the particle entrainment by post processing of simulation data

To do so, several steps are followed respectively:

- (a) Study the theory and the literature review
- (b) Make mass and energy balance for reactor design
- (c) Calculate the fluidization conditions for the reactor design
- (d) Find the proper sizing and conditions of the reactor
- (e) Draw and prepare the geometry of the reactor for the CPFD simulations
- (f) Make a proper mesh and ensure the grid independence
- (g) Use proper initial and boundary conditions and make the CPFD simulation for different operating conditions
- (h) Post processing of the results and make a valid analysis over the reactor performance.

1.2 Report outline

The thesis is made up of 6 chapters. The first chapter includes a short introduction and the main goals of the thesis, the second chapter includes a theory and relevant literature review, and the third chapter includes design calculation process of the electrified calciner. Chapter 4 includes the CPFD simulation theory and conditions, while results and discussion comes in the 5th chapter. The last chapter is the 6th one, which includes the conclusion of the whole report and some suggestions for the future work.

2 Theory and literature review

This chapter includes some theory background and literature review about the carbon capture in the cement industry, electrified calciner and the fluidized bed reactor.

2.1 Carbon capture

With an estimated 2600 million tons of CO₂ emissions in 2020, the cement industry holds the second-largest share of direct industrial CO₂ emissions worldwide [5]. Furthermore, because of urbanization and the growing global population, cement production is predicted to increase by 12–23% by 2050 [6]. By 2050, the European Union (EU) wants to cut its greenhouse gas emissions by 80–95% from 1990 levels [7]. Achieving this objective will largely depend on decarbonizing the cement sector. The international energy agency (IEA) examined a number of cutting-edge approaches to decrease CO₂ emissions from the cement sector and discovered that using cutting-edge technologies, like carbon capture technology, is one of the most effective way to meet the goal [6].

Carbon capture technologies are commonly classified into four categories: integrated capture, oxy-fuel, post-combustion, and pre-combustion. In the cement industry, oxyfuel combustion, post combustion and a third technology “direct capture” can be applied for capturing carbon emissions [8]. Since pre-combustion capture methods could only address CO₂ emissions connected to energy, their potential for mitigation in the cement industry would be limited [9]. They could be useful in newly constructed cement plants that combine gasification technology with syngas or H₂ fuel production [10]. Nevertheless, hydrogen flames are not appropriate for clinker manufacture in traditional kilns due to their comparatively low emissive power [11]. It would be necessary to install cement kiln lines and new, more effective hydrogen burners.

In the following section, a brief review of the post combustion carbon capture in the cement industry and the role of electrified calciner in this regard is written.

2.1.1 Carbon capture technologies in the cement industry

At first glance, it seems that traditional kilns in both existing and new cement plants could be upgraded with CO₂ capture technologies after combustion without big changes to how cement is made. The main things affected would be energy management and the way the kilns start up and shut down.[12]. The nature of the industry and the fact that current kilns are expected to last for another 30–50 years, along with the likelihood that new kilns meeting legal standards won't be built soon, highlight the promise of post-combustion CO₂ capture technologies[8].

One of the most effective post combustion carbon capture technologies is chemical absorption. Industries have been using chemical absorption with amine solutions since 1930 [13].

On a commercial scale, this method has been demonstrated in power plants. While the exact process can vary depending on the plant, a typical process involves three main steps[14]:

1. Treating the flue gas in a Direct Contact Cooler (DCC) to remove sulfur dioxide (SO₂), nitrogen oxides (NO_x), and dust particles.

2. Passing the pretreated flue gas through an absorber column, where it comes into contact with an aqueous amine solution. At temperatures of 40–60°C and atmospheric pressure, carbon dioxide reacts with the amine, producing a gas stream with reduced carbon content that is released into the atmosphere.
3. Regenerating the spent solvent in a stripper column, typically at temperatures of 100–120°C and pressures of 1.5–2 atm. This process, which may vary slightly depending on the solvent used, separates a high-purity CO₂ stream for recovery while sending the depleted solvent back to the absorber column to repeat the cycle.

The main differences between the flue gas emitted by a power plant and that from a cement factory lie in their temperature, composition, and the size distribution of particulate matter. The hotter gases from kilns in cement factories can lead to the degradation of amines and increased losses through evaporation, necessitating additional cooling [15]. While the higher CO₂ pressure in cement flue gas initially seems advantageous, it can pose challenges for CO₂ absorption. With a smaller volume of flue gas, more heat of absorption is released, potentially raising the temperature of the CO₂ absorber, and shifting the equilibrium in a less favorable direction [16]. Figure 2-1 shows a generic flow sheet of chemical absorption carbon capture in a cement plant.

The main drawback of amine scrubbing is its high energy demand, mostly due to solvent regeneration, which accounts for 50–80% of total energy needs [17]. In cement plants, there's typically no low-pressure steam available for solvent regeneration. Providing the necessary 2 GJ per ton of CO₂ captured would require a combined heat and power facility (CHP) or waste heat recovery[12]. Additionally, modern cement plants already utilize a significant amount of waste heat for drying raw materials and preheating raw meals. Although simulations suggest that only up to 15% of the additional thermal energy needs can be recovered from the cement kiln, the actual surplus waste heat varies by site[18].

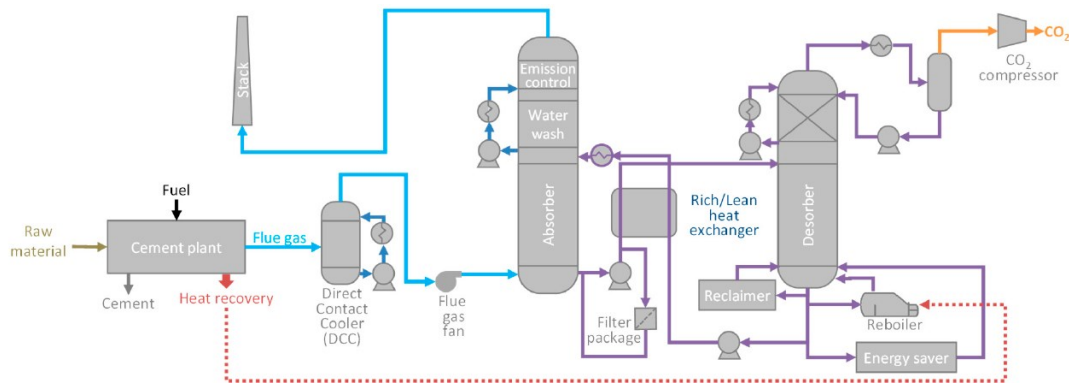


Figure 2-1: Amine carbon capture technology employed in cement plant [8]

Another post combustion carbon capture technology is membrane separation. The main drawback of membrane separation technology is that membrane-based separation has limited selectivity, capturing only a portion of the incoming CO₂. Moreover, the purity of captured CO₂ is restricted, often necessitating multiple stages for meeting product standards. While membranes theoretically could achieve capture rates exceeding 80%, only laboratory-scale

demonstrations have shown recoveries of up to 60–70% [9]. In the Norcem CO₂ capture project (2013–2017) at the Brevik cement plant in Norway, membrane separation was piloted. The pilot facility, depicted in Figure 2-2 was designed and built by Yodfat Engineers and operated by the Norwegian University of Science and Technology (NTNU) and DNV GL. Initial tests conducted in 2014 using a portion of the plant's flue gas after the SNCR, ESP, FGD, and baghouse filter, revealed challenges in achieving stable and high performance with the membrane system. For short periods, a CO₂ purity of up to 72 vol% was attained when all process parameters were well regulated [19].

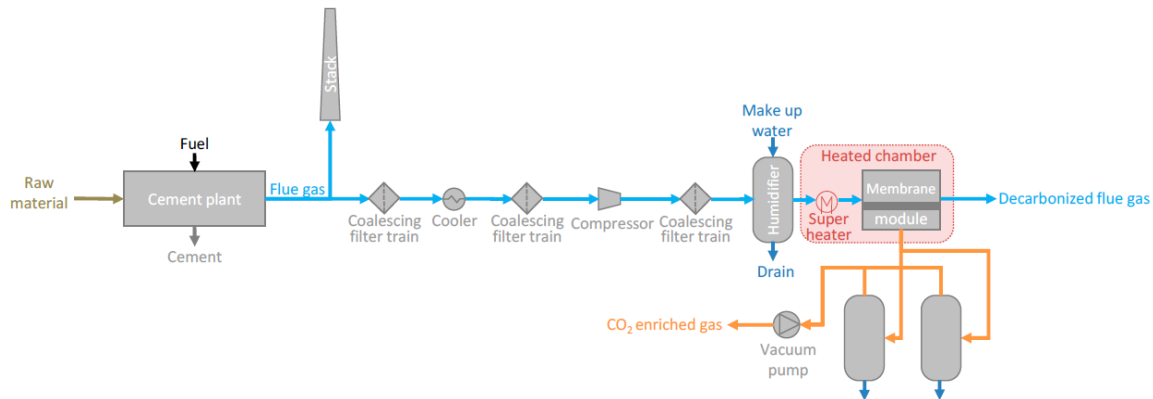


Figure 2-2: Flow diagram illustrating the simplified setup of the pilot membrane unit tested at the Brevik cement plant [8]

Calcium looping (CaL) stands out as a highly promising CO₂ capture method for the cement industry. It revolves around the reversible process of carbonation ($\text{CaCO}_3 \rightleftharpoons \text{CaO} + \text{CO}_2$), typically executed within two linked circulating fluidized beds: a carbonator and a calciner[20].

In the carbonator, CaO interacts with flue gas containing CO₂ at temperatures of 600–700°C. The resulting CaCO₃ is then sent to the calcination reactor, where it is heated to 890–930°C to release the CO₂ product and regenerate CaO, which is cycled back to the carbonator. Achieving a pure CO₂ stream typically requires oxyfuel combustion in the calciner, which, however, necessitates a cryogenic air separation unit (ASU). The resulting CO₂-rich stream is then purified in a compression and purification unit (CPU), reaching purities exceeding 95%. The sorbent tends to degrade over cycles, necessitating the addition of fresh CaCO₃ and extraction of a purge stream rich in CaO to prevent inert species buildup [21]. However, integration of the Calcium looping process into a cement plant can utilize this purge stream as a feedstock for cement production. This technology can achieve capture rates of up to 98%[22]. Notably, much of the energy input into the calciner can be reclaimed as high-temperature heat (~650°C) in the cooled carbonator, enabling efficient electricity generation[21]. Figure 2-3 shows a simplified diagram of calcium looping process installed in a cement plant.

The main drawback of this method is the need for oxyfuel combustion which requires a cryogenic air separation unit. This significantly raises both capital and operating costs. An alternative is indirect heating of the calciner, eliminating the need for an ASU [21]. Using an electrified calciner could be a possible alternative. The concept of electrified calciner is discussed in this thesis.

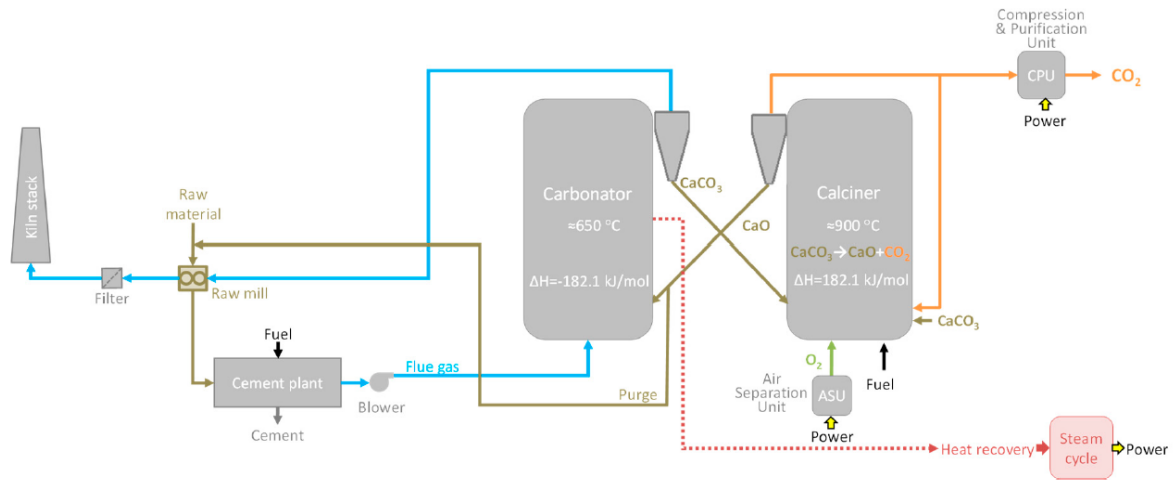


Figure 2-3: Calcium looping process simplified block flow diagram [20],[8].

2.1.2 Combination of electrified calciner and CO₂ capture

By switching from fuel combustion to electrical energy for the cement process both in calciner and in the rotary kiln, two things happen at once. Firstly, the CO₂ produced from burning fuel in the calciner is eliminated, reducing the overall CO₂ emissions from making clinker. Secondly, the exhaust gas from the calciner is almost pure CO₂, so it can go straight to a CO₂ processing unit without needing a separate CO₂ separation plant [3].

Having said that, if only the calciner uses the clean electricity instead of burning fuels while the kiln still uses the fuel combustion for providing heat there are also some significant advantages including:

- A significant reduction (around 70%) in emissions can be achieved.
- Heat needs to be supplied to a zone of only about 900°C; the extremely high temperature required in the rotary kiln doesn't have to be addressed.
- Only one of the main equipment units in the kiln system (the calciner) needs to be altered.

Figure 2-4 shows a typical cement kiln system. The working principle is as follows:

The raw meal starts at the top of the preheaters, where it's warmed to around 700°C by hot gases from the calciner. In the calciner, most of the meal is heated to about 900°C by contact with hot gases from burning fuel. Then, in the rotary kiln, the preheated meal is fully calcined, heated further until some minerals start to melt, and clinker forms at temperatures of 1400-1450°C. This kiln process also involves burning fuel. Afterward, the clinker is cooled by ambient air in the clinker cooler. A big part of the heated air from the cooler is used as combustion air in both the rotary kiln ("secondary air") and the calciner ("tertiary air"), capturing a lot of the heat. However, some lower-temperature heat (about 200°C) is lost to the surroundings ("cooler vent air"). The hot exhaust gas from the kiln mixes with the calciner gas, providing some of the energy needed for pre-calcination. Additionally, some air is supplied for

fuel conveying and cooling ("primary air") in both the rotary kiln and the calciner, and there might be some air leakage ("false air") in the rotary kiln, calciner, and preheater tower [3].

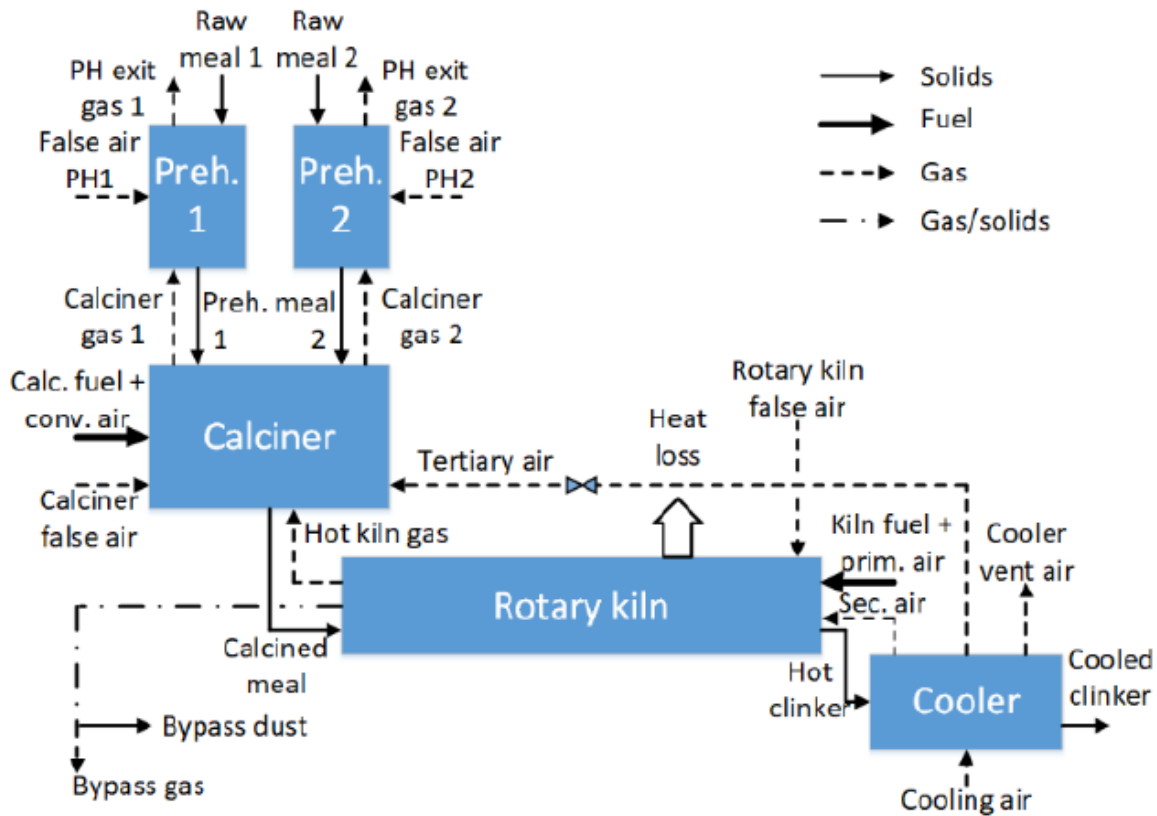


Figure 2-4: Block flow diagram of a regular cement plant using coal combustion [3]

On the other hand, Figure 2-5 depicts a conceptual setup for combining calciner electrification with CO₂ capture. The working principle is defined as follows [3].

- All fuel used in the calciner is replaced with heat indirectly provided by electrical energy.
- The tertiary air, previously directed into the calciner, is now redirected to the preheater, where its heat is utilized.
- The hot gas exiting the rotary kiln bypasses the calciner and is sent to the preheater instead. This allows its heat to be used effectively.
- As a result, the main component in the gas leaving the calciner is CO₂ from decarbonation.
- A gas-to-gas heat exchanger called "CO₂ HEX" captures the heat from the hot CO₂ leaving the calciner.
- A fan (not shown in Figure 2-5) positioned after the CO₂ HEX draws the CO₂ out of the calciner and through the heat exchanger.

- Another fan is required to push the cooler air from the cooler, through the CO₂ HEX, and to the preheater tower.

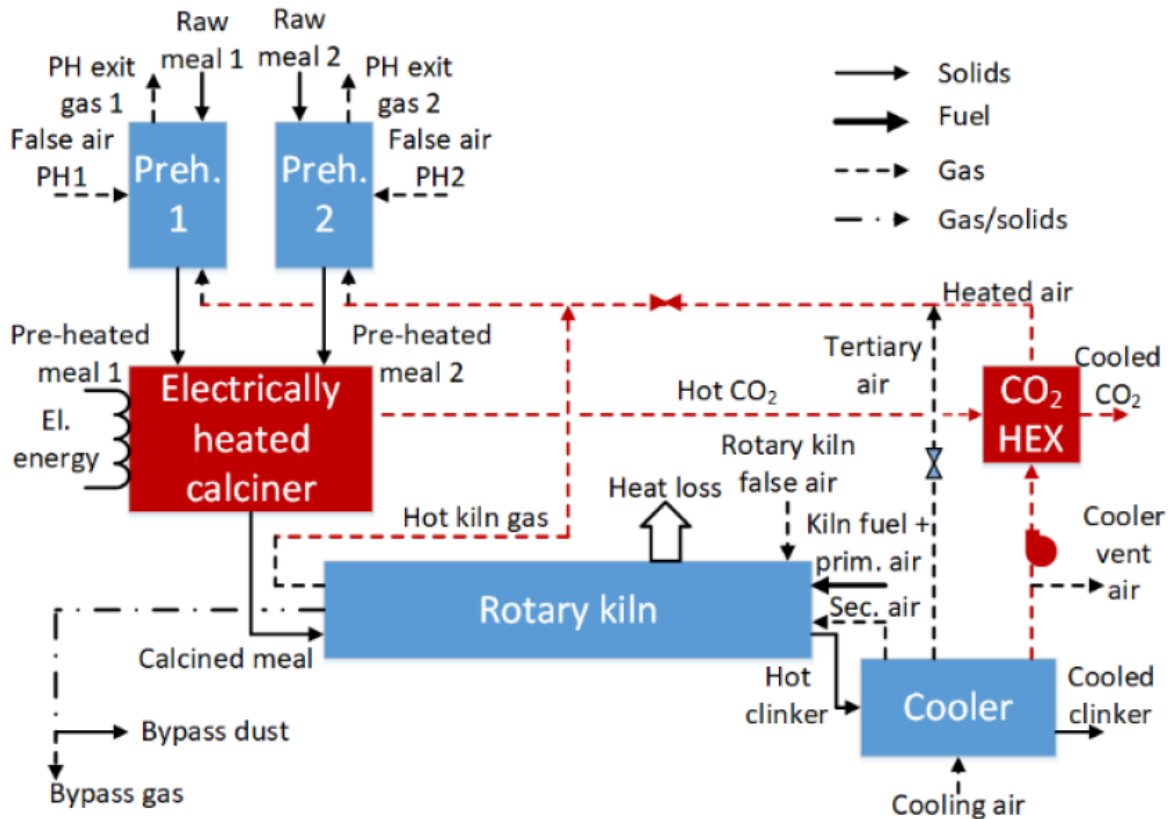


Figure 2-5: Block flow diagram of a cement kiln system with electrified calciner [3]

In this thesis the focus is on the design of the electrified calciner. The reactor is a fluidized bed reactor that is heated by clean electricity. The electricity is warming up the horizontal cylinders in the reactor. These hot cylinders provide energy in the bed, mainly with conduction and radiation heat transfer. The fluidized bed includes both coarse and fine particles. Fine particles are the raw meal which is injected to the reactor to be calcined and the coarse particles are used to make the bed. More details of the design and working principle of the electrified calciner are provided in the third chapter of this thesis. A brief description of the fluidized bed theory is provided in the next section.

2.2 Theory of fluidized bed

Fluidization refers to the transformation of stationary solid particles into a fluid-like state induced by a flowing stream of gas or liquid directed upward into a reactor filled with solids. This process finds extensive applications across various engineering domains, broadly categorized into two groups:

- Physical operations encompass tasks such as heat transfer, absorption, conveying systems, and fine powder mixing.

- Chemical operations involve reactions between gases and solid catalysts or among solid particles themselves.

Among the notable techniques in the Process industry is the employment of fluidized bed reactors. These reactors have been utilized commercially since the 1920s, notably with the introduction of the Winkler coal gasifier in Germany. Fluidized bed reactors offer several advantages, including high rates of heat and mass transfer, efficient mixing capabilities, and conditions close to isothermal. Owing to these benefits, the concept of fluidization finds widespread application in various engineering endeavors such as hydrocarbon reforming, gasification, aluminum production, and calcination [23],[24],[25].

2.2.1 Fluidization regimes

The fluidized bed behaves variably depending on gas velocity and solid properties. As illustrated in Figure 2-6, there are various fluidization regimes. Figure 2-6(a) demonstrates that the fluid enters the void spaces between the particles at a low flow rate, but the height remains constant while the bed is at rest. This step involves a fixed bed. As the superficial gas velocity increases, the drag force of upward flow gas eventually equals the weight of the particles in the bed (Figure 2-6(b)). This point marks the beginning of fluidization and is one of the most important aspects of fluidization, the minimum fluidization velocity (U_{mf}). When the superficial gas velocity exceeds the minimum fluidization velocity in a gas-solid system, the bed may expand smoothly. The bed in Figure 2-6(c) can only be seen when small particles are exposed to high-pressure dense gas. Bubbles arise when the superficial gas velocity exceeds the minimum fluidization velocity, and bubble coalescence and channeling occur. At this point, the bubbling fluidized bed occurs at a superficial gas velocity that is a little larger than the minimum fluidization velocity, also known as the minimum bubbling velocity (U_{mb}). Figure 2-6(d) shows that the bed's height does not significantly grow beyond its minimum fluidization height. This bed is bubbling fluidization and can occur under the specific circumstance of the fluidization of highly dense particles by low density fluids. As the velocity increases, bubbles integrate and rise in the fluidized bed. The bubble's size can grow to be as large as the bed's diameter if the height to diameter ratio is enough. Figure 2-6(e) shows the condition known as slugging. When the velocity exceeds the terminal settling velocity, particles from the upper surface eject from the bed, causing turbulent motion of solid clusters and gas voids, as seen in Figure 2-6(g). This is referred to as turbulent beds. As the velocity increases, the fluidized bed transforms into an entrained bed with a dilute or lean phase, resulting in pneumatic solid transport, as seen in Figure 2-6(h) [23],[24],[25].

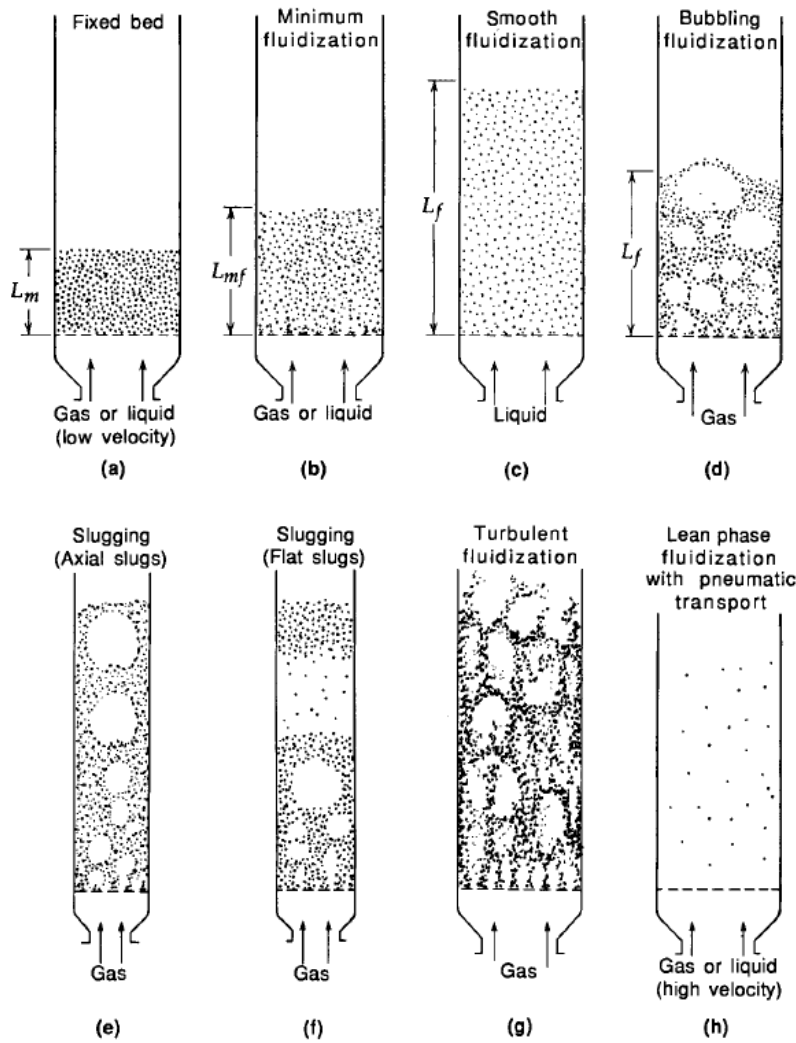


Figure 2-6: Fluidization regimes [24]

2.2.2 Minimum fluidization

The minimum fluidization velocity (U_{mf}) is the lowest superficial gas velocity at which particles begin to fluidize. U_{mf} is calculated by balancing the pressure drop in the particle bed, as described by the Ergun equation, against the weight of the particles. The equation for this is given as follows:

$$\frac{1.75}{\varepsilon_{mf}^3 \varphi_s} \left(\frac{d_p U_{mf} \rho_g}{\mu_g} \right)^2 + \frac{150(1-\varepsilon_{mf})}{\varepsilon_{mf}^3 \varphi_s^2} \left(\frac{d_p U_{mf} \rho_g}{\mu_g} \right) = \frac{d_p \rho_g (\rho_s - \rho_g) g}{\mu_g^2} \quad (2-1)$$

Where ε_{mf} is the void fraction at minimum fluidization condition, φ_s is the sphericity of particles, d_p and ρ_s show the particle diameter and envelope density, ρ_g and μ_g show the fluid density and viscosity [26]. In a fluidized bed reactor, the minimum gas velocity should be well above the U_{mf} to ensure good mixing conditions.

2.2.3 Settling velocity

The terminal settling velocity (U_t) is the steady free-fall velocity of a particle in a stationary fluid. If the local gas velocity exceeds the terminal settling velocity of a particle, the particle begins to get entrained. The terminal settling velocity is determined by balancing the drag forces exerted by the fluid against the gravitational forces due to the particle's mass. It can be calculated by solving the relevant equations below where u_t^* is the dimensionless terminal settling velocity and d_p^* is the dimensionless particle diameter [26].

$$U_t = u_t^* \left(\frac{\mu_g(\rho_s - \rho_g)g}{\rho_g^2} \right)^{\frac{1}{3}} \quad (2-2)$$

$$u_t^* = \left(\frac{18}{(d_p^*)^2} + \frac{2.335 - 1.744\phi_s}{(d_p^*)^{0.5}} \right)^{-1} \quad (2-3)$$

$$d_p^* = d_p \left(\frac{\rho_g(\rho_s - \rho_g)g}{\mu^2} \right)^{\frac{1}{3}} \quad (2-4)$$

The operating velocity in the segregation chamber should ensure that coarse particles stay in the bed while fine particles are entrained. This is accomplished by maintaining a velocity between the terminal settling velocity of the largest fine (raw meal) particles and that of the smallest coarse (inert) particles.

2.3 Fluidization conditions of fine particles

Before starting to describe the fluidization conditions specifically in the calciners, it is needed to briefly mention the Geldart particle classification.

Geldart classified particles into four categories, based on experimental data and empirical observations. The particles are categorized into A, B, C, and D, depending on particle size and the density differential between solids and the fluidization gas [27]. The graph of classification is shown in Figure 2-7 and it is noted that the fluidization gas in this graph was air. As shown in the Figure 2-7, group A particles are the ones with mean diameter between 20 μm to 100 μm and having low density ($<1.4 \text{ g/cm}^3$) which are easy to fluidize at low superficial gas velocities. Group B includes particles with density between 1.4 g/cm^3 and 4 g/cm^3 and particle diameter between 40 μm and 500 μm . These particles are easy to fluidize, once superficial gas velocity goes slightly higher than the minimum fluidization velocity, bubble formation starts in the bed. But group C particles includes fine powders with particle diameter smaller than 30 μm which are too difficult to fluidize due to having large inter particle forces in comparison with the drag forces applied by the gas. Group D includes very large particles with high density which are also difficult to fluidize in deep beds [27].

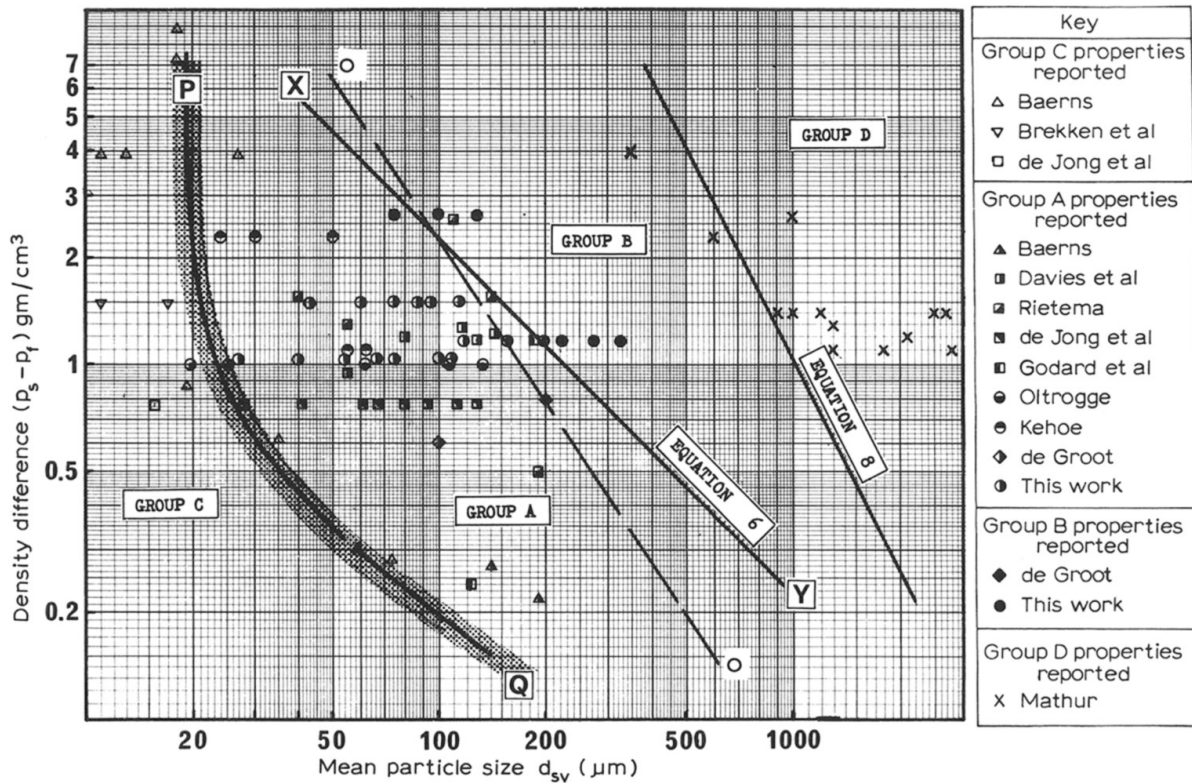


Figure 2-7: Geldart classification of particles [27]

2.3.1 Binary particle Fluidized bed

In this thesis the aim is to design a fluidized bed reactor to calcine the cement raw meal. This raw meal is classified in Geldart C particle group which are too difficult to fluidize, as mentioned above. So, one of the ways to tackle this problem is using binary particle fluidized bed. In other words, Mixing the fine powder of raw meal with bigger particles like Geldart B particles can solve this problem. After blending these particles, separation, and entrainment of Geldart C particles by modifying the superficial gas velocity is possible. This was investigated in several scientific articles.

First, Kato et al. [28] in 1991 investigated the distribution of residence of fine particles in a powder-particle fluidized bed. They supplied fine particles continuously while the coarse particles were fluidized and investigated the particle residence time in different conditions. In another study Tashimo et al. [29] investigated the calcination of fine powder raw meal (Geldart C) in a powder-particle fluidized bed. Powder-particle is another way of calling binary particle fluidized bed which includes fine and coarse particles. In their experiment in 1999, several factors such as the effect of temperature, static bed height, superficial gas velocity and limestone particle size on the calcination of Geldart C limestone was investigated. The results showed that having the reaction temperature higher than 850°C and the average gas residence time higher than 0.2 seconds leads to more than 90% calcination of fine limestone particles.

Also, they concluded that operating in high temperature may reduce the effect of CO₂ concentrations as the fluidization gas.

In 2002, Nakagawa et al. [30] studied the minimum fluidization velocity for different binary particle fluidized bed reactors, including coarse and fine particles. The weight fraction of fine particles in their study was less than 15%. In this study they concluded that increasing the weight fraction of fine particles decreases the minimum fluidization velocity. The reason for this reduction in the systems with Geldart C particles was the formation of aggregated particles. They also concluded in this study that in a specific range of fine particle weight fraction, Geldart C particles can be fluidized and homogeneously mixed with the coarse particles. This specific range is not a specific value for all reactors, and it depends on the system conditions.

In another study, in 2014, Kim et al. [31] studied the Geldart C particles entrainment in binary particles fluidized bed. They used a mix of Geldart B and Geldart C particles in the fluidized bed reactor and the results showed that the amount of entrainment of fine particles (Geldart C) is adjustable and depends on the superficial gas velocity and the mass ratio of fine and coarse particles.

In recent years, some studies have been conducted in this field in the University of South-Eastern Norway. In 2020, Samani et al. [4] investigated a fluidized bed calciner for calcination of fine powder limestone with particle size of 0.2 μm to 180 μm . Due to the difficulty of fluidization of these small particles, especially the ones smaller than 30 μm , they have used some inert coarse particles (Geldart B with 550 μm -800 μm particle diameter) for fluidization. They mentioned in their numerical simulation study that using this technique not only clustering and aggregation of the fine particles is decreased due to the colliding with coarse particles which leads to a more homogenous bed, but also existence of coarse particles helps having a more stable temperature in the bed as they may enhance the heat transfer.

In 2021 Jacob et al. [32] worked on an experimental and numerical investigation of using coarse particles for fluidization of fine powder limestone in the calciner. In their study, they have used sand as coarse particles (for experiments) and the weight fraction of fine particles in the bed was 0.25 and 0.50. They concluded that for this reactor and with the superficial gas velocity of 0.3 m/s, the mentioned weight fractions of fine particles work well and leads to a stable bed. They also conducted CPFD simulations using the commercial software Barracuda and validated the results (Pressure drop) with the experiments. They mentioned that after this validation, the CPFD simulation can be used for a scaled up calciner in industrial size. Their experimental setup is shown in Figure 2-8.

In another study, conducted in 2023 by Jacob et al. [33], an electrified calciner with vertical channel were designed and investigated by CPFD simulation. The performance of the calciner was assessed using time and space-averaged data collected within the simulation of the calciner. The results revealed that at the exit, the raw meal temperature was approximately 912°C, and the average size of the particles leaving the calciner closely resembled the original size of the raw meal particles. They also concluded that for proper segregation, the gas speed at the top of the calciner should be between 1-1.3 m/s. While slower velocities are possible, they might not achieve enough segregation, causing particles to build up. Figure 2-9 shows the geometry of the calciner and the velocity distribution along the height of the reactor.

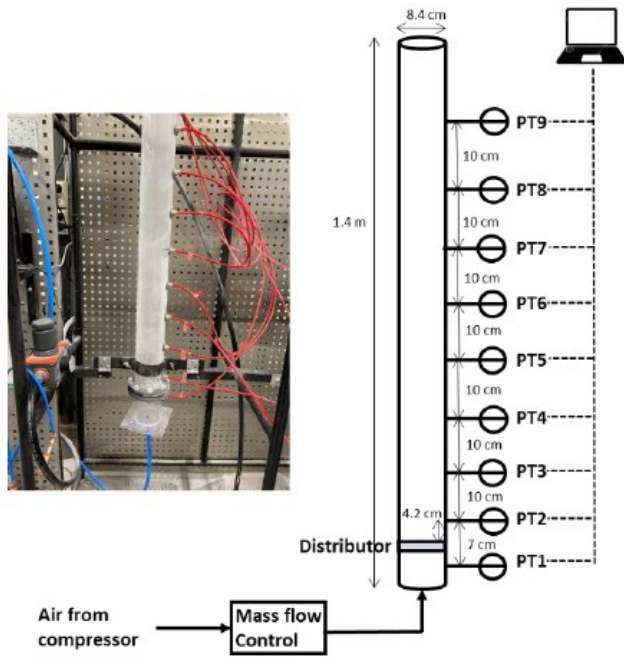
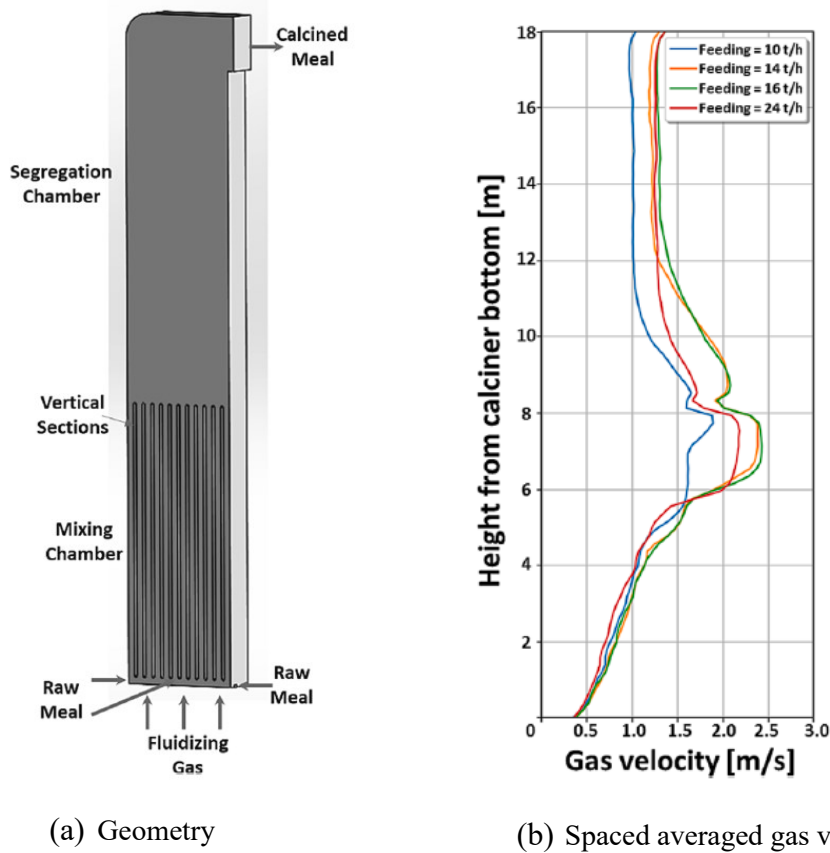


Figure 2-8: Experimental setup for investigation of binary particle fluidized bed calciner [32]



(a) Geometry

(b) Spaced averaged gas velocity in the calciner

Figure 2-9: The electrified calciner with vertical channel (a) Geometry, (b) space averaged gas velocity in the height of the calciner [33]

Following the previous studies, in the current thesis a lab scaled electrified calciner with immersed horizontal hot cylinders (for providing heat both for reaching the calcination temperature and the calcination reaction) is designed, sized, and different operating conditions are investigated by the CPFD simulations.

3 Reactor design

In this chapter designing and sizing the reactor is described. The reactor is designed as a binary fluidized bed reactor for calcination reaction (R-1) and the required heat is provided by electric resistance heating.



The reactor includes two different main types of particles: coarse particles and fine particles.

The fine particles are the raw meal which is injected to the bed and includes 0.77 weight calcium carbonate (which consumes energy and takes part in the reaction) and 0.23 weight inert particles. The size distribution is shown in Figure 3-1. The coarse particles are used to make the fluidized bed, provide a good mixing and heat transfer condition and should stay inside the reactor as much as possible. These particles are assumed to be pre-calcined particles (CaO), which do not take part in the reaction and if a small amount of these coarse particles find the way to the cement kiln, it doesn't make a disaster. The size distribution of the coarse particles is shown in Figure 3-1.

The reactor includes hot horizontal cylindrical elements with 55 mm diameter and as mentioned they are heated by electric resistance heating. The heating elements are assumed to keep the high temperature 1050°C and act as isothermal elements which provides heat both for heating up the raw meal and the calcination reaction. The overall available electric energy for the reactor is assumed to be 100 kW based on the data received from the ELECTRA project.

Another constraint from the ELECTRA project was the top outlet of the reactor should have 170 mm diameter to be connected to other piping and equipment in the lab.

The design of reactor includes several steps including:

1. Mass and energy balance:

- a. How much raw meal (including calcium carbonate) can be injected into the reactor and how much CO₂ and CaO will be produced.
- b. How much energy is needed in the reactor both for the reaction and heating up the feed and how much energy is available.
- c. How much heat transfer area is needed for transferring the required amount of heat.

2. Fluidized bed design calculations:

How much CO₂ is needed to be injected to fluidize the coarse particles based on the minimum fluidization velocity and the size of bottom cross section of the reactor. Calculation of the size of bottom cross section of the reactor and the arrangement of heating elements needs trial and error. It should satisfy:

- a. The height of the bed should be only slightly higher than the height of the area with heating elements.
- b. The height of the reactor and the top cross section area should be in a way that having enough entrainment velocity for the fine calcined particles and have as little as possible entrainment of coarse particles.

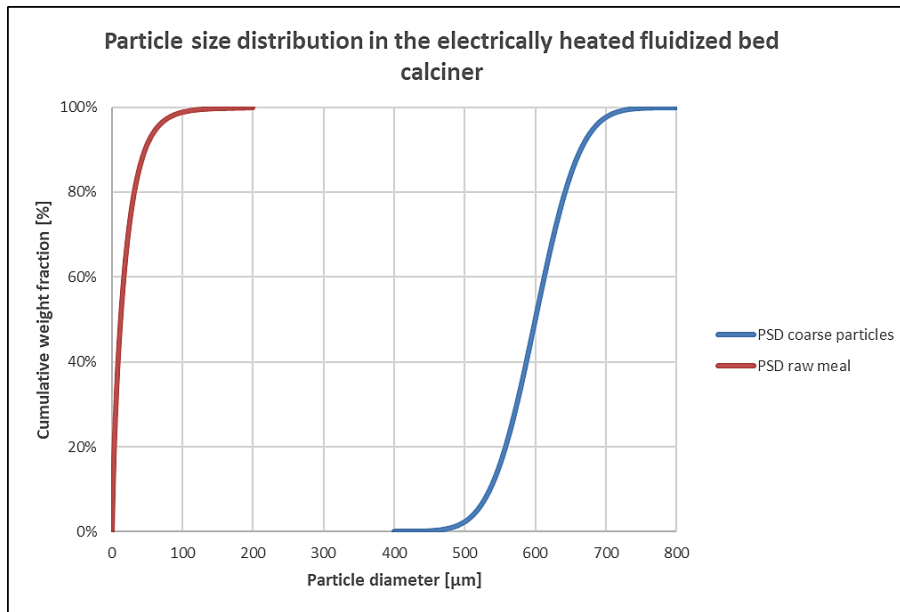


Figure 3-1: Particles size distribution

3.1 Design basis values

In this section all the design basis values, constraints and constants are summarized. (Table 3-1, Table 3-2 and Table 3-3)

Table 3-1: Table of design basis values

Parameter	Description	value	unit
u_F	Fluidization velocity	0.3	$\frac{m}{s}$
$u_{CO_2,out}$	Minimum entrainment velocity of gas	1.7	$\frac{m}{s}$
w_{CaCO_3}	Weight fraction of calcite in the raw meal	0.77	-
η	Degree of calcination	0.94	-
$T_{in,RM}$	Inlet temperature of the raw meal	20	°C
T_{cal}	Calcination temperature	920	°C
T_{cyl}	Cylinders' wall temperature	1050	°C
U	Overall heat transfer coefficient	0.3	$\frac{kW}{m^2 K}$
D_{cyl}	Cylinders' diameter	0.055	m

Table 3-2: Table of constraint values

Parameter	Description	value	unit
D_{top}	Top cross section diameter	0.170	m
\dot{E}	Available energy (electricity)	100	kW

Table 3-3: Table of constant values

Parameter	Description	value	unit
R	Ideal gas constant	8.314	$\frac{J}{mole \cdot K}$
ρ_{coarse}	Density of lime coarse particle	1512	$\frac{kg}{m^3}$
ρ_{CaCO_3}	Density of limestone	2700	$\frac{kg}{m^3}$
H_{cal}	Enthalpy of calcination	1700	$\frac{kJ}{kg_{CaCO_3}}$
C_{rm}	Specific heat capacity of raw meal	1	$\frac{kJ}{kg \cdot K}$

3.2 Step 1, mass and energy balance:

The available energy from the electricity provided in the lab would be 100 kW. The energy consumers are two-fold:

- Energy needed for heating up the meal to the calcination degree. The raw meal particles are injected into the bed at 20°C temperature and they should be heated up to the calcination degree which is 920°C. The required energy can be calculated as follows:

$$Q_{sensible} = \dot{m}_{rm} C_{rm} (T_{in} - T_{cal}) \quad (3-1)$$

- Energy needed for the calcination reaction. The reaction is endothermic which requires $1700 \frac{kJ}{kg_{CaCO_3}}$ for a complete calcination [34]. However, the design of this reactor is made for a 94% degree of calcination. The required energy can be calculated as follows:

$$Q_{cal} = \dot{m}_{rm} w_{CaCO_3} \eta H_{cal} \quad (3-2)$$

So, the energy balance can be shown as follows:

$$\dot{m}_{rm} w_{CaCO_3} \eta H_{cal} + \dot{m}_{rm} C_{rm} (T_{cal} - T_{in}) = \dot{E} \quad (3-3)$$

Where the parameters are shown in Table 3-1 and the only unknown parameter is the mass flow rate of raw meal (\dot{m}_{rm}) which can be calculated as follows:

$$\dot{m}_{rm} = \frac{\dot{E}}{w_{CaCO_3} \eta H_{cal} + C_{rm} (T_{in} - T_{cal})} \quad (3-4)$$

Using the formula above, and the data shown in Table 3-1, raw meal should be injected to the reactor with the mass flow rate of $0.047 \frac{kg}{s}$.

Having the raw meal calculated, the amount of $Q_{sensible}$ and Q_{cal} will be defined. So, one may calculate the amount of heat transfer area required for each.

Starting with the sensible heat, which is consumed by raw meal particle to be heated up from 20 °C to 920°C:

$$Q_{sensible} = \dot{m}_{rm} C_{rm} (T_{cal} - T_{in}) = 0.047 \times 1 \times (920 - 20) = 42.2 \text{ kW} \quad (3-5)$$

In order to calculate the heat transfer area of the hot cylinders needed for heating up the meal, we need an energy balance:

$$A_{sensible} U \Delta T_{LMTD} = \dot{m}_{rm} C_{rm} (T_{cal} - T_{in}) \quad (3-6)$$

Where $A_{sensible}$ is the heat transfer area we need to calculate, U is the overall heat transfer coefficient and ΔT_{LMTD} is the LMTD temperature difference. For calculation of ΔT_{LMTD} we assume having a heat exchanger, where in one side the raw meal is being heated from 20 °C to 920°C and in the other side we have isothermal hot cylinder with wall temperature of 1050°C. So, the calculation of this parameter is as follows:

$$\Delta T_{LMTD} = \frac{(T_w - T_{in, RM}) - (T_w - T_{cal})}{\ln \frac{(T_w - T_{in, RM})}{(T_w - T_{cal})}} \quad (3-7)$$

For the overall heat transfer coefficient, U, the value is assumed to be $0.3 \frac{kW}{m^2 K}$ getting the idea from studying scientific papers (for example [35]) and the previous experiments and studies in USN (for example [25]). Having said all the above, the heat transfer area needed for sensible heat transfer is calculated as:

$$A_{sensible} = \frac{\dot{m}_{rm} C_{rm} (T_{cal} - T_{in})}{U \Delta T_{LMTD}} = 0.32 \text{ m}^2 \quad (3-8)$$

In a similar way the heat transfer area needed for calcination can be calculated as follows:

$$A_{cal} U \Delta T = \dot{m}_{rm} w_{CaCO_3} \eta H_{cal} \quad (3-9)$$

Where A_{cal} is the heat transfer area we need to calculate, U is the overall heat transfer coefficient ($0.3 \frac{kW}{m^2K}$) and ΔT is the temperature difference between the wall temperature of hot cylinders ($150^\circ C$) and the temperature of calcination ($920^\circ C$). On the other hand, the calcination heat is calculated using the data in the Table 3-1, equation 3-2, and equation 3-9. The heat transfer area needed is calculated as follows:

$$A_{cal}U\Delta T = \dot{m}_{rm}w_{CaCO_3}\eta H_{cal} \quad (3-10)$$

$$A_{cal} = \frac{0.047 \times 0.77 \times 0.94 \times 1700}{0.3 \times (1050 - 920)} = 1.5 \text{ m}^2$$

These calculated heat transfer areas will be used in the next step of design to find the arrangement of hot cylinders in the bed.

To continue with the mass balance, let's get back to the value calculated for raw meal injection, which became $0.047 \frac{kg}{s}$.

The amount of $CaCO_3$ in the raw meal is:

$$\dot{m}_{CaCO_3} = \dot{m}_{rm}w_{CaCO_3} = 0.047 \times 0.77 = 0.036 \frac{kg}{s} \quad (3-11)$$

Based on the reaction, we know that each mole of $CaCO_3$ produces one mole CO_2 and one mole of CaO based on the stoichiometric reaction. The molar flow of $CaCO_3$ is calculated as follows:

$$\dot{n}_{CaCO_3} = \frac{\dot{m}_{CaCO_3}}{M_{CaCO_3}} = \frac{0.036}{0.1} = 0.36 \frac{mole}{s} \quad (3-12)$$

The molar flow rate of CaO and CO_2 produced from the reaction is also 0.36 moles per second. So, the mass flow rate of CO_2 and CaO produced from the reaction is as follows:

$$\dot{m}_{CaO} = \dot{n}_{CaO}M_{CaO} = 0.36 \times 0.066 = 0.020 \frac{kg}{s} \quad (3-13)$$

$$\dot{m}_{CO_2,prod} = \dot{n}_{CO_2,prod}M_{CO_2} = 0.36 \times 0.044 = 0.016 \frac{kg}{s} \quad (3-14)$$

3.3 Step 2, fluidized bed calculations:

To start with the fluidized bed calculations, we need to define some assumptions before mentioning the steps for trial and error. The assumptions are as follows:

- All of the cylinders are the same size. The diameter of all the hot cylinders is 0.055 meters and they will be arranged horizontally in the bed in several rows. ($D=0.055 \text{ m}$)
- The distance between each two hot cylinders in a row should be $3D$ center to center.
- The distance between each cylinder to the wall should be D .
- The length of the cylinders should be equal to the length of one side of the bottom cross section of the reactor (L_I). It is noted that the bottom cross section is assumed to be rectangular.

- e) The height of bed is assumed to be 1.2 of hydraulic diameter of the bottom cross section of the reactor ($H_{bed} = 1.2D_h$).
- f) The height of the expanded bed is assumed to be two times of the bed height before fluidization ($H_{Exp} = 2H_{bed}$).
- g) The minimum fluidization velocity of the bed is assumed to be $0.3 \frac{m}{s}$.
- h) The entrainment velocity in the outlet should be at least $1.7 \frac{m}{s}$.
- i) The outlet cross section is a circle with 0.17 m of diameter.

The trial and error procedure is as follows:

A: Fluid calculations:

1. Assume two values for the rectangular bottom cross section of the reactor. (L_1 and L_2). We prefer to keep the area as small as possible.
2. Calculate how much CO_2 volume based should be injected to have $0.3 \frac{m}{s}$ fluidization velocity, the injected CO_2 in this system can be called recycled CO_2 . Because after running the system of electrified calciner, a part of the outlet CO_2 will be injected as fluidization fluid.

$$\dot{V}_{CO_2,rec} = u_F(L_1L_2) = u_F A_{bottom} \quad (3-15)$$

3. The total amount of CO_2 in the bed includes the injected CO_2 and the produced CO_2 based on the mass balance. This amount of CO_2 can show how much would be the outlet velocity which is as follows:

$$\dot{V}_{CO_2,out} = \dot{V}_{CO_2,rec} + \dot{V}_{CO_2,prod} \quad (3-16)$$

$$u_{CO_2,out} = \frac{\dot{V}_{CO_2,out}}{A_{top}} \quad (3-17)$$

Where A_{top} is the top cross section of the reactor, which is a circle with 0.170 m diameter. In this step $u_{CO_2,out} > 1.7 \frac{m}{s}$ should be satisfied. If it is not satisfied, calculation should be repeated from step A.1.

B: arrangement of hot cylinders in the bed

1. Set the length of each hot cylinder to L_1 .
2. Calculate the surface area for one cylinder based on the selected length.

$$A_{cyl} = \pi D_{cyl} L_1 \quad (3-18)$$

3. Divide the heat transfer area by the surface area of one cylinder to calculate the number of cylinders.

$$N_{cyl} = \frac{A_{sensible} + A_{cal}}{A_{cyl}} \quad (3-19)$$

4. Using assumptions b and c, the maximum number of cylinders in the bed is calculated. And having the whole number of cylinders (N_{cyl}) from the previous step, it can be easily calculated how many rows of cylinders are needed.
5. Having the number of rows of cylinders, the height of the area including cylinders is calculated (H_{cyl}). It is noted that the cylinders are assumed to be arranged segregated, so the number of cylinders in even rows and odd rows are different. (Figure 3-2)

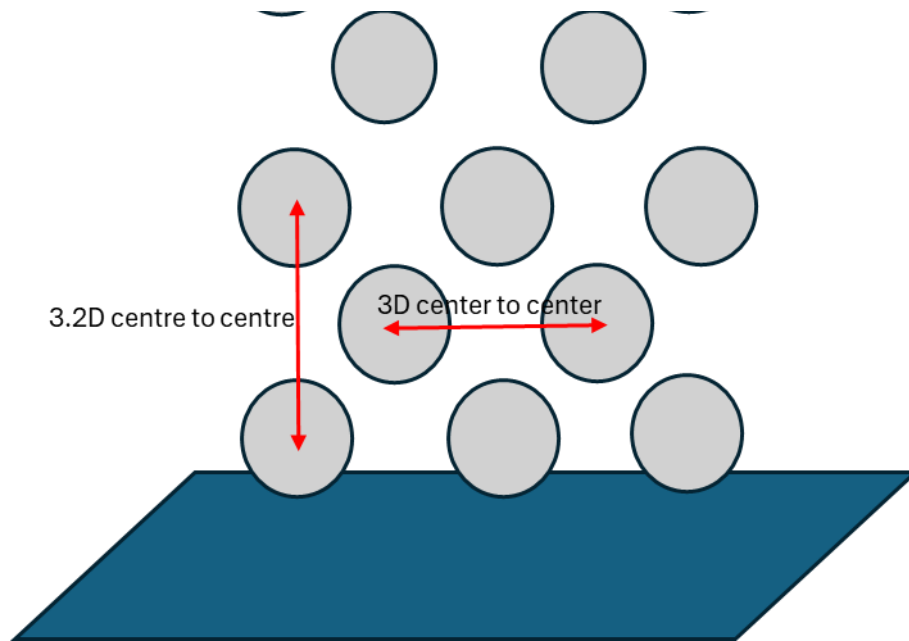


Figure 3-2: The segregated arrangement of the rows (as a sample)

C: Bed sizing

1. Using L_1 and L_2 from step A-1, calculate the hydraulic diameter of the cross section. The rough calculation for the height of bed before fluidization (including only the coarse particles) is:

$$H_{bed} = 1.2D_h \quad (3-20)$$

Where D_h is the hydraulic diameter of the bottom cross section.

2. Compare the height of bed with the height of the area with cylinders (H_{cyl}). They should be quite the same and it is preferable to have the height of cylinders slightly higher than the height of bed before fluidization.
3. If the mentioned condition was not satisfied, change the dimensions of the bottom cross section, in step A-1 and repeat all the next steps again.

This trial and error continue until finding the number of cylinders, arrangement of the cylinders and the cross-section area of the bed in a way that satisfies the requirement.

4. After defining the size of the bottom cross section and height of the bed before expanding, it is assumed that height of the bed after expanding would be double. The

total height of the reactor should be designed to be higher than H_{exp} so the coarse particles cannot leave the reactor from the outlet. But it should also be short enough for the fine particles to be calcined and entrained after calcination with enough velocity. The height of reactor should be selected in a way that outlet velocity stays between the terminal settling velocity of the largest fine (raw meal) particles and that of the smallest coarse (inert) particles.

3.4 Reactor specifications and working principles

After doing several trial and errors and satisfying all of the requirements, the final size of reactor, the bed and the arrangement of hot cylinders is defined. The final specification of the reactor is shown in Table 3-4.

Table 3-4: Final size definition of the reactor

Symbol	Definition	Value	unit
L_1	One side of the bottom cross section	0.650	m
L_2	Other side of the bottom cross section	0.440	m
H_{bed}	Height of bed before expansion	0.610	m
H_{total}	Total height of the reactor	1.880	m
N_{cyl}	Total number of cylinders	17	-
L_{cyl}	Length of each cylinder	0.650	m

The geometry is designed using the Autodesk Inventor Professional, student version. The final geometry is shown in Figure 3-3. It should be noted that geometry is designed in a way to be used in CPFDF simulations, so all the solid parts (cylinders) are subtracted, and the fluid part is drawn in the software. Another point to be mentioned is that the project had a constraint of using rectangular cross section in the bottom and circular cross section in the top. So, a transition piece should have been used. The transition piece tried to be as short as possible.

The reactor has two main sections, the mixing section, and the segregation section. The first section, called the mixing section, is at the bottom. Its main job is to mix fine raw meal with hot coarse particles to transfer heat efficiently [33]. The hot cylinders which are electrically heated warm up the mixing section. Raw meal enters from different injection points¹ located

¹ The effect of different types of injection points is investigated in the results and discussion chapter.

below the first row of the cylinders, then mixes with coarse lime particles, gets heated enough and calcined. During the calcination reaction, CO_2 gas is released, carrying particles to the second chamber, known as the segregation section. This section is meant to carry the calcined raw meal but leave the coarse particles in the bed. However, if a few coarse particles get carried, they can be replaced by adding extra material with the raw meal.

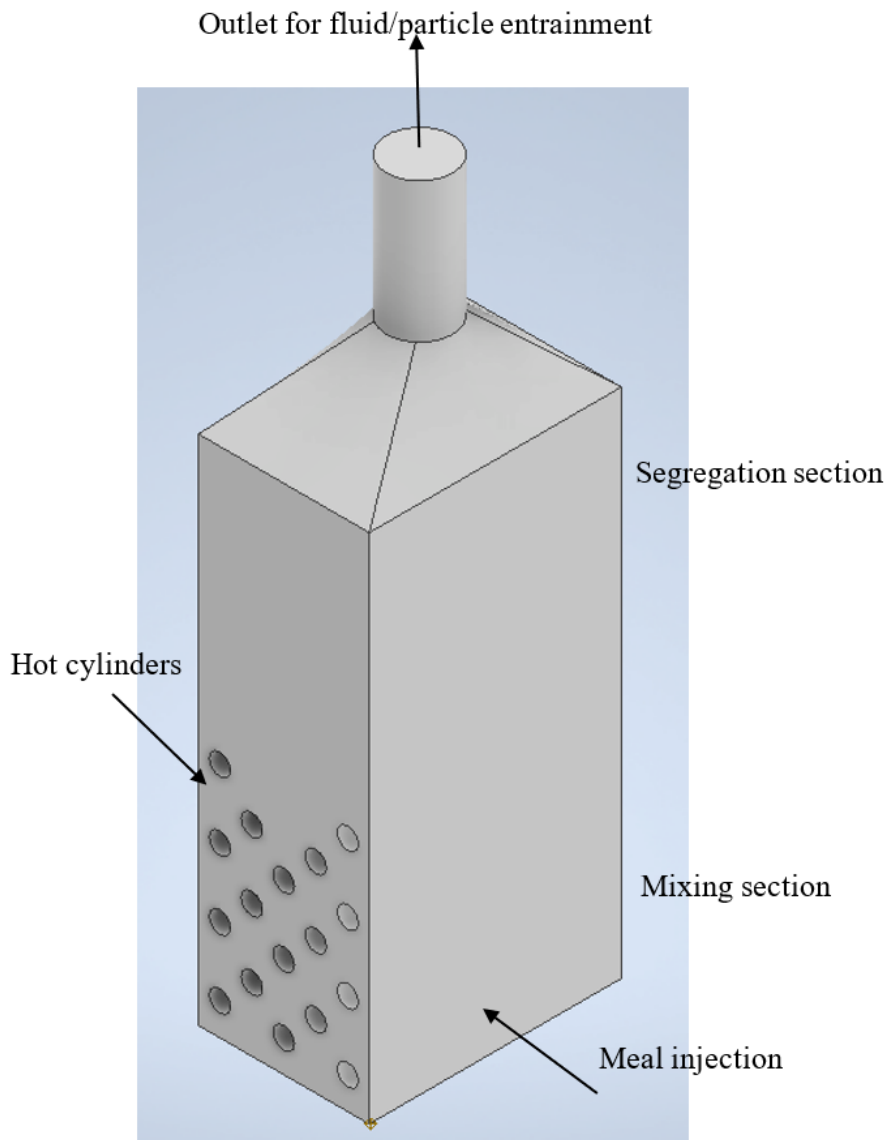


Figure 3-3: Schematic of the reactor with the designed size

4 CPFD Simulation

In this chapter, the aim is to realize the theory behind the CPFD simulation software, where all the CPFD simulations are made with the commercial software, Barracuda 21.1.1, and to describe the important specifications of the CPFD simulations.

At the end of this chapter, a review of the simulation cases is made to be used in the result and discussion section.

4.1 Theory and governing equations

In this project, the CPFD simulations are being used as a tool to investigate the fluid particle interaction and behaviors in an electrified calciner. The result of this project is being used before building a lab-scaled electrified calciner for the ELECTRA project. Different operational conditions can be investigated former than building the pilot system.

Barracuda 21.1.1 is used for the CPFD simulations. Barracuda technology uses a special method called 3D Multiphase Particle-in-Cell (3D-MP-PIC) developed by CPFD Software. It's great for simulating how fluids and particles move together in reactors, considering factors like temperature and chemical reactions. This method can handle any number of different particles and sizes, giving an accurate virtual picture inside the reactor.

The MP-PIC method solves equations for both the gas and solids phases. It uses a mix of approaches: Eulerian for gas and a mix of Eulerian and Lagrangian for solids. Instead of tracking each physical particle, it groups similar ones into numerical parcels. This makes calculating properties like particle stresses faster in the gas phase. The method can handle various particle phases, sizes, and materials efficiently [36],[34].

Governing equations for the MP-PIC method which are solved in the software are described in references [37] and [34] in details. In this thesis, the main equations are briefly shown.

4.1.1 Flow governing equations

To define the fluid behavior in a CPFD simulation the continuity, momentum, energy as well as species transport should be solved. A brief description of the equations and the order of solving the equations is defined in this section.

The continuity equation is as follows:

$$\frac{\partial(\theta_f \rho_f)}{\partial t} + \nabla \cdot (\theta_f u_f \rho_f) = \delta \dot{m}_p \quad (4-1)$$

Where, θ_f , ρ_f and u_f shows the volume fraction, density and the velocity of fluid. It should be mentioned that due to having particle-fluid reaction (calcination) in the reactor, the term $\delta \dot{m}_p$ is shown in the continuity equation and will be defined in the next sub-chapter.

The next equation is the momentum equation for the fluid which can be written as follows:

$$\frac{\partial(\theta_f \rho_f u_f)}{\partial t} + \nabla \cdot (\theta_f \rho_f u_f u_f) = -\nabla p + F + \theta_f \rho_f g + \nabla \cdot (\theta_f \tau_f) \quad (4-2)$$

In this equation ∇p denotes the pressure gradient in the gas flow, τ_f symbolizes the stress exerted by the fluid, F shows the inter-phase momentum transfer rate per unit volume (will be defined in the particle equations), and g represents the gravity acceleration.

The stress tensor in form of constitutive equation is written as follows:

$$\tau_f = \mu \left(\frac{\partial u_{f,i}}{\partial x_j} - \frac{\partial u_{f,j}}{\partial x_i} \right) - \frac{2}{3} \delta_{i,j} \mu \frac{\partial u_k}{\partial x_k} \quad (4-3)$$

Where μ is sum of the laminar shear viscosity and a turbulence viscosity from the Large Eddy Simulation turbulence model.

The equations above (4-1 to 4-3) should be solved separately for each gas species based on their mass fraction calculated from species transport equation.

The species transport is defined as follows:

$$\frac{\partial(\theta_f \rho_f Y_{f,i})}{\partial t} + \nabla \cdot (\theta_f u_f \rho_f Y_{f,i}) = \nabla \cdot (\rho_f D_t \theta_f \nabla Y_{f,i}) + \delta \dot{m}_{i,chem} \quad (4-4)$$

Where $Y_{f,i}$ and $\delta \dot{m}_{i,chem}$ show the mass fraction of species i in the fluid and the chemical source term respectively. The term D_t shows the turbulent mass diffusivity which can be related to the flow viscosity by the Schmidt number correlation ($Sc = \frac{\mu}{\rho D}$).

In the case of having non-isothermal simulation, the energy equation should also be solved. Since we have fluid-particle interactions, the energy equation should also be dependent on the particle behavior which is defined as follows:

The energy equation for the fluid is:

$$\begin{aligned} \frac{\partial(\theta_f \rho_f H_f)}{\partial t} + \nabla \cdot (\theta_f \rho_f H_f u_f) \\ = \theta_f \left(\frac{\partial p}{\partial t} + u_f \nabla p \right) + \phi - \nabla \cdot (\theta_f \dot{q}_f'') + Q + S_h + \dot{q}_D + \dot{q}_w \end{aligned} \quad (4-5)$$

Where H_f is the enthalpy of fluid, ϕ shows the viscous dissipation rate, \dot{q}_f'' is the fluid heat flux, Q Represents the energy source and S_h is the energy exchange between fluid and particles which depends on the particle behavior and will be defined in the next sub-chapter (Particle governing equations). More details can be found in references [37] and [34].

4.1.2 Particle governing equations

In the MP-PIC method, the movement of particles is forecasted by solving a transport equation for the particle distribution function (PDF) "f". Here (in ref [37]) it is simplified by assuming that "f" depends on the spatial location of particles " x_p ", their velocity " u_p ", mass " m_p ", temperature " T_p ", and time " t ".

So, the term $\delta\dot{m}_p$ in equation (4-1), can be defined as:

$$\delta\dot{m}_p = - \iiint f \frac{dm_p}{dt} dm_p du_p dT_p \quad (4-6)$$

Where $\frac{dm_p}{dt}$ is the rate of change of the particle mass producing gas through chemistry. (For more details refer to [37] and [34]).

The acceleration of the particle (A_p) is defined by:

$$\frac{du_p}{dt} = D_p(u_f - u_p) - \frac{1}{\rho_p} \nabla p - \frac{1}{\theta_p \rho_p} \nabla \tau_p + g + \frac{\bar{u}_p - u_p}{\tau_D} \quad (4-7)$$

Where u_p is the particle velocity, ρ_p is the particle density, D_p is the drag function, τ_p is the particle contact stress and τ_D is the particle collision damping time. The term θ_p is the particle volume fraction which is defined using the followed equation:

$$\theta_p = - \iiint f \frac{m_p}{\rho_p} dm_p du_p dT_p \quad (4-8)$$

It is noted that the fluid volume fraction in equations (4-1 to 4-5) is defined after solving this equation. Because, the sum of fluid volume fraction and particle volume fraction shall be 1.

The drag function that is selected to be used in the simulations is the Wen Yu Ergun model, which is a blend of two drag models from Wen-Yu and Ergun. The former is more appropriate for dilute flows, while the latter works better for dense flows[33]. More details of the drag equation can be found in [33].

Getting back to the fluid momentum equation, the term F which shows the particle force per volume of the fluid is shown as:

$$F = - \iiint f \left\{ m_p \left[D_p(u_f - u_p) - \frac{\nabla p}{\rho_p} \right] + u_p \frac{dm_p}{dt} \right\} dm_p du_p dT_p \quad (4-9)$$

In the particle energy equation, it's assumed that temperatures within the particles are consistent, there's no heat release from chemical reactions inside the particles, and any heat released from reactions on particle surfaces doesn't significantly affect the surface energy balance. The equation for particle lumped heat transfer is then simplified as follows:

$$C_v \frac{dT_p}{dt} = \frac{1}{m_p} \frac{\lambda_f Nu_{f-p}}{2r_p} A_{sp} (T_f - T_p) \quad (4-10)$$

Where C_v is the particles specific heat capacity, λ_f shows the fluid thermal conductivity, Nu_{f-p} represents the Nusselt number of heat transfer between particle and fluid, T_p is the temperature of the particle and A_{sp} shows the particle surface area.

The term S_h in the fluid energy equation, can be defined now using the particle energy equation as follows:

$$S_h = \iiint f \left\{ m_p \left[D_p (u_f - u_p)^2 - C_v \frac{dT_p}{dt} \right] - \frac{dm_p}{dt} \left[H_p + \frac{1}{2} (u_f - u_p)^2 \right] \right\} dm_p du_p dT_p \quad (4-11)$$

Where H_p shows the enthalpy of the particle.

4.1.3 Heat transfer governing equations

Considering the heat transfer between fluid and particle, the heat transfer coefficient between the two phases can be calculated as follows:

$$h_p = \left(0.37 Re^{0.6} Pr^{0.33} + 0.1 \right) \frac{k_f}{d_p} \quad (4-12)$$

Where Re and Pr are the Reynolds and Prandtl number respectively. k_f shows the fluids conduction coefficient and d_p shows the particle diameter [33, 38].

The heat transfer between the fluid and the wall (where the wall temperature assumed to be fixed) should also be considered which can be calculated as follows:

$$h_{fw} = h_l + f_d h_d \quad (4-13)$$

Where h_{fw} shows the heat transfer coefficient between fluid and wall, h_l is the lean gas phase heat transfer coefficient and h_d represents the dense particle phase heat transfer coefficient. It is noted that f_d which shows the fraction of contact time by the dense particle phase, depends on the particle volume fraction at the wall, θ_p , and the close pack value fraction, θ_{cp} . More details can be found in the Barracuda 21.1.1 user manual [38].

Another important heat transfer in the reactor is the radiation heat transfer from hot walls to the particles which is calculated using “near wall model” as follows:

$$q_{wp} = A_w F_{wp} \varepsilon_{wp} \sigma (T_w^4 - T_p^4) \quad (4-14)$$

$$\varepsilon_{wp} = \left(\frac{1}{\varepsilon_p} + \frac{1}{\varepsilon_w} - 1 \right)^{-1} \quad (4-15)$$

Where T_w, T_p show the temperature of the wall and the particle respectively. σ shows the Stefan-Boltzman constant, ε_{wp} is the particle emissivity (volume averaged), F_{wp} represents the wall particle view factor and A_w is the wall area [33, 38].

4.1.4 Reaction kinetics

The only reaction in this reactor is the calcite decomposition ($CaCO_3 \rightarrow CaO + CO_2$). The calcination kinetics can be explained using the shrinking core model. According to this model, the reaction rate depends on three factors: heat transfer to the particles and through the product layer, the decomposition of calcite, and the diffusion of CO_2 through the product layer. For

particles that are in the micrometer scale, the resistance from heat transfer and CO₂ diffusion through the product layer is usually minimal. As a result, the heat transfer to the particle surface and the decomposition of calcite are likely to be the primary factors influencing the reaction kinetics. The decomposition or production rate depends on the CO₂ partial pressure, the equilibrium pressure, stoichiometric coefficient and the molecular mass of components based on equation 4-16. In this equation $\frac{dm_j}{dt}$ represents the rate of decomposition or formation of component j within the meal. M_j denotes the molecular mass of component j, while ν_j signifies the stoichiometric coefficient related to the calcination reaction. p_{CO_2} stands for the partial pressure of CO₂ present in the calciner. A_{sp} represents the surface area of the calcite particles, and A_{eff} denotes the excess area fraction, accounting for voids present within the particles. Equations 4-17 and 4-18 show the rate kinetics and calculation of the equilibrium pressure where k_D is the rate kinetics and p_{eq} is the equilibrium pressure. [34, 39, 40].

$$\frac{dm_j}{dt} = M_j \nu_j k_D (p_{eq} - p_{CO_2}) A_{sp} A_{eff} \quad (4-16)$$

$$k_D = 1.22 \times 10^{-5} \exp\left(-\frac{4026}{T_p}\right) \quad (4-17)$$

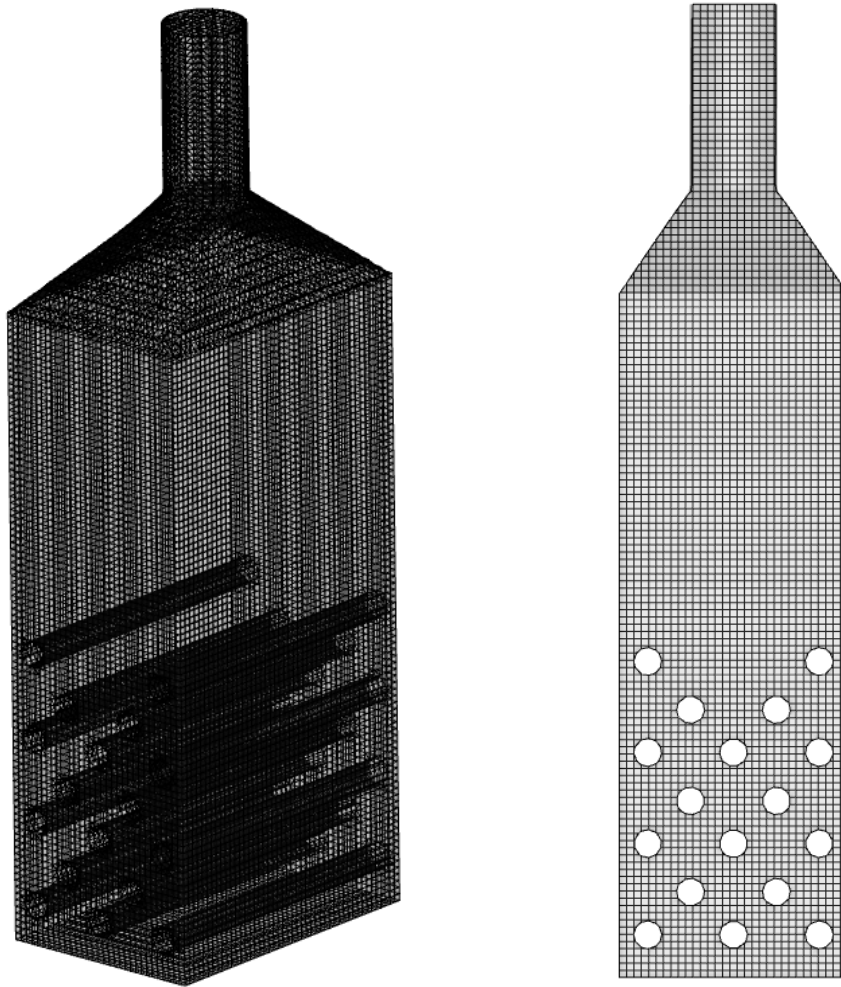
$$p_{eq} = 4.192 \times 10^{12} \exp\left(-\frac{20474}{T_p}\right) \quad (4-18)$$

4.2 Simulation specifications

After mentioning the main equations that are being solved behind the commercial simulator “Barracuda Virtual Reactor 21.1.1”, it is worth mentioning some settings and specifications of the simulation.

4.2.1 Geometry and grid

The geometry was shown in Figure 3-3. The grid type is a uniform grid as uniformity of the cell size is important to reach a stable and efficient simulation [38]. It is noted that for checking the grid independence the pressure drop in the reactor is checked for the four different number of cells including 54000, 130680, 192510, 250767 and the last three meshes have less than 0.46% difference in the result. The mesh with 192510 cells is finally selected which is fine enough for ensuring accuracy and coarse enough for not having too much calculation time. The final mesh is shown in Figure 4-1.



(a) 3D mesh

(b) Mesh in the middle slice (x-y plane)

Figure 4-1: Mesh of the reactor.

4.2.2 Specifications of the particles and the fluid

The simulation includes two phases, gas and solid. Where the gas only contains CO_2 and the solid particles are two-fold. The coarse particles which are made of CaO with the size distribution of 400-800 micron (Figure 3-1) build the bed. The fine particles known as the raw meal which include 0.77 CaCO_3 and 0.23 inert material has a size distribution less than 200 micron (Figure 3-1).

The main working principle of the reactor which is simulated in very brief wording is that the gas is injected from the bottom cross section of the reactor which makes the bed fluidized. The raw meal particles are slowly injected from the sides of the reactor in a way to have the most contact with the hot cylinders. Contact of the raw meal with coarse particles, fluidization gas and the hot cylinders as well as the radiation from hot cylinders provides the heat needed for

the raw meal to reach the calcination temperature and decomposes CaCO_3 to CaO and CO_2 . The calcined particles then exit from the outlet of the reactor. The outlet is a pressure outlet which has atmospheric pressure. A summary of the boundary conditions for each case is shown in Table 4-1. This table is referred to in the “Result and discussion” chapter to investigate the purpose of each simulation and discuss the results.

All the simulations are done time dependent, and the simulations continued to reach the pseudo-steady state. To maintain the accuracy, stability and the calculation speed the simulator checks the Courant number¹ to stay in the preferred range ($0.8 < CFL < 1.5$), and adjusts the time step if needed[38]. But the initial timestep is set to 0.001 s. The simulation data is saved each 0.1 seconds. To solve the fluid governing equations LES model is selected as the turbulence model. The conversion criteria are set to $1e-6$ for the pressure and energy calculations, $1e-7$ for the volume and velocity calculations while the radiation calculations have $1e-9$ as the conversion criteria. The conversion criteria values were suggested in Barracuda. [38]

Table 4-1: Summary of all the simulated cases with boundary conditions

Case NO	Gas inlet temperature (K)	Gas inlet velocity (m/s)	Coarse particle initial temperature (K)	Hot cylinder temperature (K)	Raw meal temp (K)	Raw meal total mass flow rate (kg/s)	Number of injection	Type of injection area
1	293	0.3	293	-	-	-	-	-
2	1193	0.3	1193	-	-	-	-	-
3	293	0.3	1193	1323	-	-	-	-
4	1193	0.3	1193	1323	293	0.047	2	point
5	1193	0.3	1193	1323	1123	0.047	6	point
6	1193	0.3	1193	1323	1123	0.047	2	Rectangular area
7	1193	0.3	1193	1373	1123	0.047	2	Rectangular area
8	1193	0.3	1193	1323	293	0.047	2	Rectangular area

¹ The Courant-Friedrichs-Lewy (CFL) number is a dimensionless measurement that shows how far a fluid travels in a specific time step. $\frac{u\Delta t}{\Delta x}$ defines the CFL number, where Δx is the cell dimension and Δt is the time step. CFL is calculated for each direction.

Case NO	Gas inlet temperature (K)	Gas inlet velocity (m/s)	Coarse particle initial temperature (K)	Hot cylinder temperature (K)	Raw meal temp (K)	Raw meal total mass flow rate (kg/s)	Number of injection	Type of injection area
9	1193	0.3	1193	1423	293	0.047	2	Rectangular area
10	1193	0.3	1193	1423	993	0.047	2	Rectangular area
11	1193	0.2	1193	1373	1123	0.047	2	Rectangular area
12	1193	0.4	1193	1373	1123	0.047	2	Rectangular area
13	1193	0.8	1193	1373	1123	0.047	2	Rectangular area

4.2.3 Mass balance check

The first step before continuing a simulation is to check the mass balance. To do so, the fluid inlet mass flow rate of fluid and outlet mass flow rate is investigated. A calculation example for case 1 is as follows.

In this case, based on the 0.157 kg/s mass flow inlet (boundary condition), fluid density of 1.79 kg/m³ (at 293 K) and having 0.38550 m³ as the total volume of the reactor, I desired that in 0.22 seconds the simulation reaches the pseudo steady state.

Checking the simulation result for the outlet mass flow rate (Figure 4-2), shows that at the start of simulation a peak in the mass flow happened and then smoothed in almost 0.3 seconds reached the desired value (0.157 kg/s). The result seems to satisfy the mass balance and is reasonable.

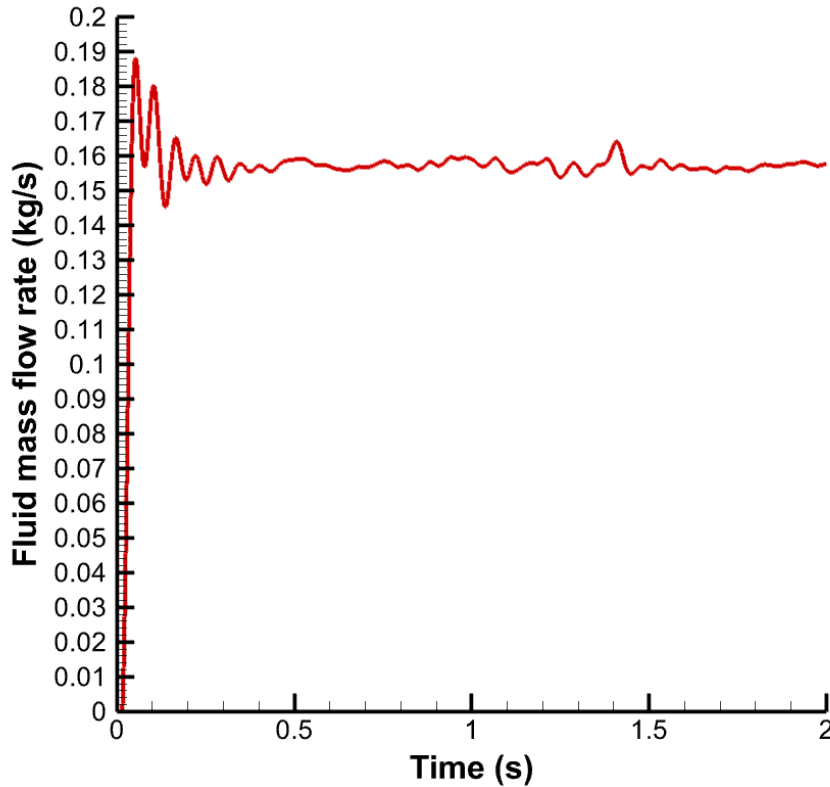


Figure 4-2: Investigation of the mass flow rate out of the reactor to ensure satisfying the mass balance (case 1)

It is noted that the mass balance is checked for all the cases and the cases which are including reaction obviously need more time to reach the pseudo-steady state. As an example, the mass balance in case 9 which includes the reaction can be checked as follows.

Based on the calcination reaction, the only reactant is calcite which converts to calcium oxide and carbon dioxide. To keep the mass balance, the injected mass of raw meal should be equal to the entrained mass of fine particles and produced CO_2 (4-19). Using a flux plane defined in the outlet, the entrainment of fine particles (Figure 4-3 (a)) and the mass flow rate of CO_2 (Figure 4-3 (b)) is shown.

$$\dot{m}_{rm,in} = \dot{m}_{rm,out} + \dot{m}_{\text{CO}_2,prod} \quad (4-19)$$

Starting with the particle entrainment, as shown in the Figure 4-3, from the 28th second the time integrated mass of fine particle entrainment started to increase with almost a fixed slope. This shows the time that the reaction happened, and the mass balance should be checked afterwards. The slope of this line (red line) from 28th to 45th second can show the mass flow rate of fine particle entrainment:

$$\dot{m}_{rm,out} = \frac{0.620 - 0.03}{45 - 28} = 0.035 \frac{\text{kg}}{\text{s}} \quad (4-20)$$

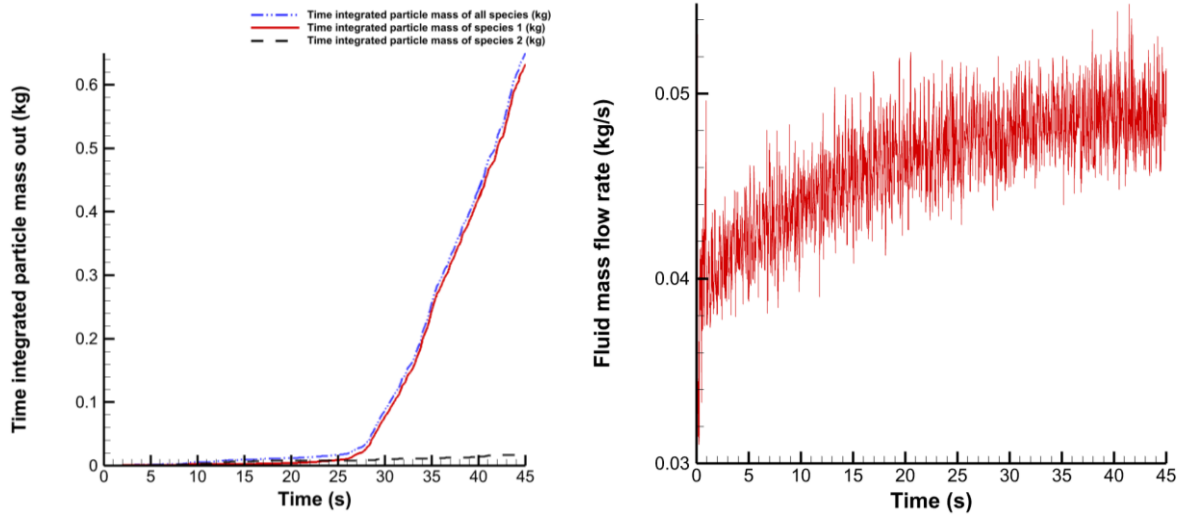
The gas mass flow out can be read from Figure 4-3 (b) as 0.0485 kg/s. However, this is not the produced gas. This value includes the injected gas too. The mass flow rate of injected gas for

this case was 0.038 kg/s based on the design calculations. So, the produced CO₂ can be calculated as:

$$\dot{m}_{CO_2,prod} = \dot{m}_{CO_2,out} - \dot{m}_{CO_2,inj} = 0.049 - 0.038 = 0.011 \frac{kg}{s} \quad (4-21)$$

The injected mass flow rate of raw meal for case 9 was 0.0470 kg/s as shown in Table 4-1. Thus, based on equation 4-19 the mass balance is satisfied. The error is less than 3% due to numerical errors and is acceptable:

$$0.035 + 0.011 = 0.046 \frac{kg}{s}$$



(a) particle

(b) gas

Figure 4-3: Particle and gas entrainment from the reactor outlet in case 9. (a) Time integrated particle mass entrainment (species 1: fine particle, species 2: coarse particle), (b) Gas mass flow rate

5 Result and discussion

After design and sizing of the reactor, simulations have been made to investigate how the reactor works in different operational conditions. The investigated operating conditions include variation in the number of injection points, the temperature of the raw meal feeding the reactor, the wall temperature of hot cylinders and the fluidization gas velocity. The calcination degree, amount of particle entrainment, the entrainment velocity and pressure drop in the reactor are some of the parameters that investigated for each case and compared among different simulation cases.

All the cases with the boundary conditions are mentioned in Table 4-1. Before starting discussion of the result, a brief description of the purpose of each simulation is mentioned.

In this thesis, the simulations include fluid and particle interactions (fluidized bed), heat transfer between wall, particle and fluid and the calcination reaction. So, the starting of simulations are made step by step. In the first step two base cases are made to check if the fluidization works properly based on the design calculations. In this step, no heat transfer or reaction were included. The fluidization has been checked for both cold and hot beds (cases 1 and 2). These cases can be used as the startup conditions, where the reactor starts cold and then gets hot enough before meal injection.

In the next step, the reaction was not included but the heat transfer was taken into consideration. This case is made to check the heat transfer works properly without any errors or problems. (case 3)

The next step, simulation cases include reaction, heat transfer and particle-fluid interaction. In case (4) the raw meal mass flow rate is injected from only two small injection points. The calcination degree reached in this case was not preferable. The reason for that was found in not spreading the raw meal particle over the hot cylinders as much as needed.

So, the number of injections were increased to three injection points on each side of the reactor (6 injection points in total), and at the same time preheating the raw meal before injection. This condition significantly improved the calcination degree reached. But not preferred value yet. (case 5)

The next simulation conducted by a well spread out of the raw meal particles over the hot cylinders and using as much as contact area possible, which made by changing the injection type from several small points to a bigger rectangular area in each side of the reactor (2 injection area in total). This condition worked best in spreading out the particles and thus this type of injection point was used to check other operational conditions. (case 6)

In cases 7 to 10, the effect of changing the temperature of hot cylinders and or raw meal on the reactor performance is investigated. And cases 11 to 13 are made to investigate the effect of fluidization velocity on the reactor performance.

5.1 The effect of fluid temperature on the fluidization

In this section the effect of temperature on the fluidization without including the reaction and heat transfer is investigated. To do so, two cases are compared with each other (Case 1 and Case 2). The boundary conditions can be found in Table 4-1. In both cases the height of bed before fluidization is 61 cm. Case 1 shows the cold conditions (293 K), while case 2 shows the hot conditions (1193 K). Both cases have been simulated up to 25 seconds and they have reached pseudo steady state. The results below are for the 25th second.

For both cases the gas is injected with 0.3 m/s velocity from bottom of reactor with an area of 0.65×0.44 . So, the inlet volume flow rate for both cases is $0.0858 \text{ m}^3/\text{s}$. However, they are different in the fluid density and viscosity in 293 K and 1193 K. By increasing the temperature from 293 K to 1193 K the viscosity of the gas and the density of the gas increases significantly (Based on the data “viscosity of carbon dioxide” in reference [41]). So, the minimum fluidization velocity and minimum bubbling velocity decreases as the temperature increases. This is in line with the previous study by Suksantraisorn et al. [42] in terms of the effect of temperature on the minimum fluidization velocity of the bed with particles smaller than 2 mm diameter. This describes why the bed height in the hot case is higher than the cold case, although the cold case has higher fluid density.

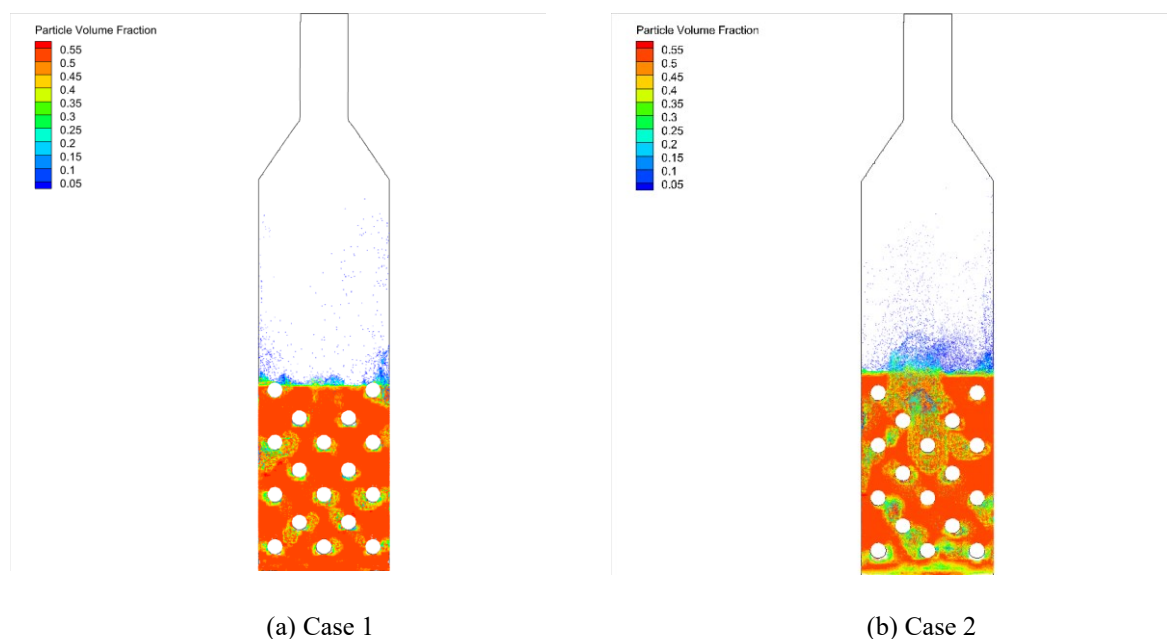


Figure 5-1: The bed expansion in 25 seconds in the middle plane of the reactor (a) case 1 (b) case 2.

The fluid velocity distribution in both cases is shown in Figure 5-2. In both cases, the fluid velocity distribution is quite similar, and the exit velocity of fluid is between 4 m/s - 5 m/s. The reason for this similarity is that the reactor geometry is the same and the inlet volume flow rate was the same. In both cases a similar (and not high) change in the density from bottom to top of the bed has happened and the exit velocity was predictable by the mass balance. Having no reaction, the gas mass flow rate injected shall be the same as gas mass flow rate exited.

The next picture, Figure 5-3, shows the pressure distribution in the bed and in the reactor. The lowest part has the maximum pressure due to the weight of the bed particles. The more moving upward the pressure decreases to reach the atmospheric pressure at last. The pressure drop in the reactor in the cold and hot case was almost 4 kPa. The difference between the two pressure distributions is about the particle movements in the bed. In the case 2 or namely the hot case, the bed has more expansion. So, the weight of the particle in the bed in the same location is a bit lower in comparison with the case 1.

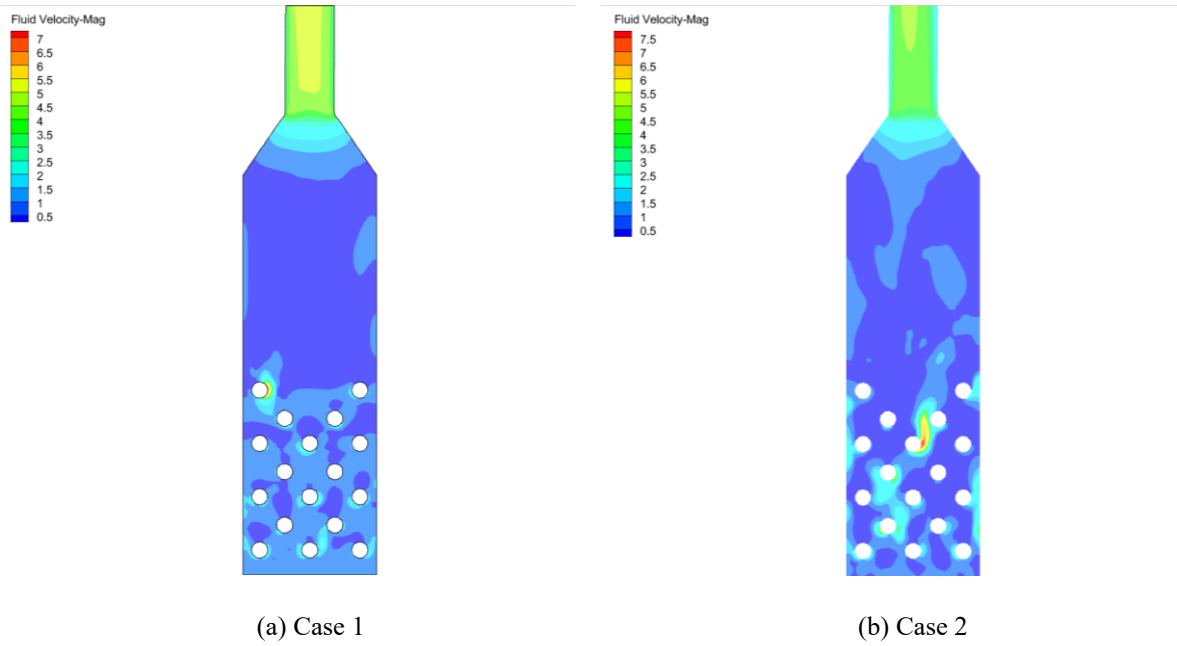


Figure 5-2: Fluid velocity magnitude in the middle plane of the reactor in cases 1 and 2. (a) Case 1, (b) Case 2.

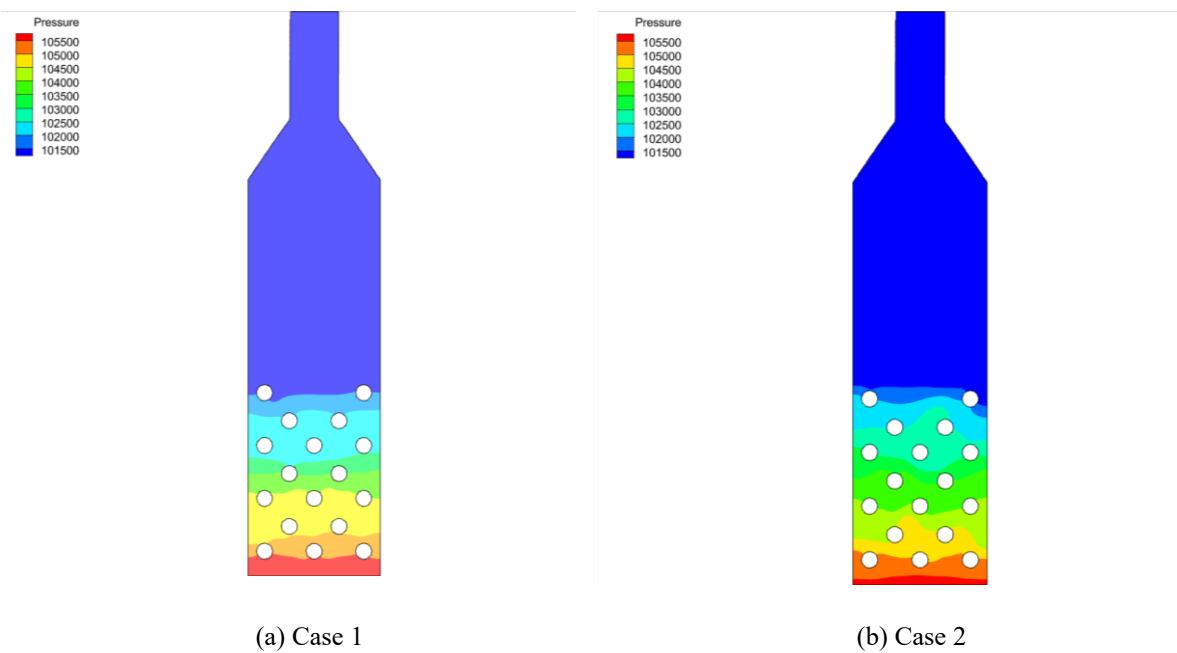


Figure 5-3: Pressure distribution in the middle plane of the reactor in cases 1 and 2. (a) Case 1, (b) Case 2.

5.2 The effect of heat transfer on particle entrainment (without considering the reaction)

Before starting to check the effect of meal spreading on the reactor performance, the heat transfer condition was checked in case 3. As shown in the Table 4-1, in this case the initial temperature of the coarse particles in the bed was 1193 K, the hot cylinders temperature was 1323 K and the injected CO₂ as fluidization gas was cold at 293 K.

Considering the boundary conditions, the main temperature difference is between the fluidization gas with particles and hot cylinders. There are no injected raw meal particles to consume the energy for being heated and take part in the reaction. Thus, in this case a big entrainment of coarse particles is happened, as expected (Figure 5-4).

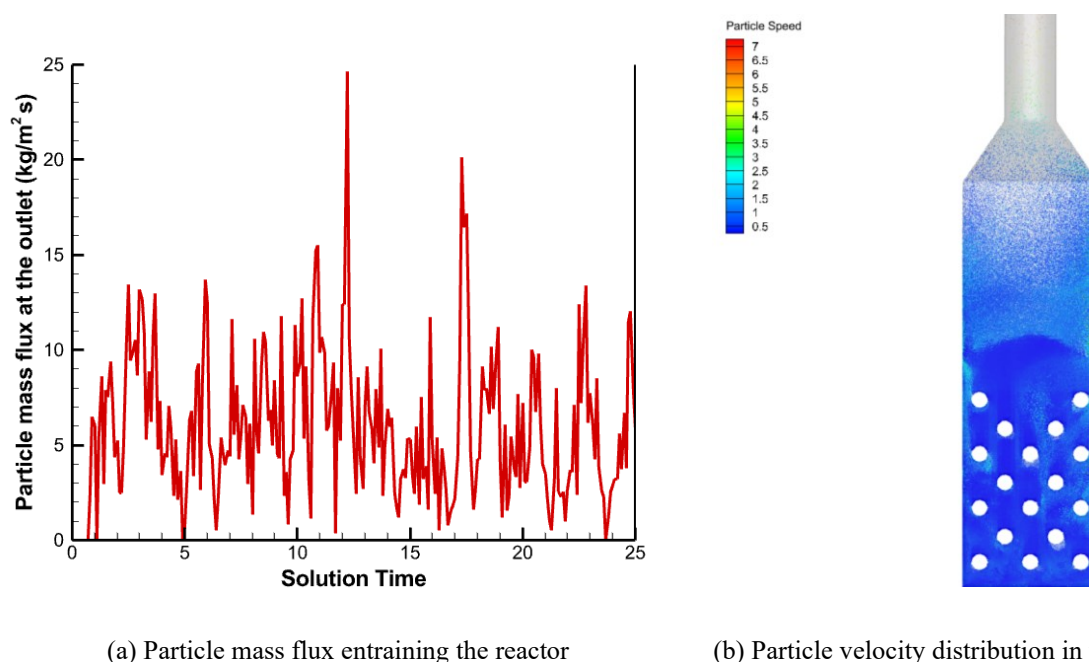


Figure 5-4: Particle condition in the reactor after 25 seconds in case 3. (a) Particle mass flux exiting the reactor from the topmost plane, (b) Particle velocity distribution in the middle of the reactor.

The main energy consumer in this case were the CO₂ gas and its temperature increased from 293 K (at the start time) to almost 1220 K (at 25th second) as shown in Figure 5-5. This significant temperature increase makes a big change in the fluid viscosity and density which can describe the reason for coarse particle entrainment. The fluid is injected with 0.3 m/s and 293 K temperature, but the fluid velocity at the exit of the reactor is much higher (almost 18 m/s) as shown in Figure 5-5. The reason for this is keeping the mass balance! As the density significantly decreases with the temperature increase, the velocity should be increased to keep the same mass flow rate.

It should be noted that the main purpose of this simulation was to check the heat transfer in the bed, while it also showed other interesting results as discussed. It was decided to use high temperature CO₂ (1193 K) as the fluidization gas for the rest of simulation cases.

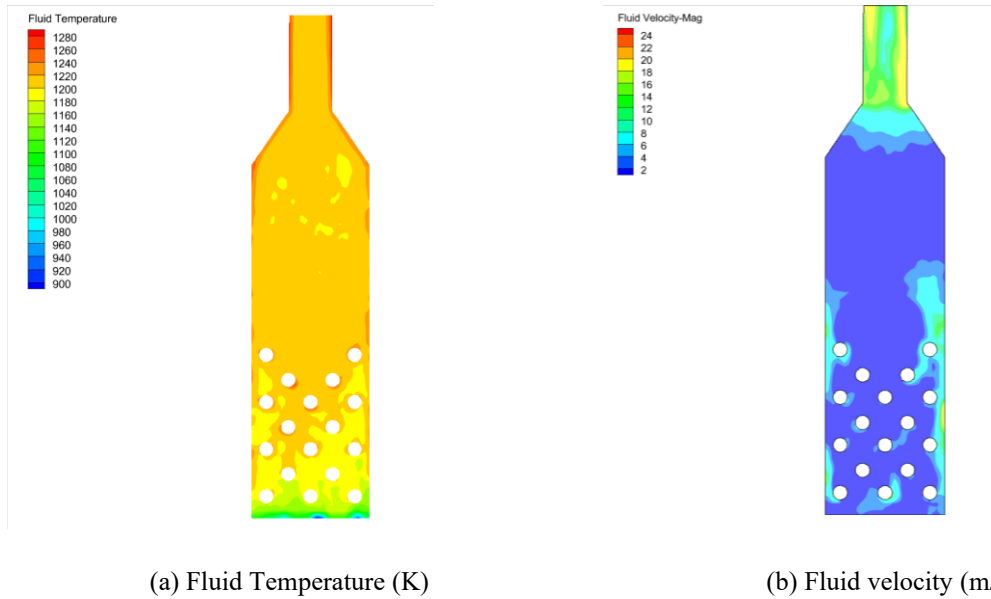


Figure 5-5: Fluid condition after 25 seconds in case 3. (a) Temperature, (b) Velocity

5.3 The effect of raw meal spreading on the reactor performance

Afterwards, cases 4,5 and 6 are simulated including the raw meal injection and the calcination reaction. As mentioned in Table 4-1, in these cases all the conditions are kept the same and the only difference is the way of raw meal injection. The injection points and the raw meal particles spreading inside the reactor are shown in Figure 5-6 and Figure 5-7.

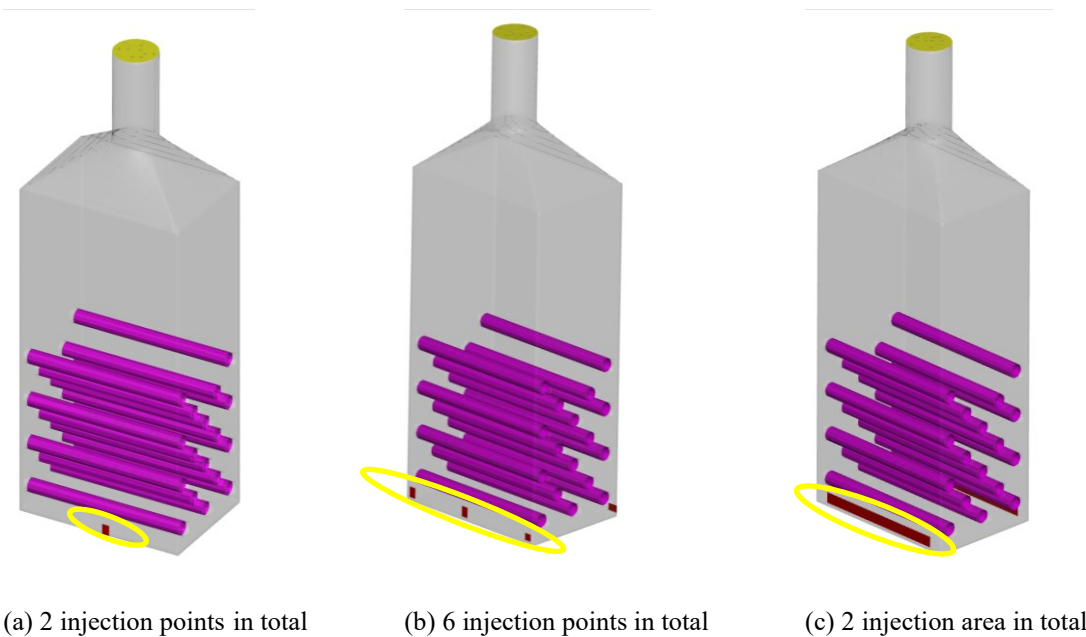


Figure 5-6: Injection types (a) 2 point injections, (b) 6 point injections, (c) 2 rectangular narrow area injections

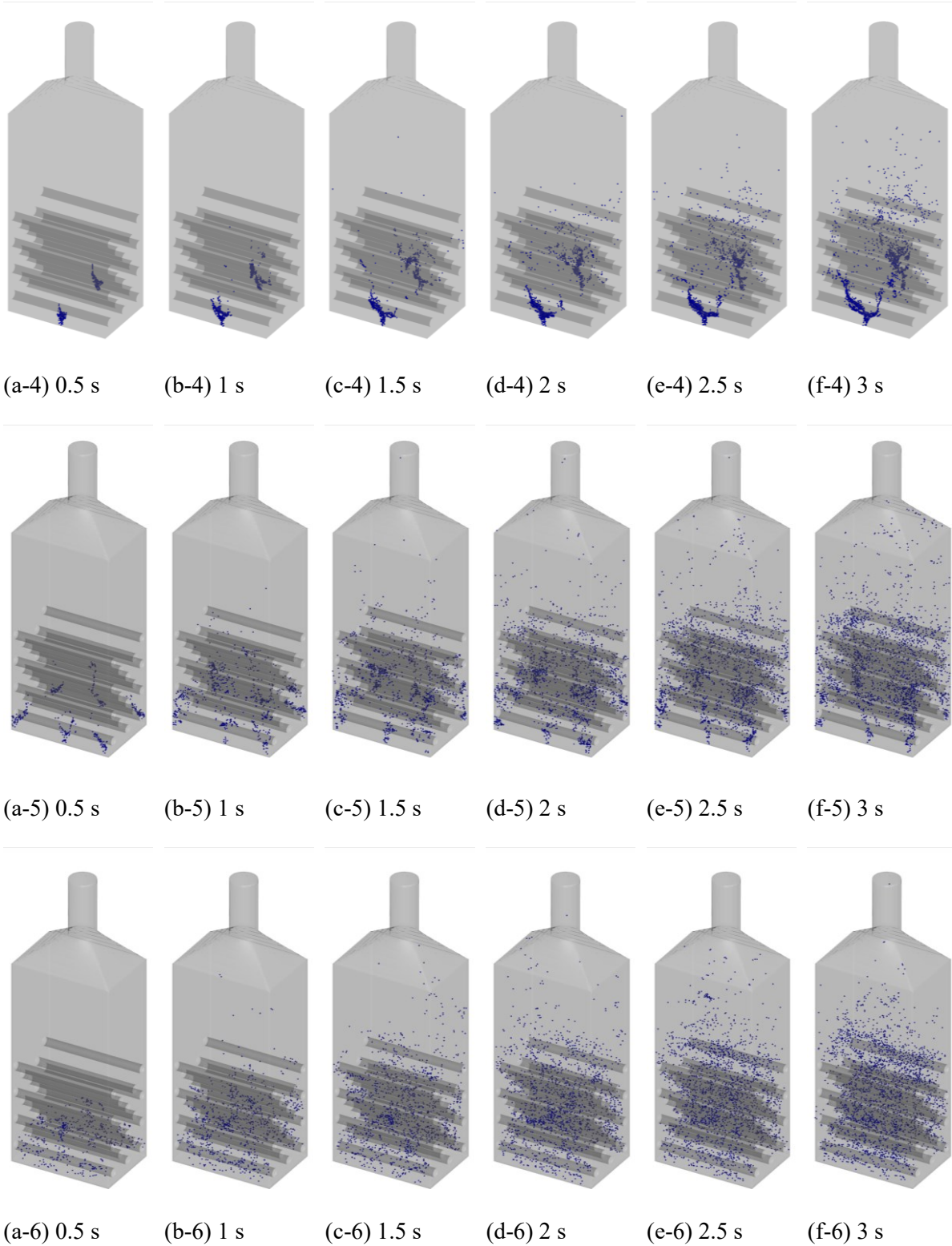


Figure 5-7: Particle spreading in 3 seconds for three different injection types (Case 4: 2 injection points, Case 5: 6 injection points and Case 6: 2 rectangular narrow area injections)

In Figure 5-8 the unreacted limestone distribution in the bed after 45 seconds is compared between cases 4 and 5. In case 4, having only one injection point on each side of the reactor (2 points in total) cannot spread the particles enough over the electrically heated cylinders, while this spreading is improved in case 5 with increasing the number of injection points (Figure 5-7). In case 4 there is unreacted raw meal accumulation above the hot cylinders area. This accumulation is significantly reduced in case 5 which has improved meal spreading and preheated meal conditions. Having lots of unreacted calcites in the free space above the cylinders shows a poor reaction in case 4 operating condition. The unreacted calcite in case 5 is decreased with having higher CO_2 production which happened because of better spreading of the meal over the heat source, namely the cylinders, improved mixing conditions and using preheated meal.

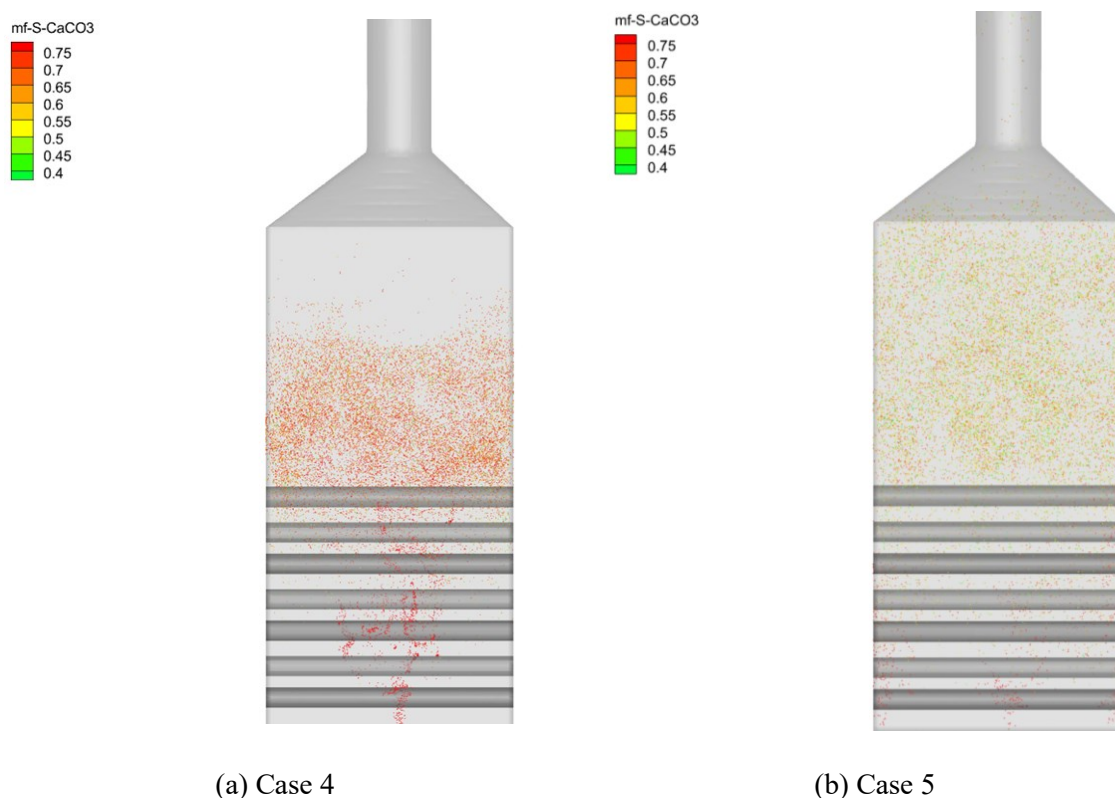


Figure 5-8: CaCO_3 distribution in the reactor after 45 seconds. (a) Case 4, (b) Case 5.

Supporting the idea mentioned above about the reaction, Figure 5-9 shows the produced CaO in the reactor in both cases. Significantly less CaO seems to be produced in case 4 in comparison with case 5. It is also accumulated and not having preferred entertainment. This accumulation has happened due to poor reaction and not producing enough CO_2 which is needed for entrainment of calcined particles.

To support the idea about CO_2 production, the graph in Figure 5-10 shows the total gas mass flow rate exiting the reactor. The inlet gas mass flow rate for the fluidization is known for each case (0.038 kg/s). So, subtracting the injected gas from the outlet gas mass flow rate shows the

CO₂ production. The produced CO₂ divided by the desired CO₂ production based on design calculations (0.016 kg/s), can be used as a calculation of the calcination degree.

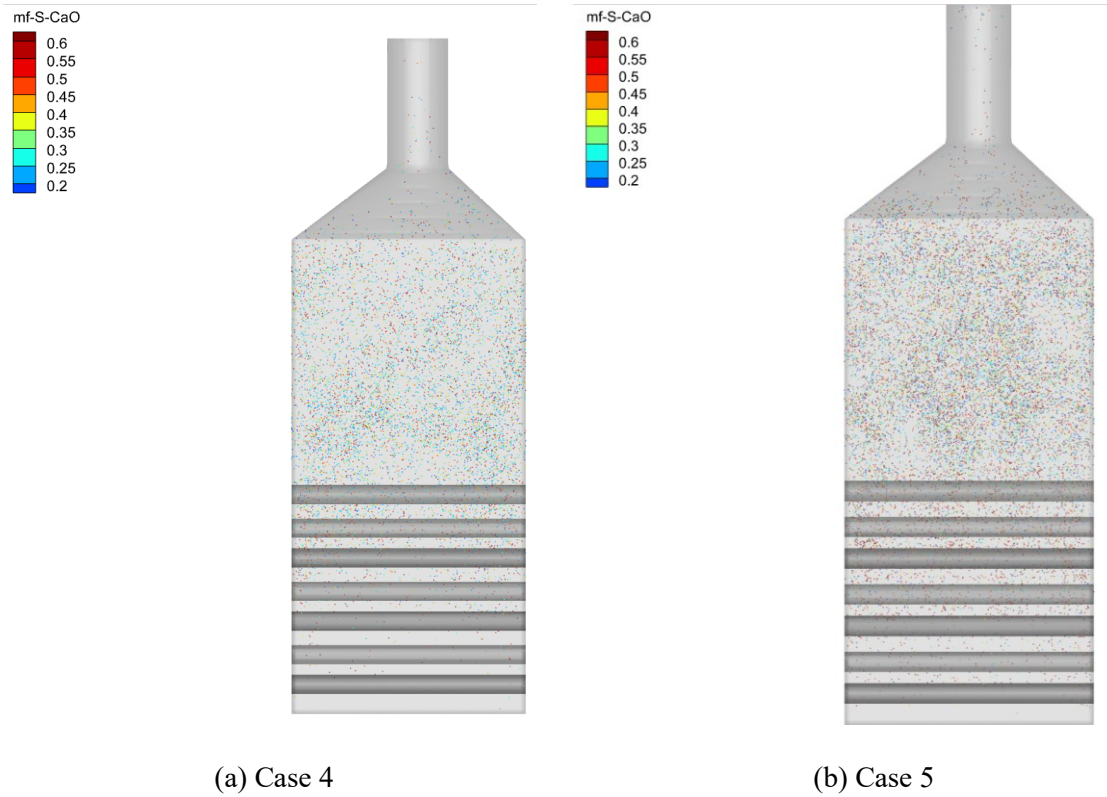


Figure 5-9: Produced CaO in the reactor after 45 seconds. (a) Case 4, (b) Case 5.

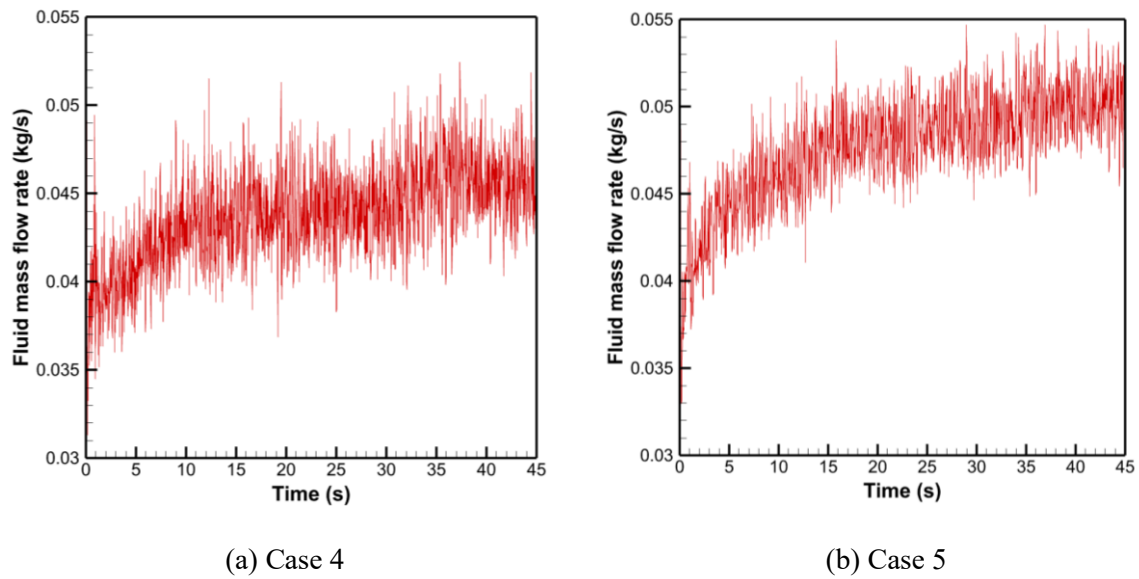


Figure 5-10: Total CO₂ gas entraining the reactor. (a) Case 4, (b) Case 5.

The calculated calcination degree for case 4 is only 43% while in case 5 with increasing the number of injection points and preheating the meal 69% calcination degree is reached. Although the reached calcination degree had a significant increase, there are some limitations in the more improvement of this case practically. The meal is preheated up to 850°C which is close to the calcination temperature and consuming energy for more preheating of the meal doesn't make sense. Apart from that, the number of injection points is 6 in this case which is not easily applicable in the lab. So, increasing the number of injections also doesn't seem a good idea in the real world. The idea for making an improvement in the calcination degree with the same operating condition was to have bigger injection areas. So, as shown in Figure 5-6 (c) there is one rectangular injection area in each side of the reactor (totally in two sides). This idea makes raw meal best spreading over the hot cylinders and mixing in the bed.

Before starting any comparison of case 6 with the previous cases, the good mixing in this fluidized bed reactor is shown in Figure 5-11. Ensuring the good mixing condition is essential for a good reactor performance. Noting that this can also be seen from Figure 5-7 third row which shows the spreading of raw meal inside the reactor during time. Figure 5-11 shows the bed before injection of fluidization CO_2 and then after starting, it shows every 15 seconds the mixing condition. It is obvious that the CO_2 is produced after 15th and before 30th second as the bed is more expanded and particles start to entrain. Moreover, it can be seen that from 30th to 45th second there is no significant change in the mixing condition which seems a sign of reaching pseudo steady condition.

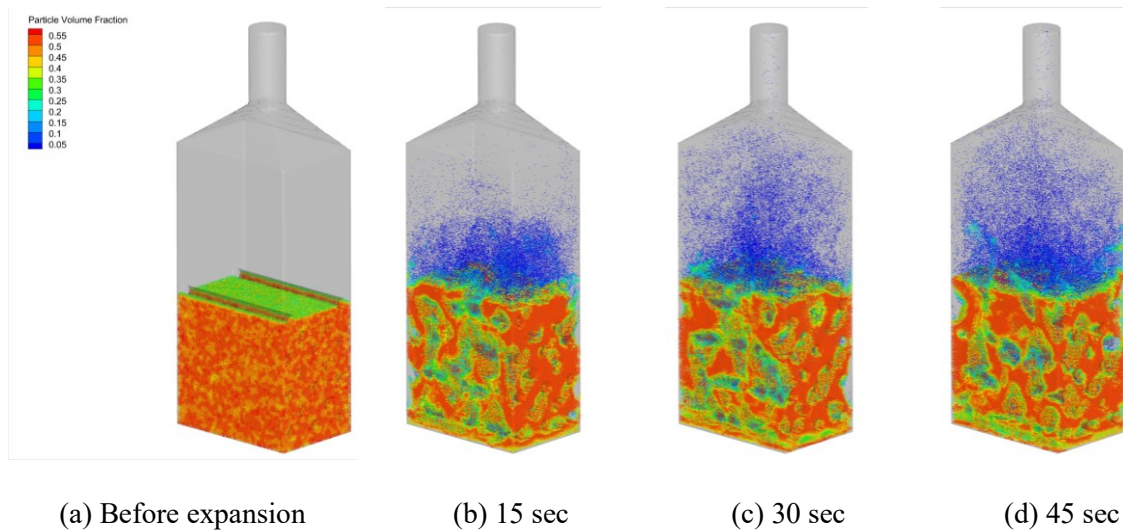


Figure 5-11: Mixing condition in the reactor (a) before expansion (b) after 15 s (c) after 30 s, (d) after 45 s.

Comparing the two cases, case 5 (six point injections) and case 6 (two rectangular injection areas), in terms of having unreacted raw meal after 45 seconds is shown in Figure 5-12. This figure shows more accumulated unreacted CaCO_3 in the case with point injection. This shows the reaction rate is improved in case 6, due to better spreading the meal.

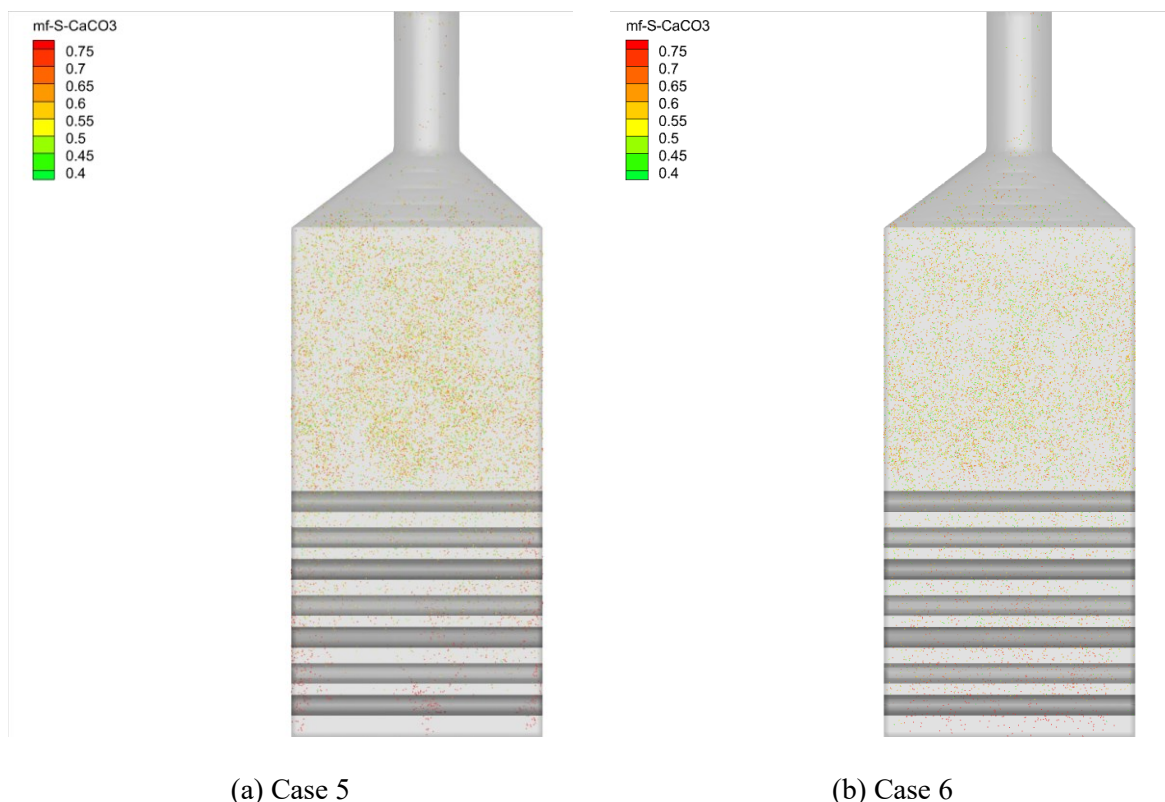


Figure 5-12: CaCO_3 distribution in the reactor after 45 seconds. (a) Case 5, (b) Case 6.

Supporting this idea, the reaction products CO_2 and CaO are shown in Figure 5-13 a and b. Figure 5-13 (a) shows the total CO_2 entraining the reactor in terms of mass flow rate. This amount includes both injected and produced CO_2 . Subtracting the injected gas (0.038 kg/s) from the total CO_2 shows the produced gas due to reaction. This value is almost 0.81 of the desired CO_2 based on the design calculation. So, using this injection type, increased the calcination degree from 69% to 81%, which is a nice improvement. Also, Figure 5-13 shows the distribution of CaO in the reactor after 45 seconds. This is obvious that the CaO is well distributed and there is no high accumulation in any specific area.

Figure 5-14 shows the time integrated particle mass entrained the reactor. This graph shows that the fine calcined particles are well entrained while only a little amount of coarse particle escapes the reactor which shows a good reactor performance.

The final result from this set of simulations (cases 4-6) shows the importance of spreading the raw meal particles to use as much as heat transfer area possible. This will significantly improve the reached calcination degree in the reactor. Also, the results showed that the reactor works preferably in not letting the coarse particles escape and entraining the fine calcinated particles. However, I believe that there is always a way for improvement!

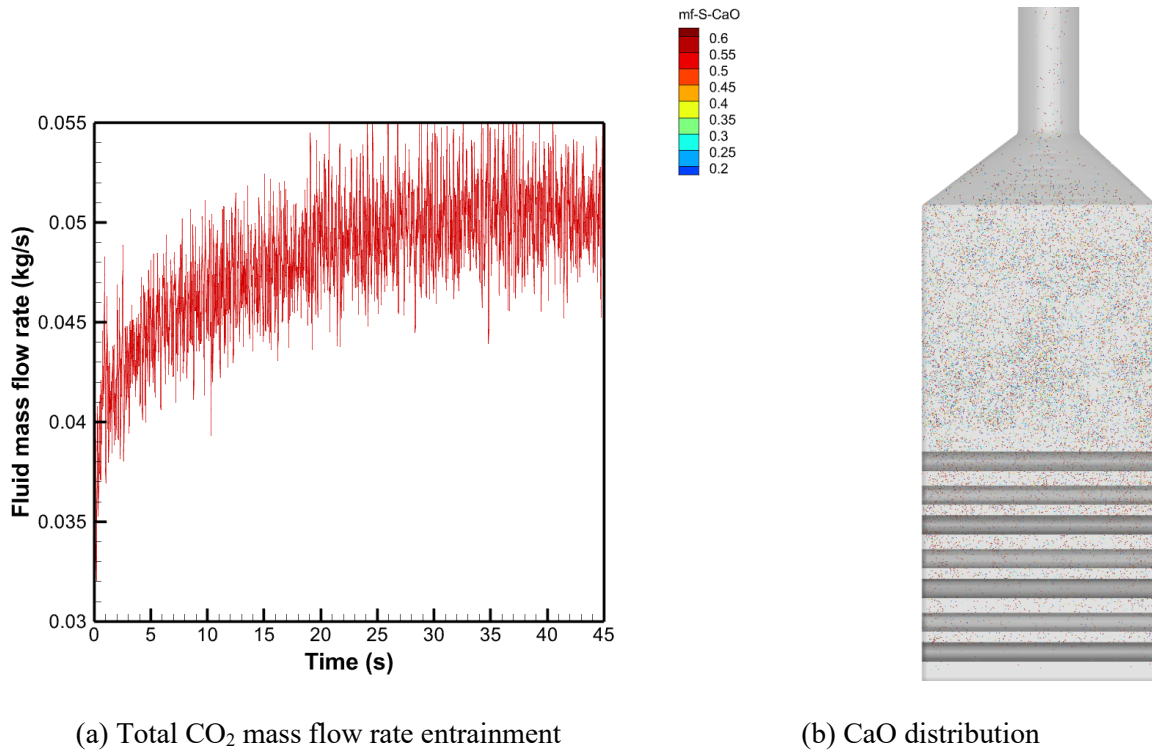


Figure 5-13: Reaction products after 45 seconds in case 6 (a) CO₂ entrainment, (b) CaO distribution in the bed.

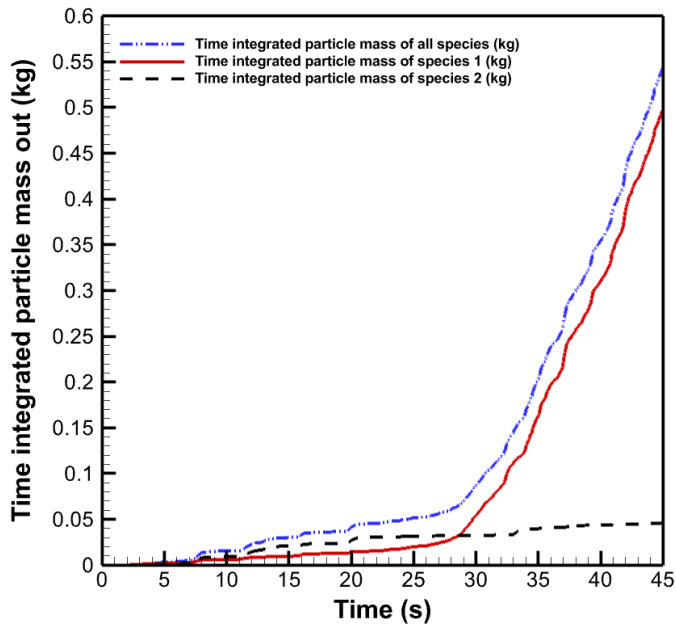


Figure 5-14: Time integrated particle entrainment in case 6. Species 1: Fine particles, Species 2: Coarse particles.

5.4 The effect of temperature on the reactor performance

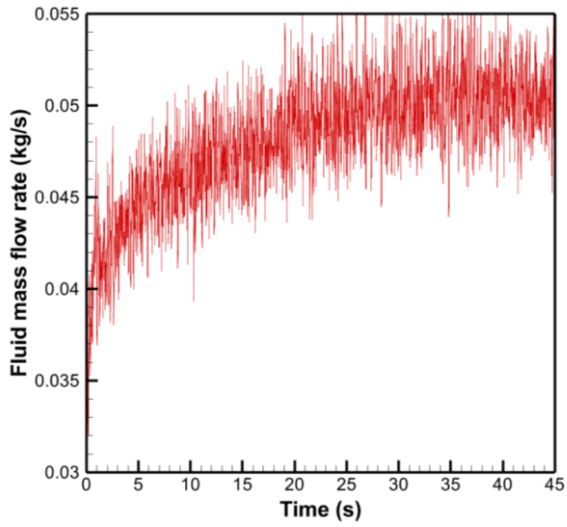
In this section the effect of preheating the raw meal and or changing the temperature of hot cylinders on the reactor performance is investigated.

5.4.1 The effect of increasing the temperature of hot cylinders on the reactor performance

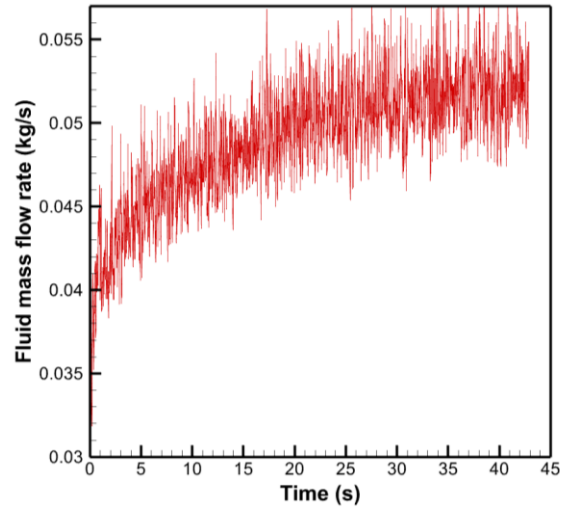
In the previous section, case 6 with preheated raw meal (850°C) and 1050°C of hot cylinder temperature was investigated. But, what if the temperature of hot cylinders increased to 1100°C? This makes the simulation of case 7. In case 7 the mixing is good just like condition shown for case 6. The meal is well spread over the hot cylinders in the bed and most of the designed heat transfer area is being used. Increasing the temperature of hot cylinders provides more energy for the particles to reach the calcination temperature and to be calcined. So, more CO₂ production is also expected. Figure 5-15 shows the total CO₂ exiting the reactor. Using this data and indicating that 0.038 kg/s gas was injected into the reactor as the fluidization gas, this reactor produces 90% of the desired CO₂ in case 7. In other words, the calcination degree in this reactor is almost 90% while with the same operation conditions and having a 50°C lower temperature of hot cylinders 81% calcination degree was reached.

The particle temperature in case (6) and (7) is compared in Figure 5-16. As shown in Figure 5-16, at the start of operation the temperature of particles is higher in case (7) due to having 50°C hotter cylinders. The calcination temperature seems to be almost 1170 K as in both cases after reaching steady conditions, the temperature reaches the same value (1170 K).

The raw meal particles residence time is shown in Figure 5-17. The vertical axis shows the percentage of the raw meal particles that are entraining the reactor. The coarse particles, or the raw meal particles recently injected that are not entrained yet are not included in this calculation. As shown in Figure 5-17, the mean particle residence time in case 7 is slightly lower than case 6 which is reasonable due to having slightly higher gas produced in the reactor. The figure shows that the weighted average residence time of the fine particles is 25.8 in case 6 and 24.5 in case 7.

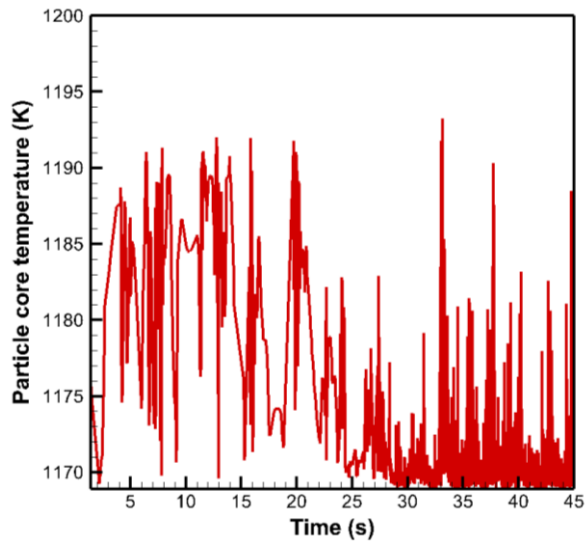


(a) Case 6

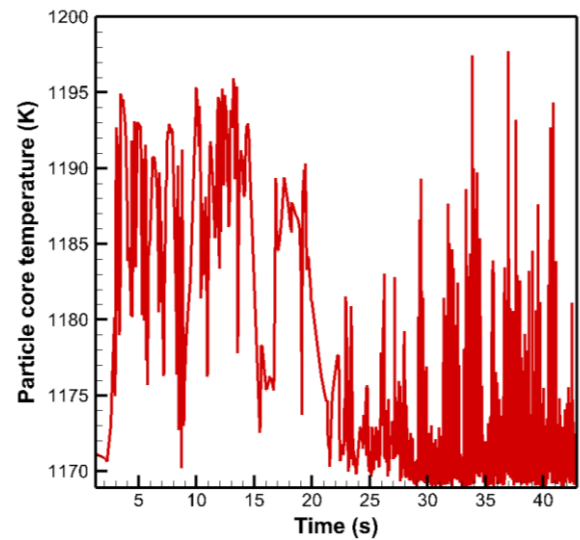


(b) Case 7

Figure 5-15: Total CO₂ mass flow rate exiting the reactor (a) Case 6 and (b) Case 7.



(a) Case 6



(b) Case 7

Figure 5-16: Particle temperature at the exit of reactor (a) Case 6, (b) Case 7.

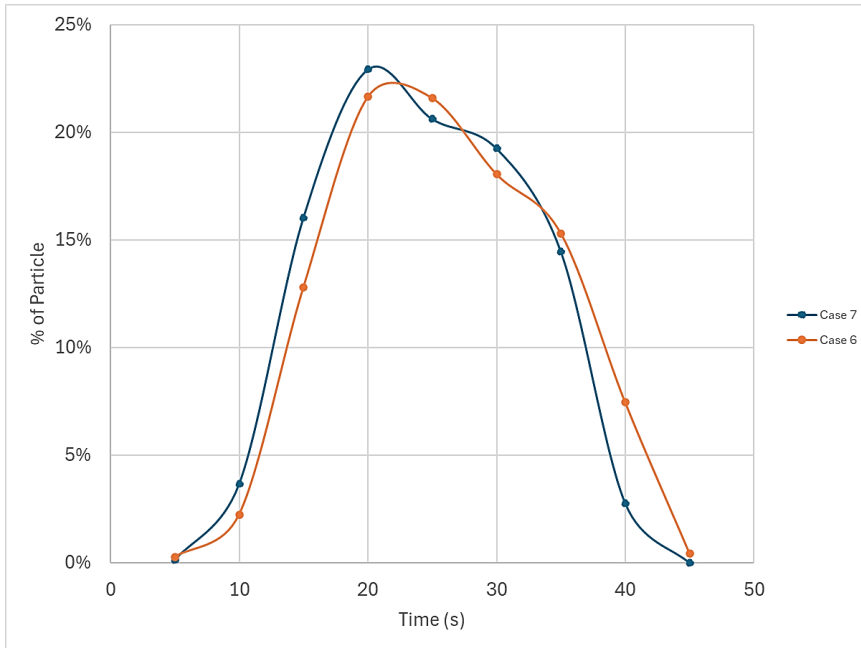


Figure 5-17: Particle residence time distribution in Cases 6 and 7.

Also, Figure 5-18 shows the time integrated particle mass exiting the reactor. The results show that the particle mass entrained in this case is slightly higher than case 6 (Figure 5-14). And in case 7 almost 47 gr of coarse particle escaped the bed in 43 seconds which is still not a very significant value.

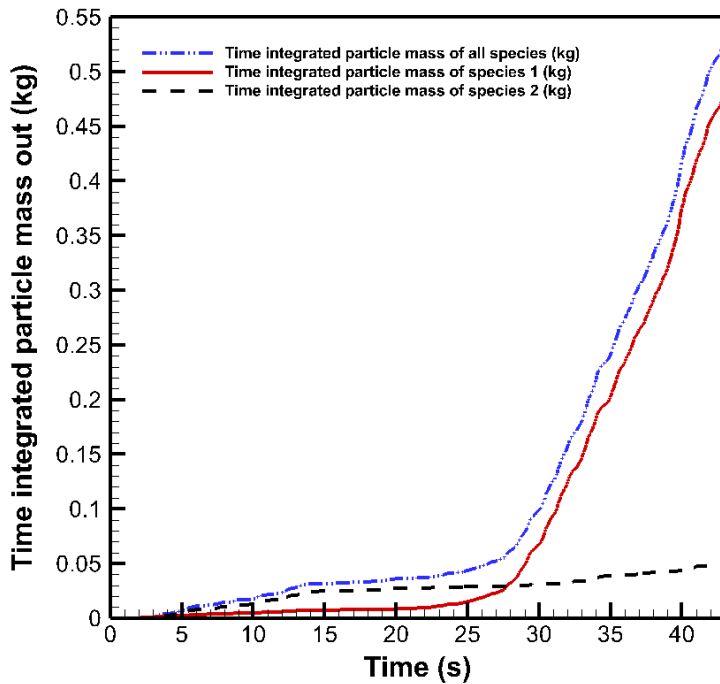


Figure 5-18: Time integrated particle entrainment in case 7. Species 1: Fine particles, Species 2: Coarse particles.

The comparison between these two cases with 50°C temperature difference in the hot cylinders' temperature shows the importance of this temperature. Having a higher temperature not only leads to higher calcination degree but also reaches steady state a bit faster. Having said that, in practice, a proper material should be selected for the hot cylinders which have high durability in very high temperatures in the order of discussed values as well as high corrosion resistance. Because the hot cylinders in this reactor are in contact with many particles all the operating period.

5.4.2 The effect of the raw meal temperature on the reactor performance

Another investigation can be made for the effect of raw meal temperature on the reactor performance. Taking case 6 with preheated meal as a reference, it can be checked what if the raw meal was not preheated?! This operating condition is investigated in case 8 with a cold (20°C) raw meal injection.

Starting with investigation of the CO₂ gas produced in the reactor, Figure 5-19 should be considered. This figure shows the total CO₂ gas exiting the reactor which includes the fluidization gas as well. However, the fluidization gas was kept the same for both cases. So, the graphs in Figure 5-19 can show the significant reduction in the gas production in the reactor. Calculating the calcination degree shows that not preheating the meal reduced the calcination degree from 81% to less than 44% which is a very significant deduction. This reduction can be explained by the heat transfer. Same amount of heat was available in both cases (hot cylinders with 1050°C) but in case 8, a larger amount of energy was required for heating up the meal.

In Figure 5-20, the average temperature of particles exiting the reactor during the time of operating the reactor (0 - 45 s) is shown. It is obvious that after some time the temperature decreased to 1170K and remained almost the same which can be assumed as the calcination temperature in the simulation.

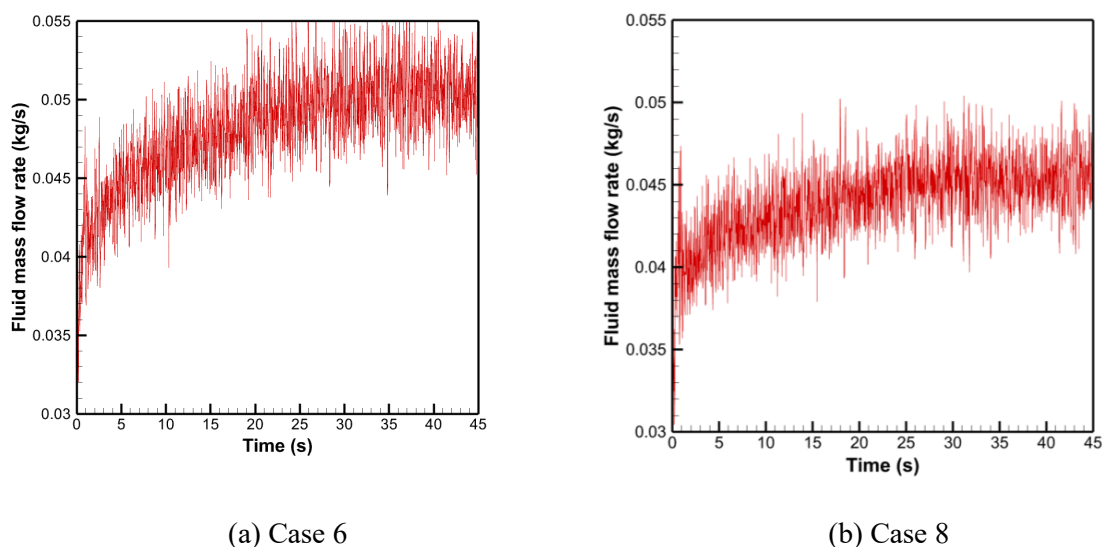
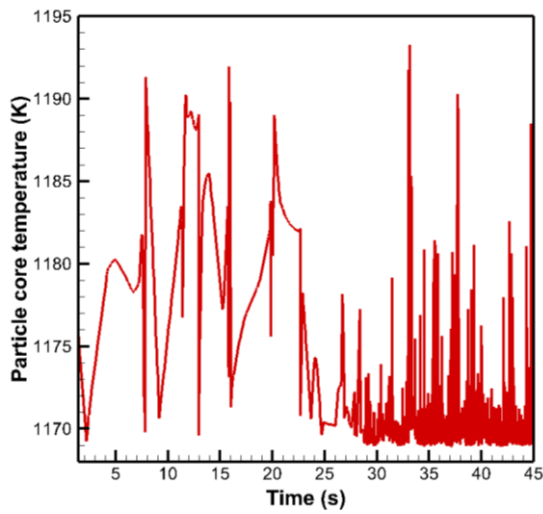
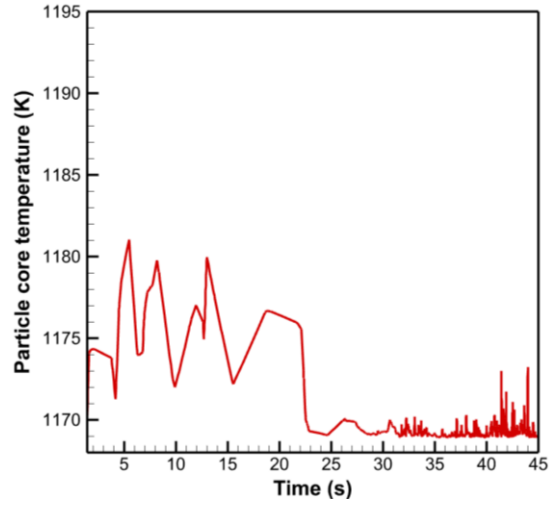


Figure 5-19: CO₂ mass flow rate exiting the reactor during time (a) Case 6, (b) Case 8.



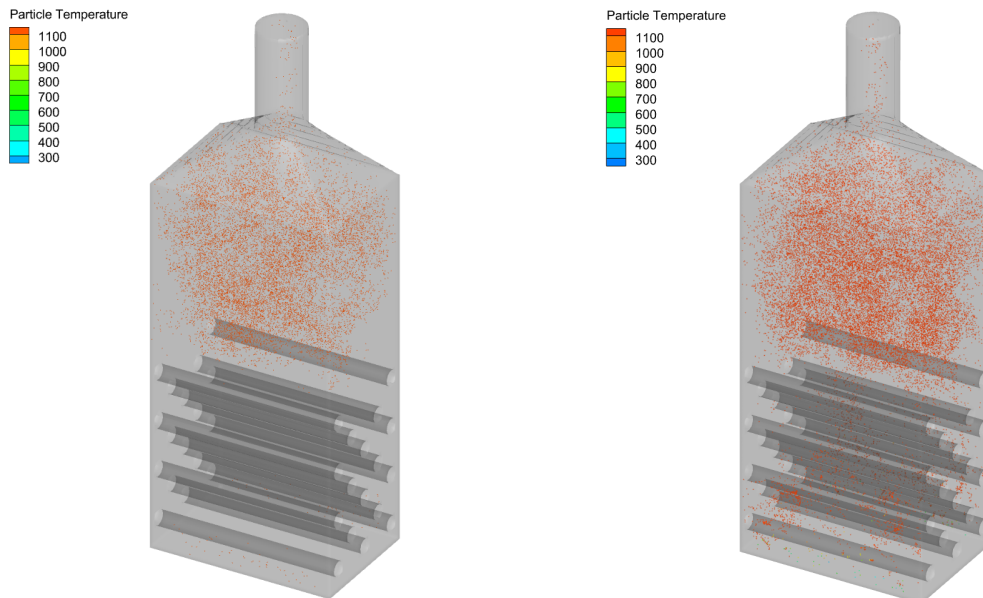
(a)Case 6



(b)Case 8

Figure 5-20: Particle temperature entraining the reactor during time (a) Case 6, (b) Case 8.

Assuming almost 1170K (897°C) as the calcination temperature, Figure 5-21 shows the particles with temperature lower than 1170K in a specific time frame (45th second of operation). This is obvious that the number of particles that haven't reached the calcination temperature in case 8 is many more. This can also describe the reduction in the calcination degree from 81% in case 6 with preheated meal to 44% in case 8 with the cold injection of meal.



(a)Case 6

(b)Case 8

Figure 5-21: Particles with less than 1171K temperature in the 45th second. (a) Case 6, (b) Case 8.

Also, the time integrated particle entrainment is shown in Figure 5-22. This figure shows that the entertainment of particles is significantly decreased in comparison with case 6. And this is completely reasonable due to the low calcination degree. Having this low calcination means that only 0.44 of the desired CO₂ is produced. And it is obvious that in this fluidized bed reactor gas is responsible for entraining the calcined particle. So, lower calcination degree due to lower temperature of raw meal leads to significantly lower entrainment. This operating condition (case 8) is not recommended.

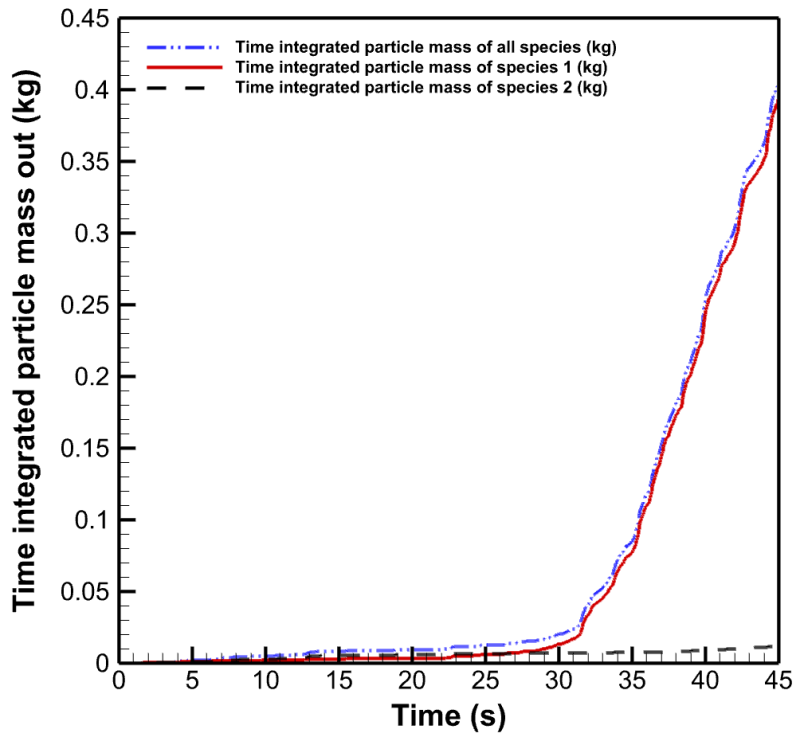


Figure 5-22: Time integrated particle entrainment in case 8. Species 1: Fine particles, Species 2: Coarse particles.

5.4.3 The effect of increasing hot cylinders' temperature on the calcination of cold injected raw meal

Investigating cases 6 and 8 showed the important effect of preheating the meal before injection. However, the previous comparison made with cases 6 and 7 showed that increasing the hot cylinders' temperature can have a positive effect on the calcination degree which is somehow the main goal. So, in case 9 the meal is stayed cold (not preheated, at 20°C) but the temperature of hot cylinders is increased to 1150°C.

As shown in Figure 5-23, the amount of CO₂ exiting the reactor has increased significantly. As the amount of fluidization gas in both cases was the same (0.038 kg/s), this increase shows an increase in the CO₂ production in the reactor. Calculating the calcination degree shows that increasing the hot cylinders' temperature from 1050°C to 1150°C and keeping all the other operating conditions the same, the calcination degree increases from 44% to 69%.

Based on Figure 5-24, the calcination temperature could be 1170K for both cases. At the early seconds, the temperature of particles exiting the reactor is almost 10°C higher in case 9 which has 100°C hotter cylinders in comparison with case 8. Then after almost 27seconds in both cases the temperature resonates around 1170 K (or 897°C) which can be assumed as the calcination temperature.

The particles with temperature lower than the calcination temperature in a specific time frame is shown in Figure 5-25. From Figure 5-25, it is obvious that the number of particles that in the 45th second of operation did not reach the calcination temperature (1170 K) yet, is decreased in case 9. This is what were expected to see. Also, Figure 5-26 shows the good mixing condition in both cases.

After calcination degree investigation for case 9, the particle entrainment is another important factor to be checked. As in case 9 more gas has been produced, the entrainment of particles should be more than case 8. Figure 5-27 shows the time integrated particle entrainment for both fine and coarse particles. The amount of entrained coarse particles in case 9 after 45 seconds is 0.018 kg, which was 0.012 kg in case 8. This shows an increase, but is it in an acceptable range?

For case 9, taking a more detailed look into the numbers, and assuming that the reactor reached steady condition in 27th second, the time integrated mass of coarse particles escaping the reactor increased from 0.007 kg to 0.018 kg between 27th and 45th seconds. This shows that after the reactor reached steady condition, in each second 0.6 gr of coarse particles might be escaped. The initial mass of coarse particles in the bed can be calculated:

$$m_{p,coarse} = \rho_{p,coarse}(V_{bed} - N_{cylinder}V_{cylinder})\alpha = 1512 \frac{kg}{m^3} \times (0.61m \times 0.286 - 17 \times \pi \times \left(\frac{0.055}{2}\right)^2 \times 0.65) m^2 \times 0.55 = 123.26 kg$$

Thus, after reaching the steady state condition 0.00048 % of coarse particle mass might escape in each second which seems acceptable.

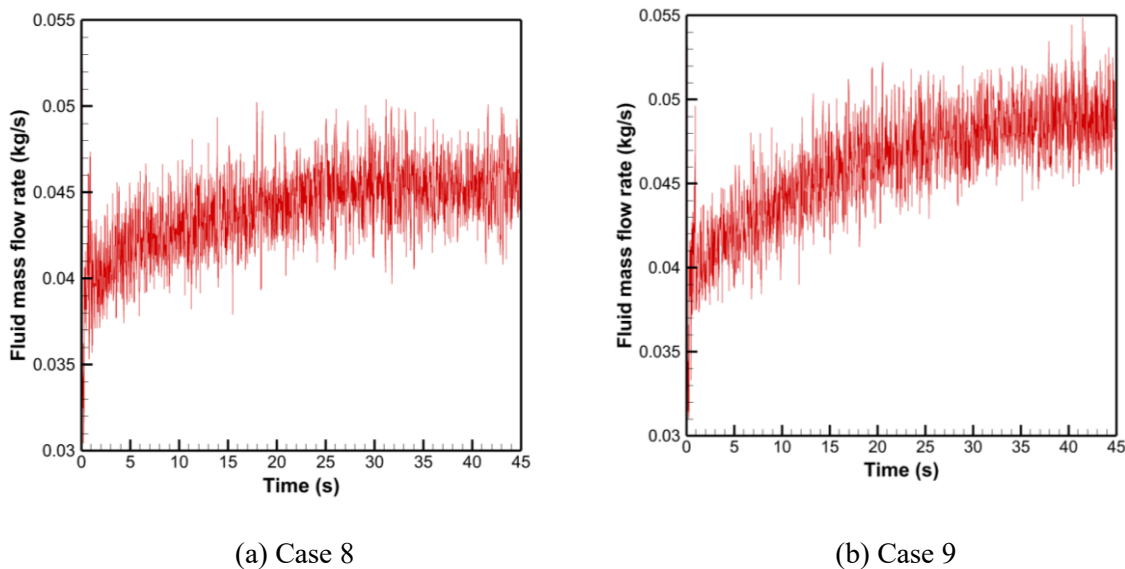


Figure 5-23: CO₂ mass flow rate exiting the reactor during time (a) Case 8, (b) Case 9.

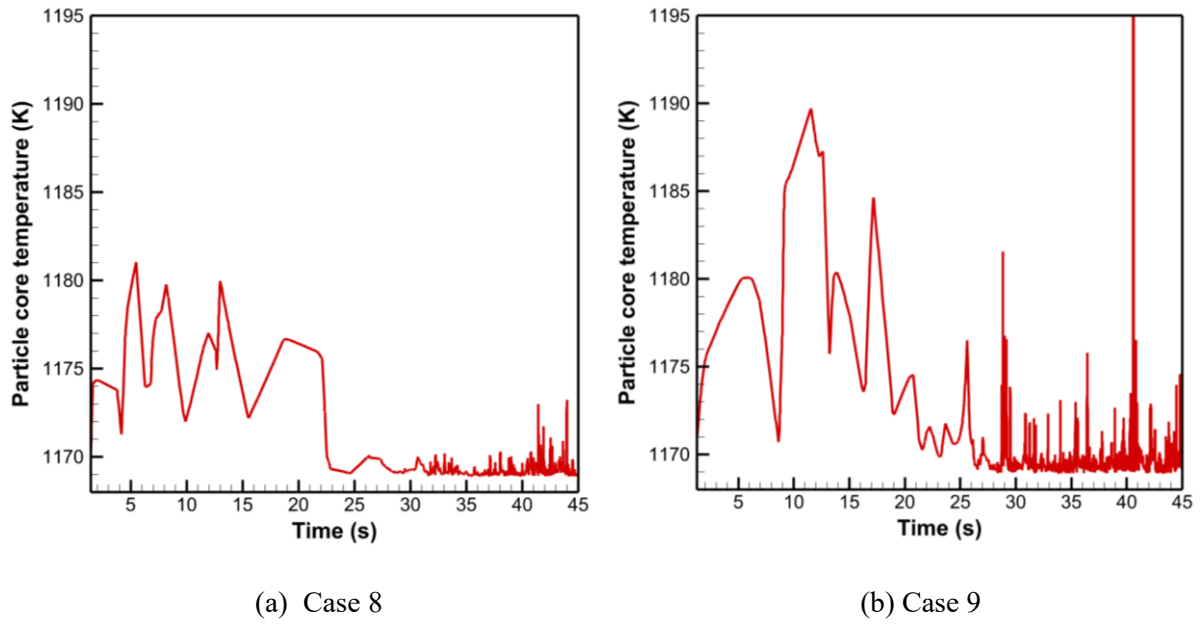


Figure 5-24: Entrained particle temperature (a) Case 8, (b) Case 9.

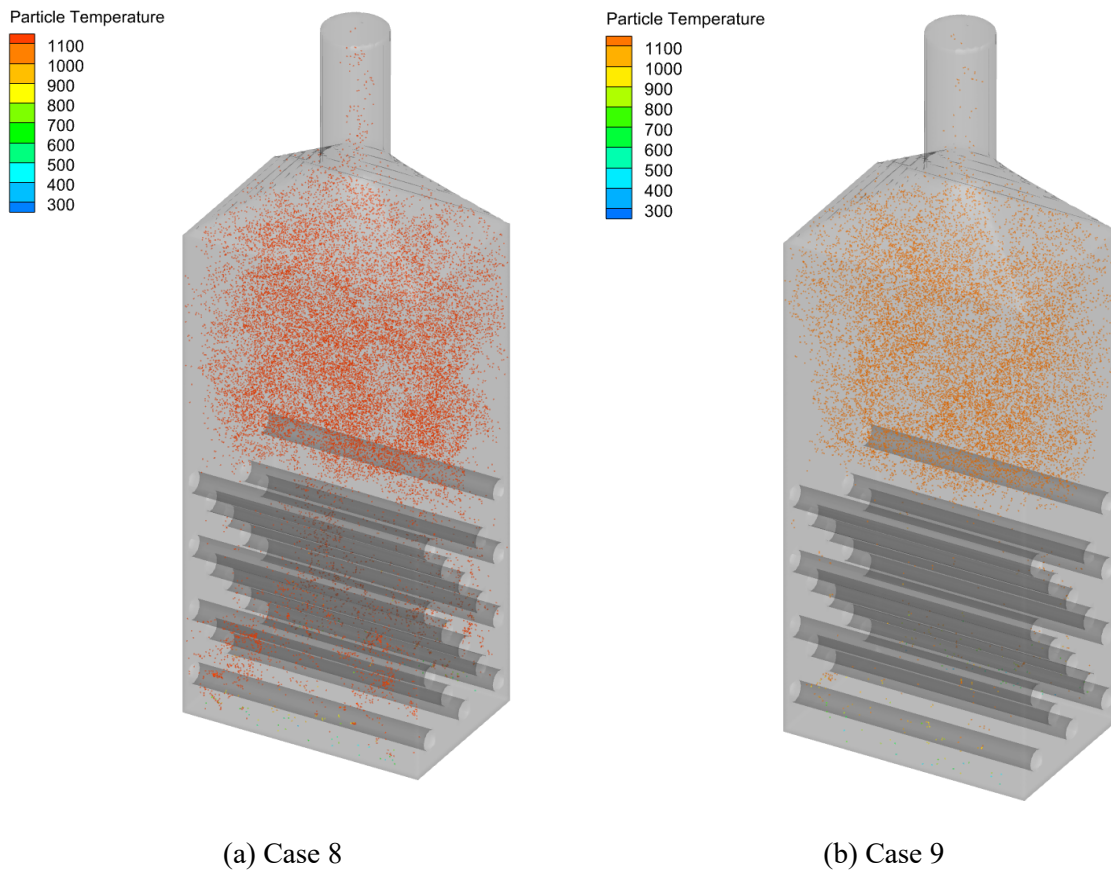


Figure 5-25: Particles with less than 1171K temperature in the 45th second. (a) Case 8, (b) Case 9.

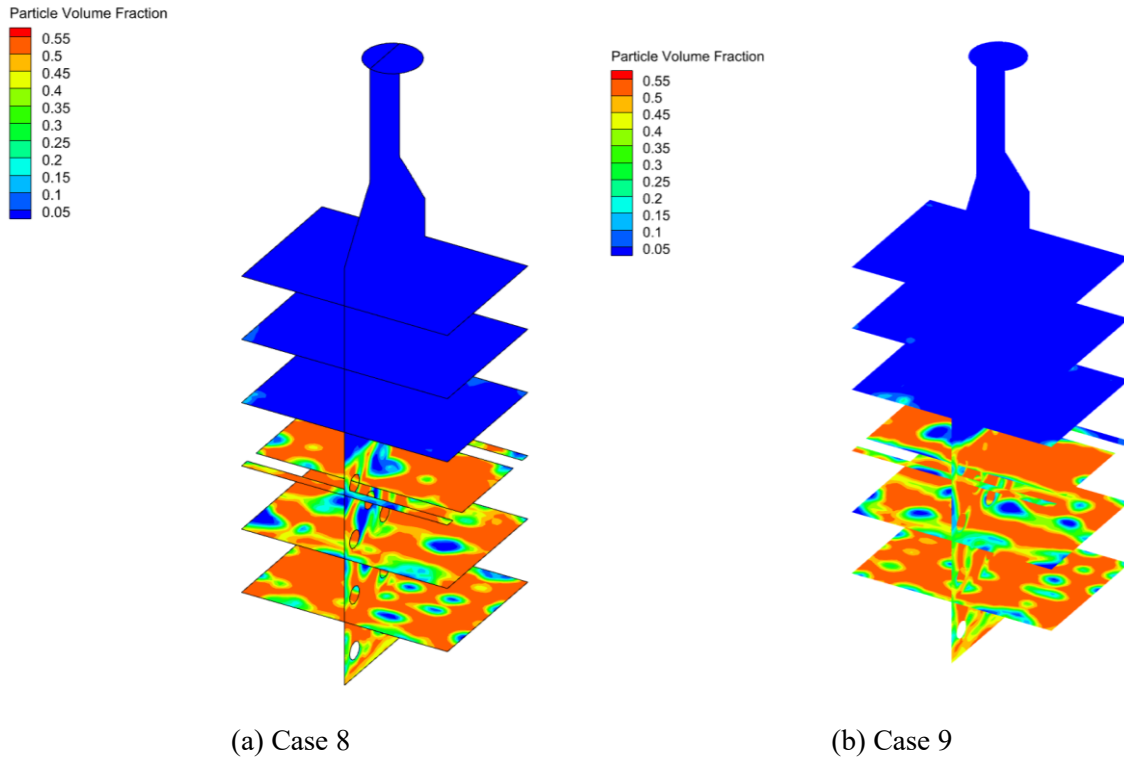


Figure 5-26: Particles volume fraction in the 45th second. (a) Case 8, (b) Case 9.

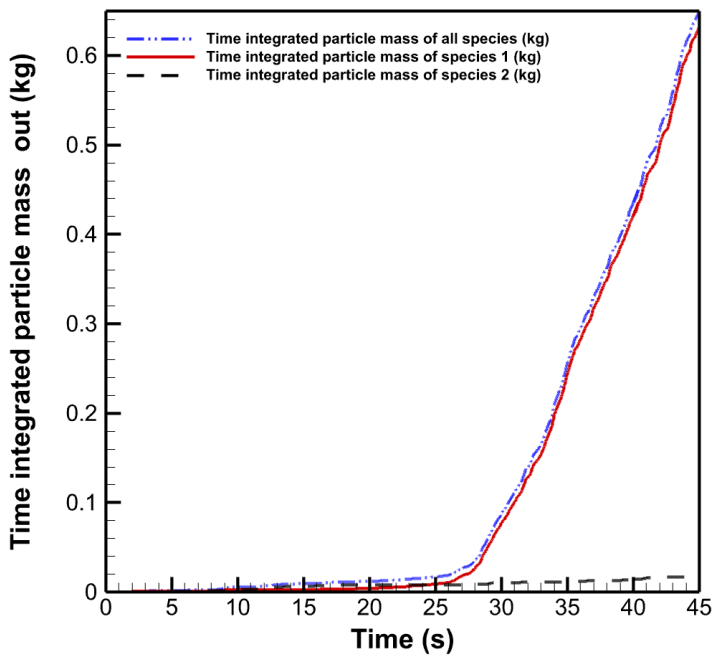


Figure 5-27: Time integrated particle entrainment in case 9. Species 1: fine particles, Species 2: Coarse particles.

Also, the simulation results show that in case 9 with cold meal conditions and the hottest cylinder temperature, the weighted average residence time after reaching the pseudo steady condition is 25.7 seconds. Figure 5-28 shows that more than 60% of the particles have residence time between 20-30 seconds.

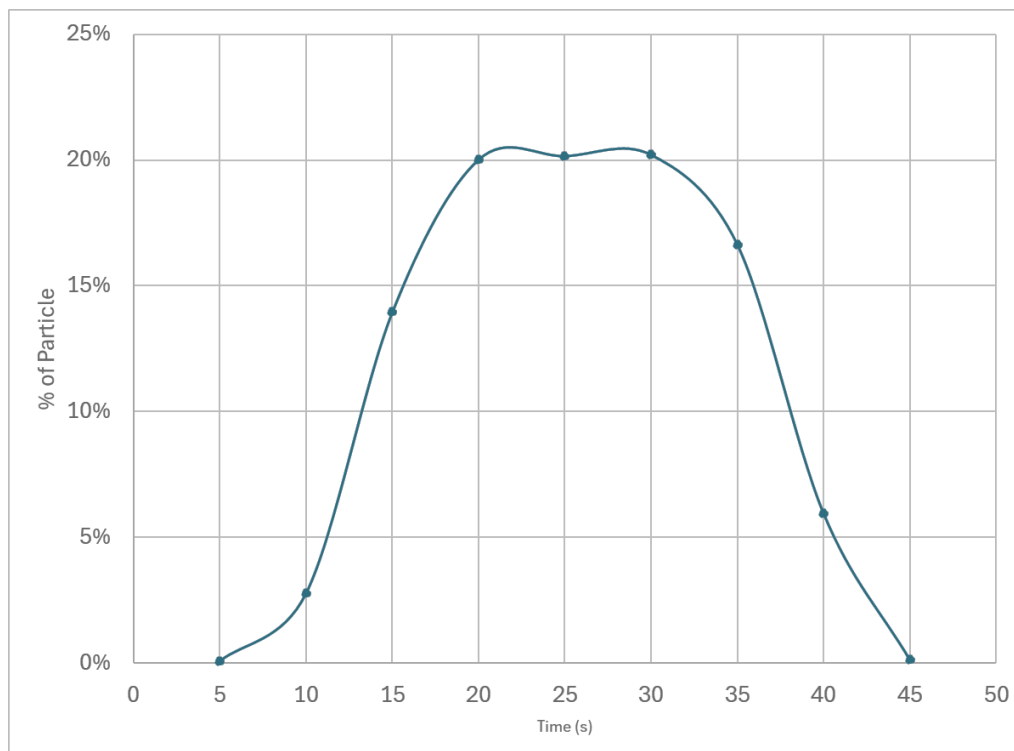


Figure 5-28: Residence time of raw meal particles entrained the reactor in case 9.

Simulation of case 9 showed that with having cold raw meal but increasing the wall temperature of hot cylinders to 1150°C almost 70% calcination degree is reachable. So, if it was not possible to preheat the meal before injection, it seems reasonable to increase the hot cylinders temperature in the bed. Having said that, simulation 7 operating conditions (using preheated meal with 850°C and hot cylinders with wall temperature of 1100°C) revealed that almost 90% calcination degree is reachable.

The drawback of these cases, 7 and 9, is that in practice usually the meal is not as hot as 850°C and not as cold as 20°C! Case 10 is simulated to stay in between those operating conditions and show a more practical result.

5.4.4 Investigation of the reactor performance in a more practical operating condition

In case 10 the meal is preheated to 720°C and the hot cylinders' temperature is at the hottest value, 1150°C. Let's calculate the calcination degree in this case with more details! Figure 5-29 shows the total mass flow rate of CO₂ exiting the reactor. This includes both injected and produced gas. As shown in Figure 5-29 the gas mass flow rate exiting the reactor is increasing until it reaches a pseudo steady value. This value is 0.0525 kg/s in this case which includes

0.038 kg/s injected CO_2 . So, it seems that after reaching the pseudo steady state 0.0145 kg/s gas is produced in the reactor. Based on the design calculations having 0.0470 kg/s raw meal with 0.77 weight fraction of CaCO_3 should produce 0.0160 kg/s of CO_2 ¹. The calcination can be calculated as the produced CO_2 in this operating condition divided by the design value for CO_2 production. Thus, in this operating condition (case 10) the calcination degree 90% is reachable which is almost similar to what has been reached in case 7 with a more preheated injected meal but less wall temperature of the hot cylinders. This shows that there should be a balance between preheating the meal and the temperature of hot cylinders. Why is that? This is because the more preheated the meal, the less energy is consumed for reaching the calcination temperature and most of the energy is used to provide required energy for the calcination reaction. On the other hand, the hotter the wall temperature of the hot cylinders, the more energy is provided to the reactor for both heat up the meal to calcination temperature and the calcination reaction.

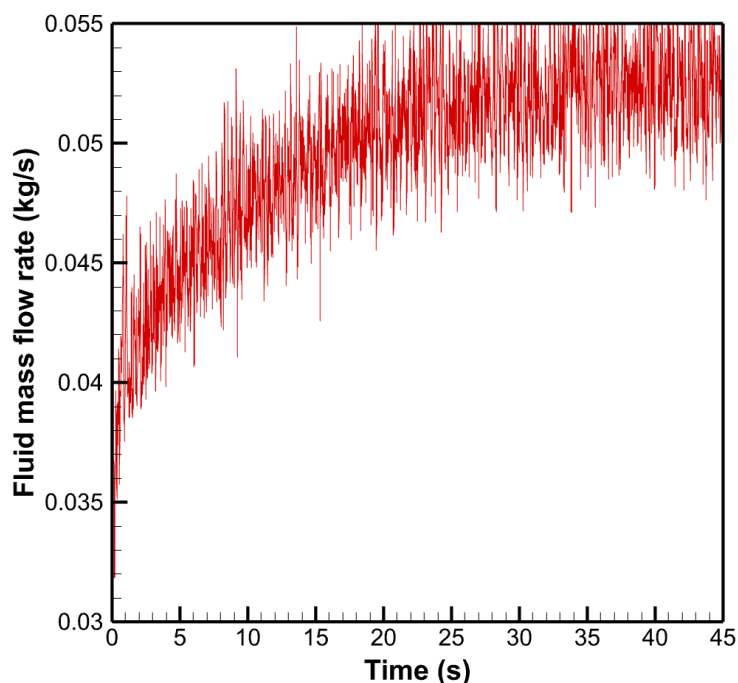


Figure 5-29: CO_2 mass flow rate exiting the reactor during time in case 10.

Having higher calcination degree means higher amount of gas is produced in the reactor and thus the particle entrainment is affected. Figure 5-30 shows the time integrated mass of particles entraining the reactor. Starting with the coarse particles, in 45 seconds of operating in this condition (case 10) almost 0.048kg of coarse particles escaped the reactor. Calculating from the time reactor reached steady condition (around 23rd second in this case) with a linear assumption, 0.0012 kg/s or 1.2 gr/s of coarse particles may escape the reactor. Based on the previous calculation, we assume that almost 123.26 kg of particles were present in the bed initially, so 0.001% mass of coarse particle can escape the bed in each second. In another point

¹ More details can be found in the mass balance calculation in chapter 3.

of view, the time integrated particle mass of all types exiting the reactor is 0.628 kg in which 0.579 kg are fine particles. So, 92% weight of the entrained particles are fine particles.

Another factor that can be investigated is the velocity of entraining the particles. Figure 5-31 shows the vertical velocity of particles entraining the reactor. As shown in this figure, the entrainment velocity is less in the early seconds of operation. It increases as the CO₂ is being produced due to calcination reaction and after almost 23rd second when the reactor reached steady the entrainment velocity keeps the 3.8 m/s (resonates around this). This value shall be less than the settling velocity of smallest coarse particles to have an acceptable condition.

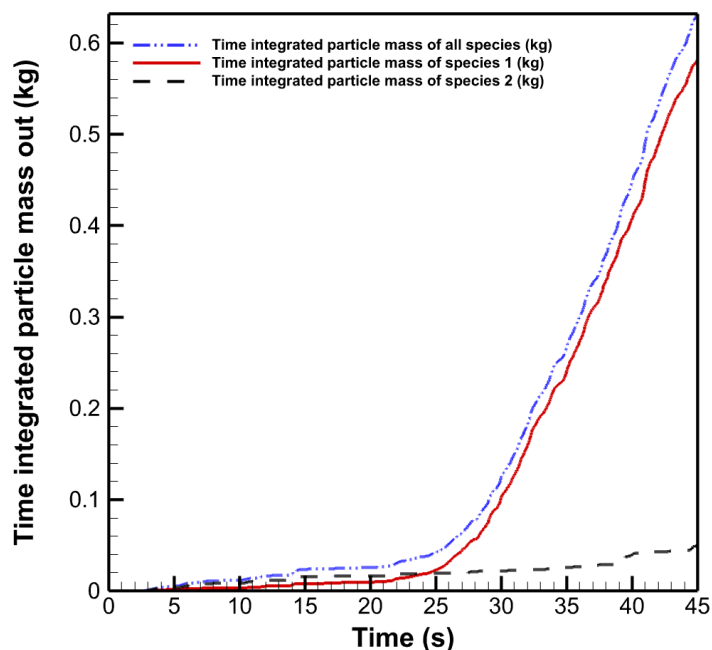


Figure 5-30: Time integrated particle entrainment in case 10. Species 1: fine particles, Species 2: Coarse particles

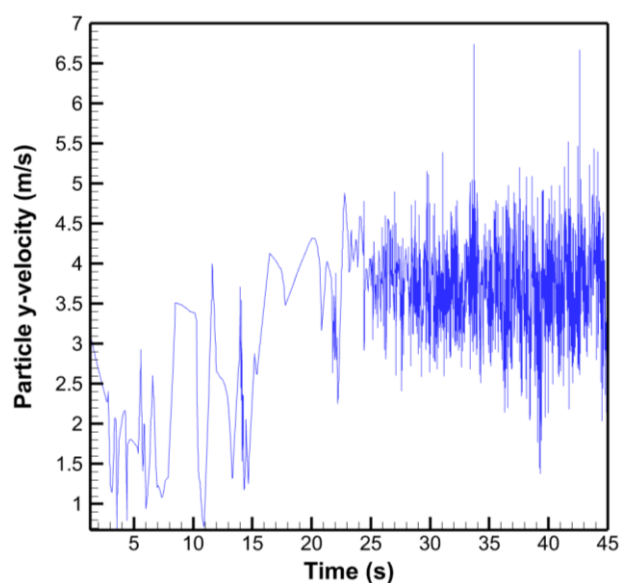


Figure 5-31: The vertical velocity of particles entraining the reactor (case 10).

After investigating the particle conditions, the fluid condition in the reactor is also of great importance. Figure 5-32 shows the fluid velocity and temperature distribution inside the reactor. In this figure, the vertical slice is exactly in the middle of the reactor and the horizontal slices are taken each 0.2 m from the bottom to the transition piece and then at the outlet of the reactor. Results are shown for the 45th second of the operation in the case 10 condition which is having 0.3 m/s fluidization velocity, 1150°C (or 1423 K) hot cylinder temperature and 720°C (or 923 K) raw meal temperature. As shown in Figure 5-32 the fluid velocity shows an increase near the walls in some slices (located at the top of the hot cylinders). This means that the cylinders arrangement and the distance to the wall could be reconsidered. The fluid temperature shows higher values near the cylinders which seems reasonable, but this also shows that a part of hot fluid is quickly moved near the walls which could have done better heat transfer if the cylinders arrangement was better. However, this case shows an acceptable performance in the reactor.

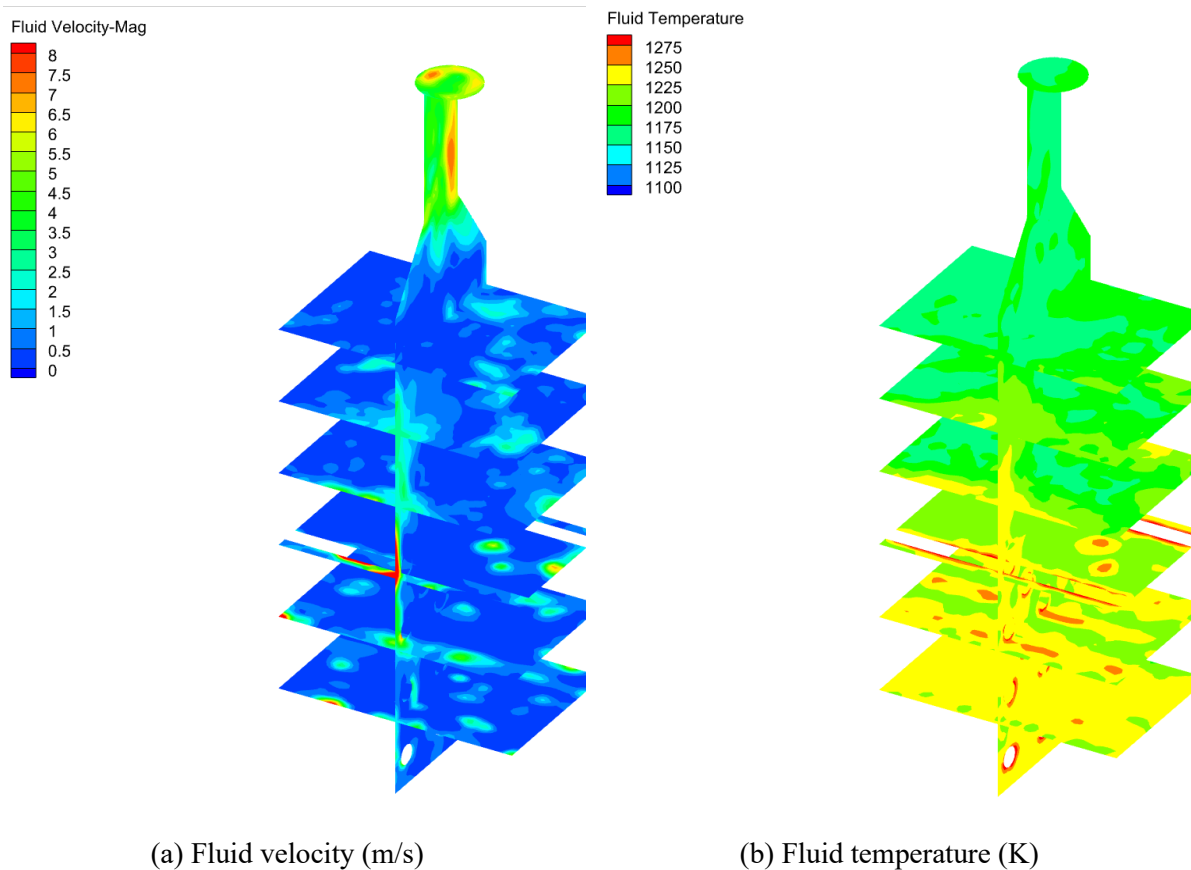


Figure 5-32: Fluid velocity and temperature distribution inside the reactor in case 10 (Vertical slice: middle, Horizontal slices: every 0.2 m)

5.5 The effect of fluidization velocity on the reactor performance

Up to now, the effect of temperature and type (and number) of raw meal injection is investigated. However, the fluidization condition is also of great importance in the fluidized bed reactor performance. To check the fluidization condition, all the operating conditions kept the same and the effect of variation of fluidization velocity is investigated. The reference temperature conditions is 1100°C temperature of hot cylinders, and using preheated raw meal with 850°C. This condition reached almost 90% of calcination degree with 0.3 m/s fluidization velocity. In cases 11-13 the fluidization velocity is changed 0.2 m/s , 0.4 m/s and 0.8 m/s.

Starting with the lowest fluidization velocity 0.2 m/s, Figure 5-33 shows the mass flow rate of CO₂ gas exiting the reactor. This also includes the injected fluidization gas. The injected fluidization gas depends on the fluidization gas velocity and density (which depends on the temperature) and the cross section of the reactor where the gas is injected. In this case the injection velocity is 0.2 m/s which is different from the previous cases. The amount of injected gas in this case is 0.025 kg/s. As shown in the Figure 5-33 the total amount of gas exiting the reactor has reached a pseudo steady state value which is 0.037 kg/s. Thus the rate of production of CO₂ is 0.012 kg/s which leads to a calcination degree of almost 75%.

The previous case with the similar temperature conditions but a higher fluidization velocity 0.3 m/s (case 7) reached a calcination degree of almost 90%. The reason for this reduction could be found in the mixing condition. Due to having lower fluidization velocity the mixing condition is not as good as case 7, this can reduce the heat transfer and reduce the calcination degree as a result. The particle volume fraction for case 7 and 11 are compared in Figure 5-34. It is reminded that all the cases boundary conditions are mentioned in Table 4-1.

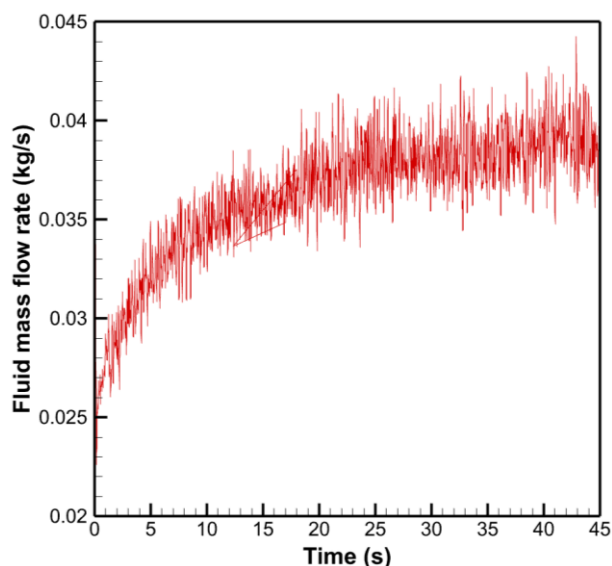


Figure 5-33: CO₂ mass flow rate exiting the reactor during time in case 11.

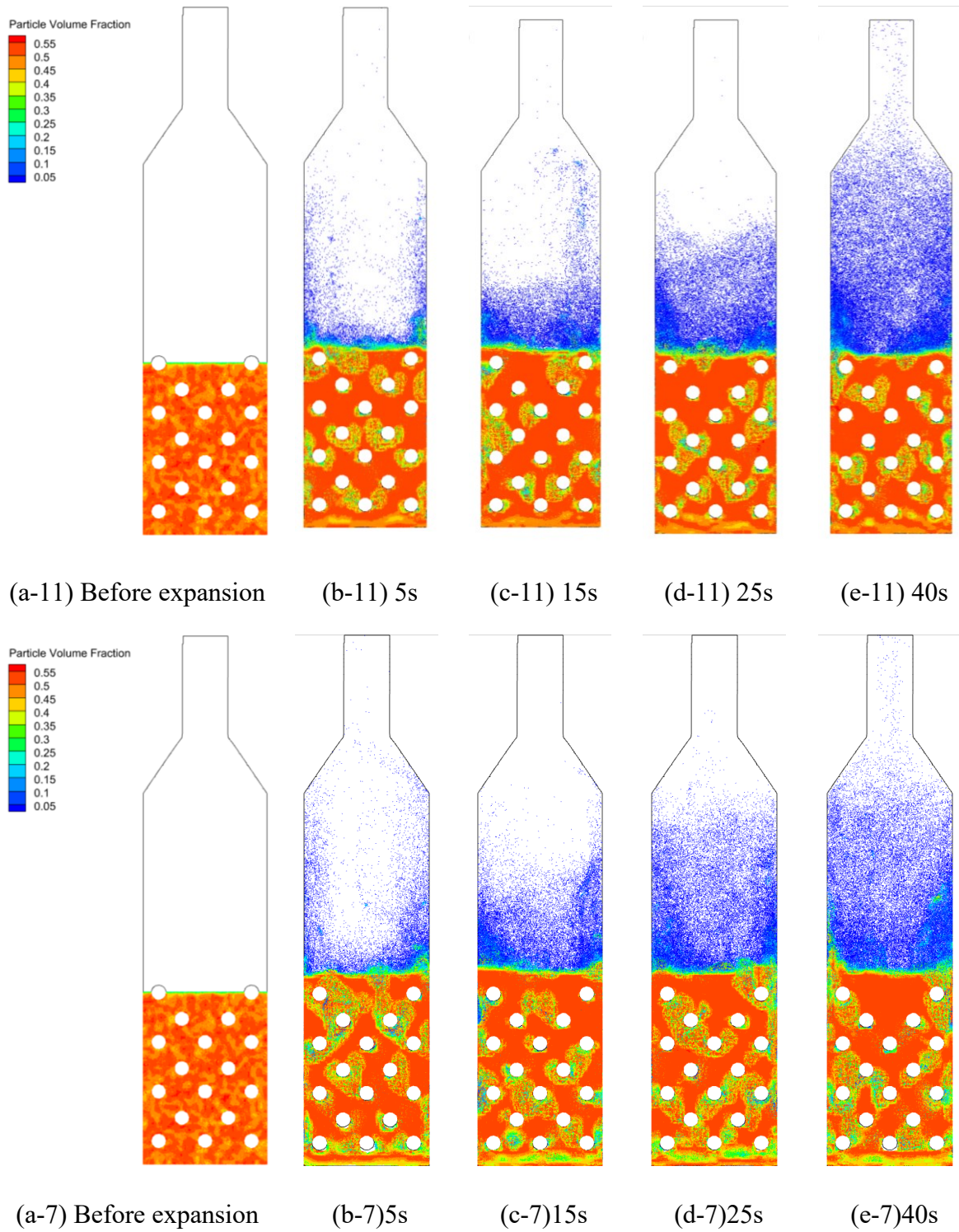


Figure 5-34: Particle volume fraction during time in the middle plane of the reactor. First row, case 11 and second row, case 7.

Figure 5-35 shows the particle entrainment condition for the case 11 with 0.2 m/s fluidization velocity. As shown in this figure, the time integrated particle mass entraining the reactor is too low. The first reason for this, is lower production of CO₂ namely lower calcination degree in comparison to case 7. However, the difference in the calcination degree cannot describe this big difference in the particle mass entrained the reactor. Looking through the Figure 5-35, the time that the reactor reached steady (where the time integrated particle mass entrainment started increasing linearly) happened much later in case 11 in comparison to all other cases. And this is due to lower fluidization velocity. Now comparing the slope of the line from 38th second for all particle entrainment, case 11 shows a 0.02 kg/s entrainment of all particle types while case 7 shows 0.03 kg/s (Figure 5-18, after reaching the linear condition from 28th second). This amount of reduction in the particle entrainment is completely reasonable.

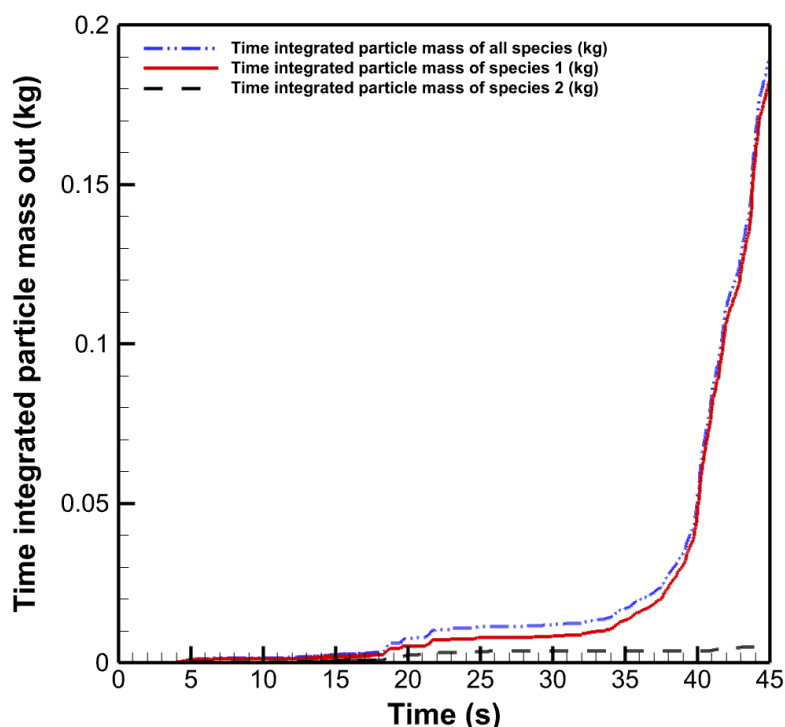


Figure 5-35: Time integrated particle entrainment in case 11. Species 1: Fine particles, Species 2: Coarse particles

Figure 5-36 shows the entrainment velocity of particles in case 11 in comparison with case 7. This shows two main things, firstly, the final steady particle entrainment velocity in case 11 is less than case 7 which shows the effect of fluidization velocity on the entrainment velocity. And secondly, it shows that the pseudo steady condition in case 11 happens much later. This is also due to having lower fluidization velocity, lower mixing efficiency and lower heat transfer effect, and thus reaction speed.

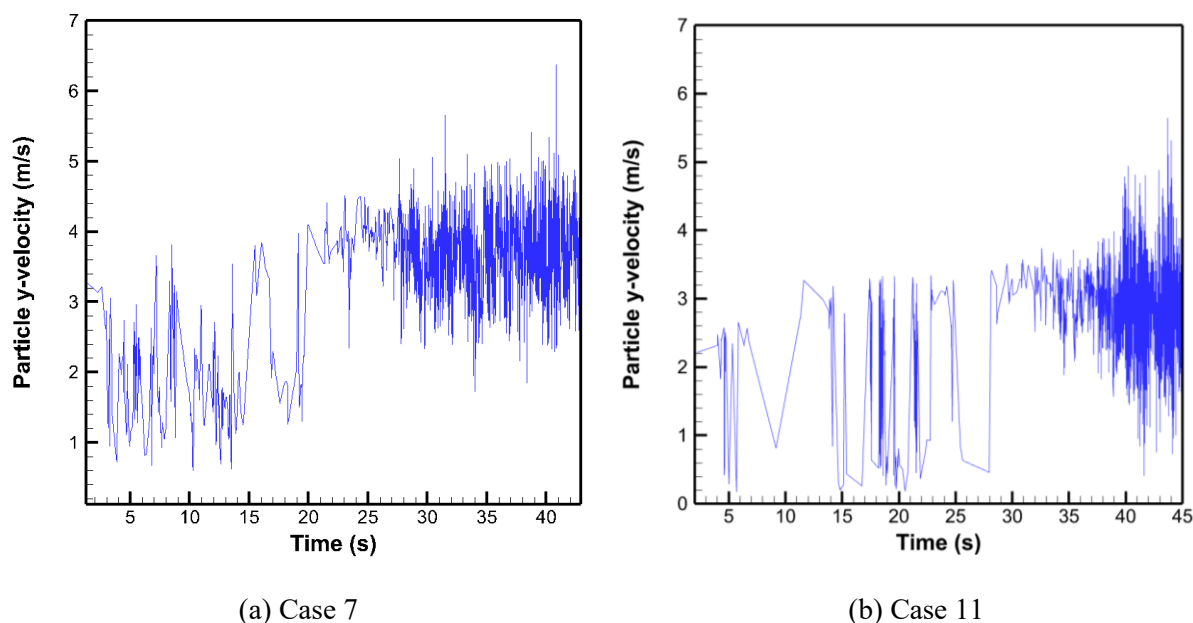


Figure 5-36: Particle entrainment velocity (a) Case 7, (b) Case 11.

Up to now, the fluidization velocity of 0.2 m/s and 0.3 m/s have been investigated, and the results showed the operating condition in case 7 with 0.3 m/s fluidization velocity, was more preferred. In cases 12 and 13 the fluidization velocity is increased to 0.4 m/s and 0.8 m/s to see its effect on the reactor performance.

Figure 5-37 shows the time integrated particle mass entraining the reactor in this operating condition (fluidization velocity 0.4 m/s, preheated meal to 850°C and hot cylinder temperature of 1100°C). As shown in Figure 5-37, the particle entrainment is significantly higher than the case 11. This also means that a higher mass of coarse particles may escape the reactor in this operating condition. The total amount of coarse particles that may escape the reactor in 45 seconds is almost 0.22 kg while it was less than one tenth of this value of case 11! However, as the time of reaching pseudo steady state in these cases is different, it is more reasonable to compare the slope of the linear part of the graph. Starting from the 20th second in case 12, it shows that the total particle mass entrainment in this case is 0.039 kg/s which is almost double of the value calculated for case 11 (0.02 kg/s). This seems reasonable due to the increase in the fluidization velocity. However, due to the high amount of entrainment of the coarse particles this operating condition is not preferred.

Figure 5-38 shows the time integrated particle mass entrainment in case 13 operating condition. This graph shows that from the start of operation the particles are escaping the bed due to a very high injection velocity! This operating condition shall be avoided during the practical tests.

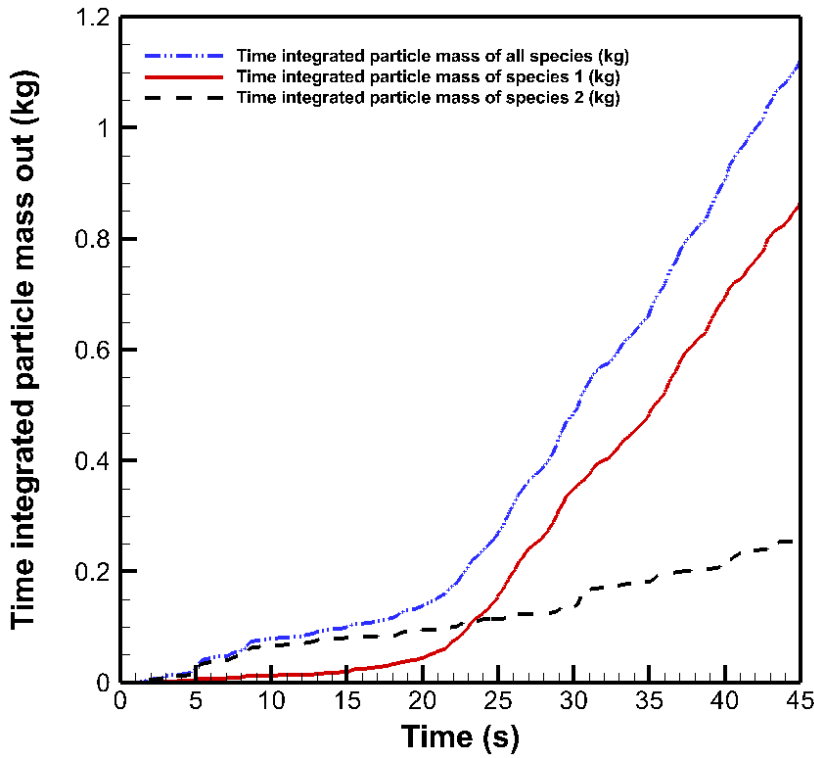


Figure 5-37: Time integrated particle entrainment in case 12. Species 1: Fine particles, Species 2: Coarse particles

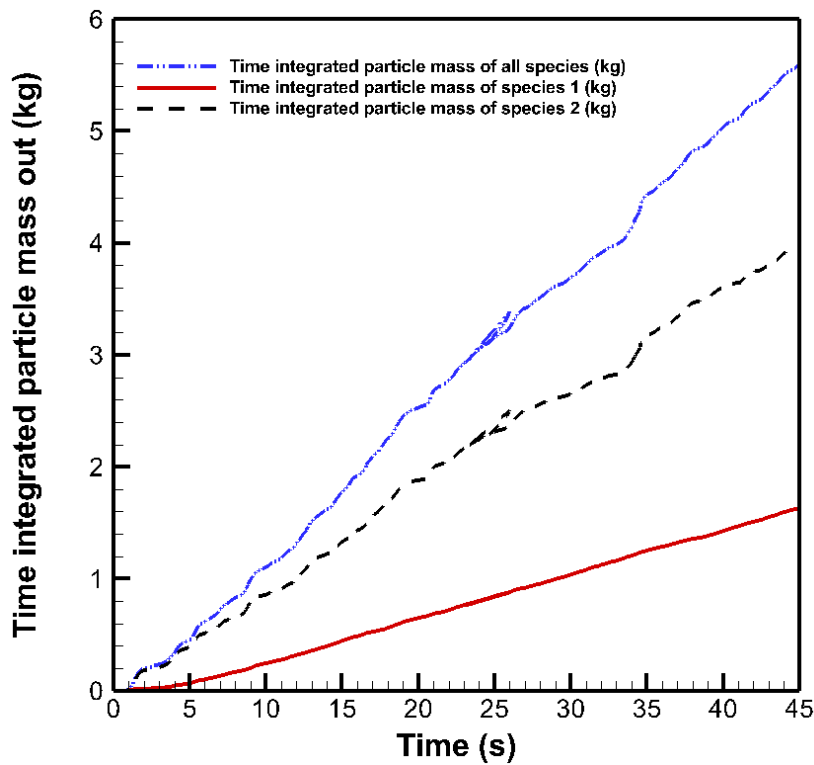


Figure 5-38: Time integrated particle entrainment in case 13. Species 1: Fine particles, Species 2: Coarse particles

The total fluid mass flow rate exiting the reactor in both cases is shown in Figure 5-39. As the amount of injected gas in these cases are different, they should be investigated separately.

In case 12, having 0.4 m/s fluidization velocity the injected gas was 0.051 kg/s. So, the produced gas in the pseudo steady state condition is 0.013 kg/s which leads to almost 81% calcination degree. However, due to having high entrainment of coarse particles they should be charged on a regular basis, if this operating condition is selected for a practical test for any reason.

In case 13, the mass flow rate of injected gas was 0.102 kg/s and the total mass flow rate exiting the reactor reached almost 0.111 kg/s based on Figure 5-39. This means a 0.008 kg/s of CO₂ production and leads to 56% calcination degree. These operating conditions shall be avoided in practice due to having very high particle entrainment and low calcination degree.

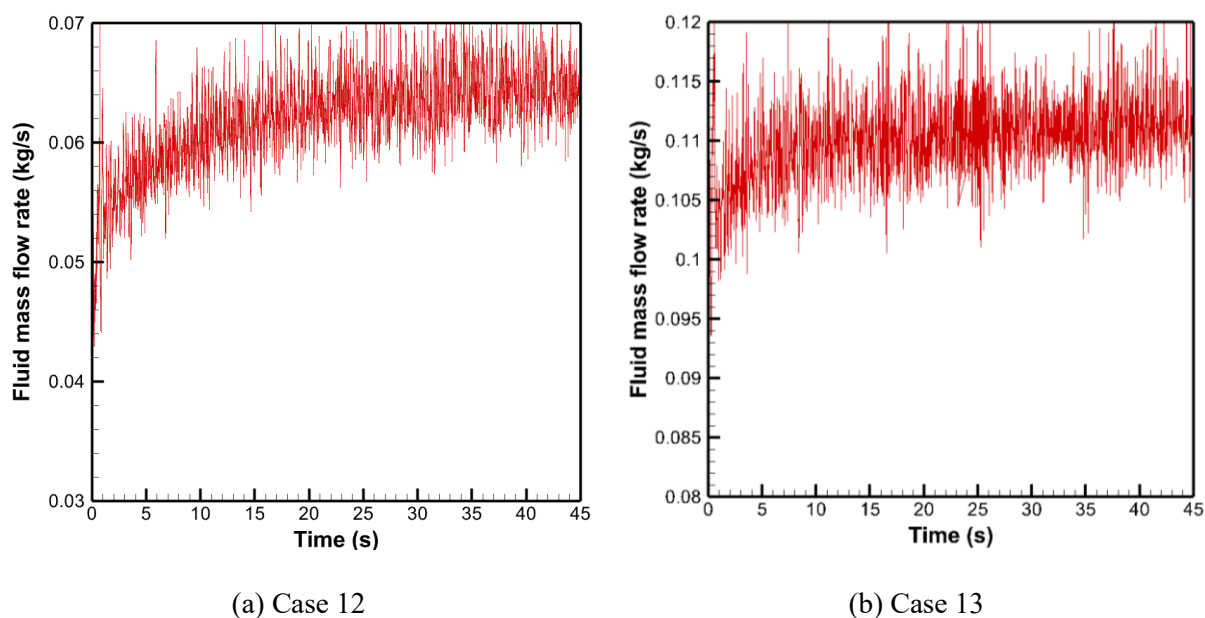
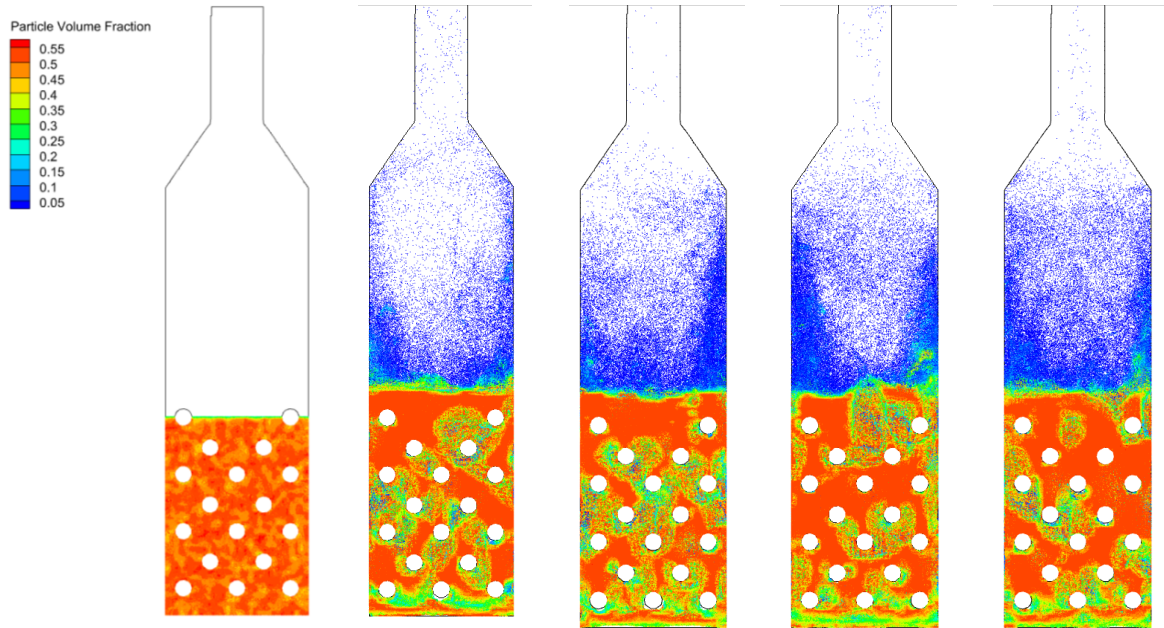


Figure 5-39: CO₂ mass flow rate exiting the reactor during time (a) Case 12, (b) Case 13.

To visualize the fluidization condition in both cases, the particle volume fraction variation during operating time of the reactor is shown in Figure 5-40. As shown in this figure, both cases have high particle entrainment but in case 13 almost all particles are escaping and the bed is far from the bubbling condition! Moreover, the fluid velocity distribution inside the reactor is visualized using several horizontal slices (each 0.2 m up to the transition piece) and a vertical slice in the middle of the reactor (Figure 5-41). As shown in Figure 5-41 the mixing conditions for the both cases is quite the same, however the fluid velocity in case 13 is much higher, as expected.



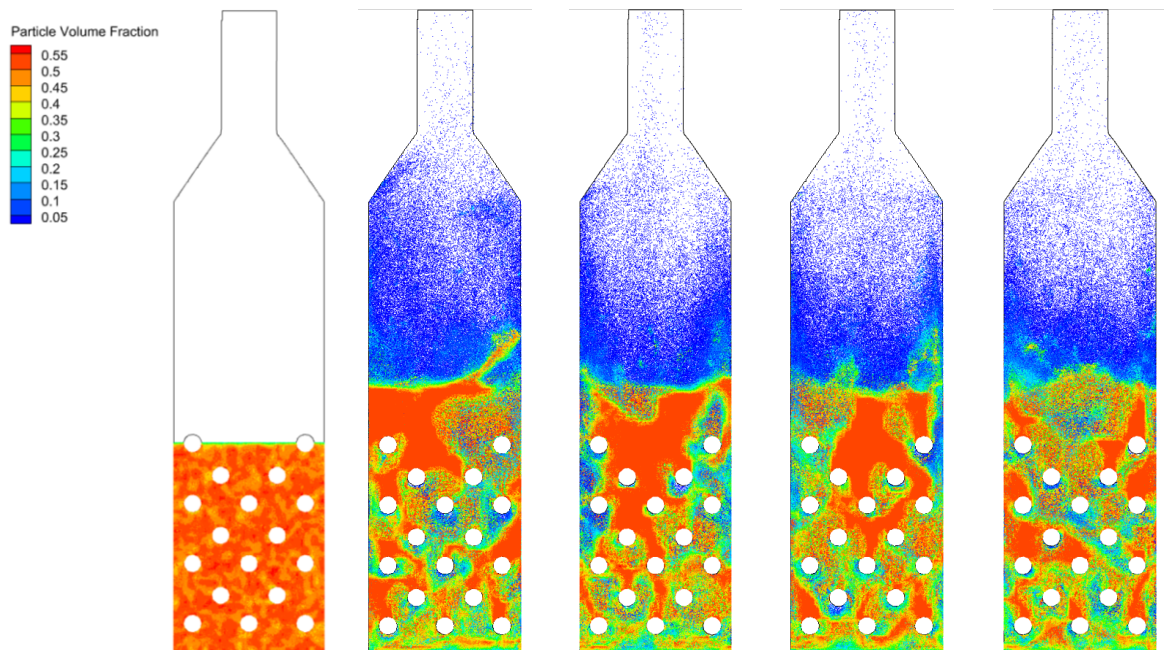
(a-12) Before expansion

(b-12) 5s

(c-12) 15s

(d-12) 25s

(e-12) 45s



(a-13) Before expansion

(b-13) 5s

(c-13) 15s

(d-13) 25s

(e-13) 45s

Figure 5-40: Particle volume fraction during time in the middle plane of the reactor. First row, case 12 and second row, case 13.

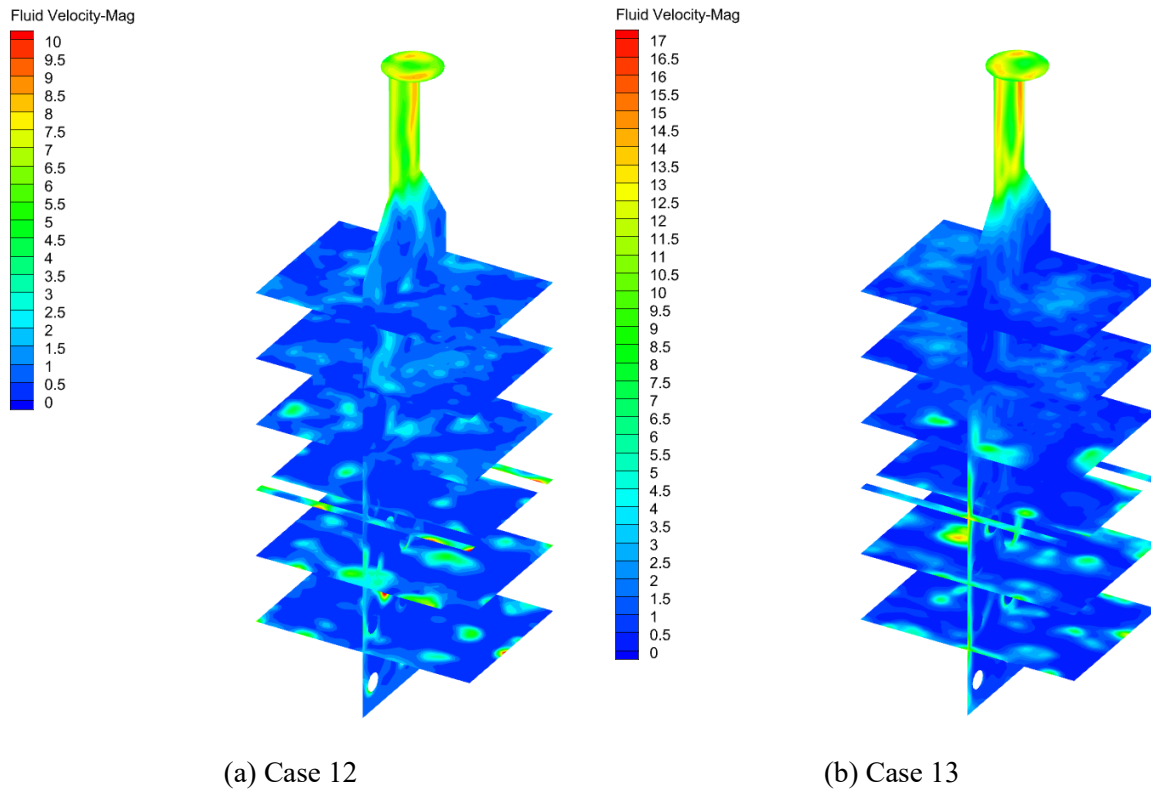


Figure 5-41: Fluid velocity distribution inside the reactor (a) Case 12, (b) Case 13.

5.5.1 The effect of fluidization velocity on the residence time of raw material in the reactor

The residence time of the raw meal is calculated for the cases with different fluidization velocities (0.2 m/s - 0.8 m/s) as shown in Figure 5-42. The calculation of the residence time is made using postprocessing of the data from Barracuda by converting the Tecplot data to a CSV file. As each particle has a unique ID during the simulation, the residence time is calculated by subtracting the injection time from the entrainment time for each particle. In Figure 5-42 the vertical axis shows the percentage of the entrained fine particles. This means that the percentage does not include the coarse particles.

This figure shows that the highest fluidization velocity caused a very low residence time of particles (maximum 10 seconds) which is not preferred. This case also lead to a very low calcination degree. In the case with 0.3 m/s fluidization velocity, which is known as one of the best operating conditions among others with having 90% calcination degree, 45% of the raw meal particles have a residence time between 15-25 seconds and almost 15% have a residence time between 25-30 seconds. In the case with the lowest fluidization velocity (0.2 m/s) the highest residence time for the raw meals is shown, as almost 15% of particles got entrained after 40 seconds!

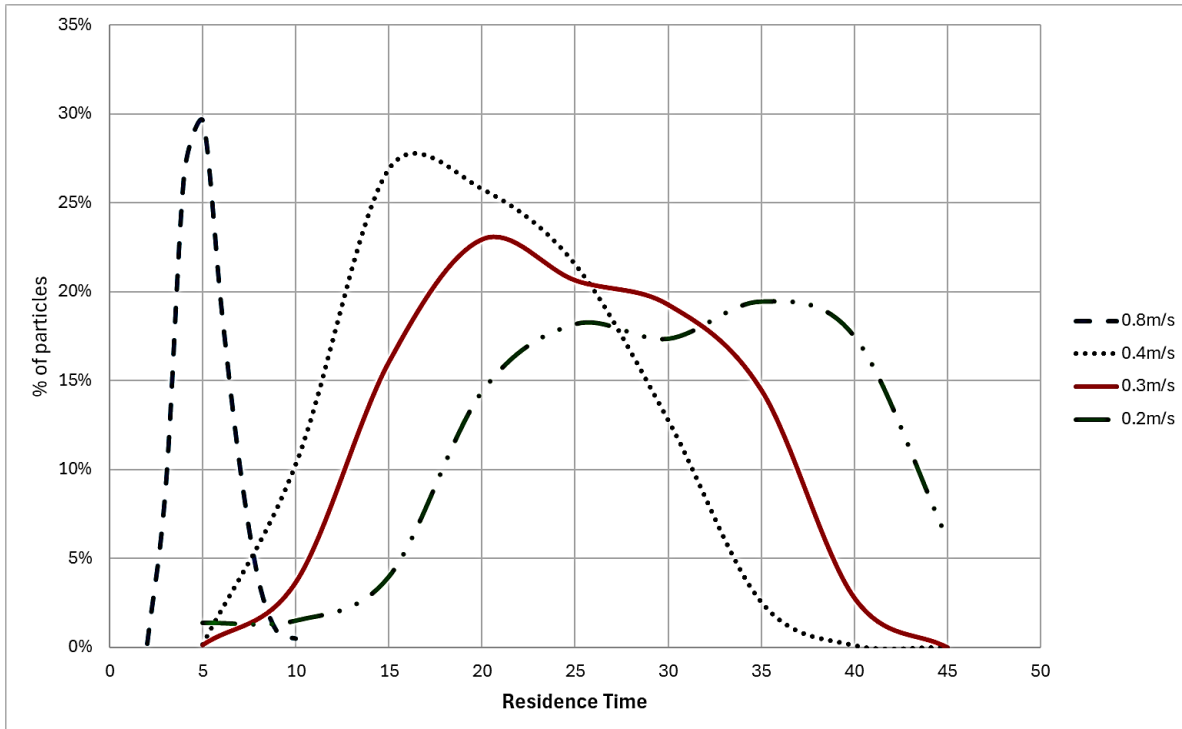


Figure 5-42: Raw meal particle residence time distribution for different fluidization velocities (All cases have 850°C injected raw meal and 1100°C hot cylinder temperature)

5.6 Overview of the results

In this thesis the focus was on the design of an electrified calciner for direct capture of CO₂ from cement raw meal and to investigate different operating conditions using the CPFDF simulations. The operating conditions includes variations in type of raw meal injection, raw meal temperature, hot cylinder wall temperature and fluidization velocity that all mentioned in Table 4-1.

The results showed that spreading the meal over the hot cylinders and using as much as possible of the heat transfer area is of great importance. Starting with a cold meal injection from two small points (one each side of the reactor), very low amount of CO₂ produced which shows a low calcination degree (43%). Increasing the injection points to 6 points totally and preheating the raw meal to 850°C significantly improved the calcination degree to 69% due to using more heat transfer area and needing less energy for reaching the calcination temperature.

The improvement continued by changing the 3 injection points on each side of the reactor to only one but long and narrow. This type of injection worked best among others and improved the calcination degree to more than 80% with same thermal conditions.

Continuing with the narrow long injection areas, the effect of changing thermal operating conditions is investigated (Figure 5-43). As shown in Figure 5-43 the hotter temperature of the cylinders and the more preheating the raw meal the more calcination degree would be reached. Also, there is a balance between the initial temperature of raw meal and the wall temperature of the cylinders. It means that if the meal is too cold the hotter temperature of cylinders is needed to reach the same calcination degree. The investigation operating conditions showed

that for a cold meal injection, if the temperature of cylinders increased to 1150°C a 70% calcination degree is reachable. Also, if there is a possibility of preheating the meal up to 720°C which is a usual preheating temperature of cement raw meal the calcination degree could be improved to 90%.

Moreover, the effect of fluidization velocity on the calcination degree and fine particle residence time is investigated (Figure 5-44). As shown in Figure 5-44 the fluidization velocity 0.3 m/s works best. Results showed that decreasing the fluidization velocity to 0.2 m/s decreases the mixing efficiency. Also in this case reaching steady state condition needs more time than the previous cases with higher fluidization velocity. The weighted average particle residence time in case of using 0.3 m/s fluidization velocity is 24.5 seconds while it can be increased to 30 seconds in case of using 0.2 m/s as fluidization velocity.

On the other hand, increasing the fluidization velocity to 0.8 m/s shows a quick entrainment of both coarse and fine particles (5 seconds average residence time) which shall be avoided.

All in all, the recommended operating setting based on this thesis results is staying between 0.2-0.4 m/s (noting that in 0.4 m/s coarse particles should be refilled after less than 2 days continuous operation). For the thermal conditions preheating the raw meal before injection is highly recommended, however if the meal was injected too cold, 1150 °C temperature of hot cylinders is recommended. In terms of injection type, the narrow long injection area that spreads the raw meal over the length of hot cylinders or any type of injection that makes most contact between the raw meal and heat sources (hot cylinders in this case) is recommended.

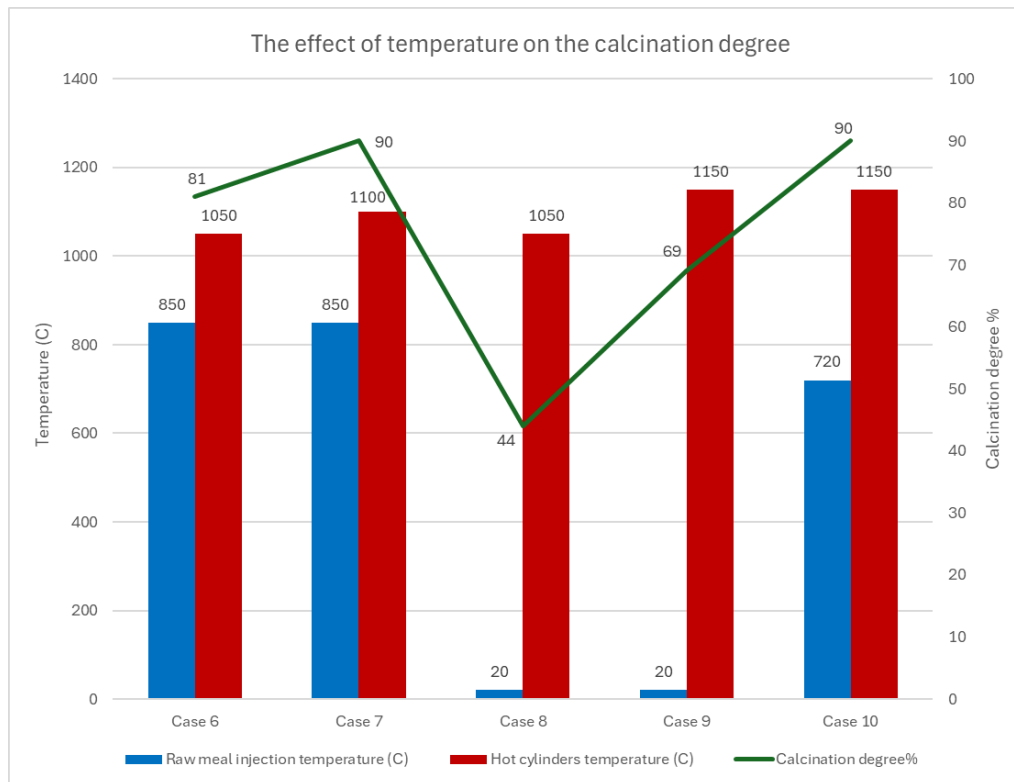


Figure 5-43: Summary of the effect of temperature on the calcination degree

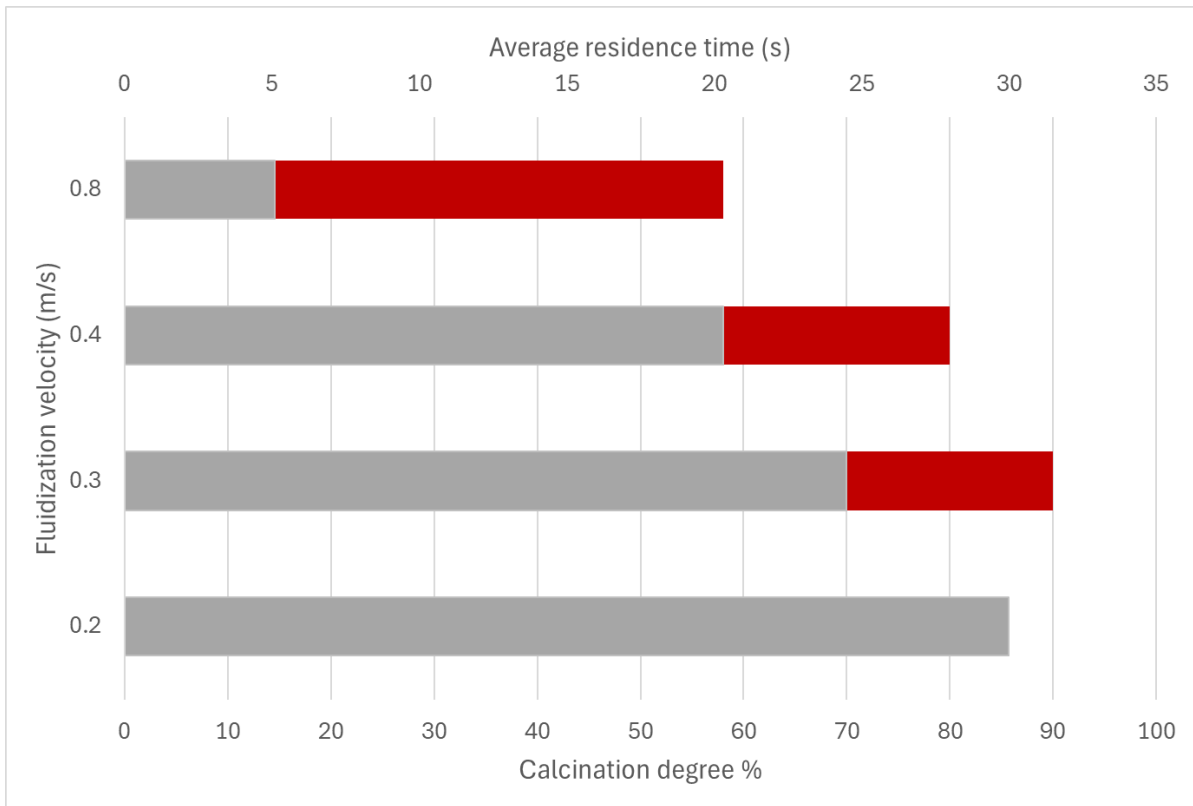


Figure 5-44: Summary of the effect of fluidization velocity on the calcination degree and average residence time

6 Conclusion and Further Work

This thesis primarily focused on the design of an electrified calciner aimed at direct CO₂ capture from cement raw meal. It also investigated various operating conditions using CPF_D simulations. The study examined different types of raw meal injection, raw meal temperature, hot cylinder wall temperature, and fluidization velocity, as detailed in Table 4.1.

The designed calciner features a binary fluidized bed reactor with 17 electrically heated cylinders immersed in the reactor. These cylinders provide the necessary heat for both heating the meal to the calcination temperature and for the endothermic calcination reaction. The bed consists of coarse lime particles with a diameter distribution between 400 μ m-800 μ m, while the raw meal, a fine powder with a diameter of less than 200 μ m, is injected from the sides of the reactor.

Key findings include:

1. **Injection points and preheating:** Initial simulations with cold meal injection from two small points resulted in a low calcination degree (43%). Increasing the injection points to six and preheating the raw meal to 850°C significantly improved the calcination degree to 69% by utilizing more heat transfer area and requiring less energy to reach the calcination temperature. Changing the injection to a single, long, narrow point on each side of the reactor (two in total) yielded the best results, improving the calcination degree to over 80% under the same thermal conditions.
2. **Thermal operating conditions:** The study found that hotter cylinder temperatures and more preheating of the raw meal led to higher calcination degrees. There is a balance between the initial temperature of the raw meal and the cylinder wall temperature. For instance, with a cold meal injection, increasing the cylinder temperature to 1150°C achieved a 70% calcination degree. Preheating the meal to 720°C, a common preheating temperature for cement raw meal, could improve the calcination degree to 90%.
3. **Fluidization velocity:** Optimal fluidization velocity was found to be 0.3 m/s. Lowering the velocity to 0.2 m/s decreased mixing efficiency and delayed CO₂ production, while increasing it to 0.8 m/s caused rapid entrainment of both coarse and fine particles, which shall be avoided.

Based on these findings, the recommended operating settings are as follows:

- **Fluidization velocity:** Maintain between 0.2-0.4 m/s, noting that at 0.4 m/s, coarse particles should be refilled after less than two days of continuous operation and 0.3 m/s works best.
- **Thermal conditions:** Preheat the raw meal before injection when possible. If the meal is injected cold, the cylinder temperature should be increased to 1150°C.
- **Injection type:** Utilize a narrow, long injection area that spreads the raw meal over the length of the hot cylinders or any configuration that maximizes contact area between the raw meal and heat sources (i.e., hot cylinders).

6.1 Suggestion for future studies

The suggestion for the further work is as follows:

- Carry out a comprehensive life cycle assessment (LCA) to evaluate the environmental impact of the electrified calciner, including CO₂ emissions, energy consumption, and potential environmental benefits. Include the electricity production energy sources as well.
- Perform a detailed economic analysis to evaluate the cost-effectiveness of the proposed calciner design (with horizontal hot cylinders) and operating strategies compared to conventional methods. This should include the cost required to change the conventional calciner to the designed electrified one, the required process and piping modifications, the cost of production and using clean electricity, the cost of material with high temperature and high corrosion resistance for the cylinders, etc.
- Use machine learning algorithms to predict and optimize calciner performance under various operating conditions based on the simulation data.
- Study the possibility of utilization of part of hot produced CO₂ to preheat the meal before injection.
- Build a pilot electrified calciner with hot condition and perform an experimental study to evaluate the simulation results and make the feasibility study before scaling up the designed calciner.

References

- [1] "COP27: UN report shows pathways to carbon-neutrality in “energy intensive” steel, chemicals and cement industries." United Nations Economic Commission for Europe. <https://unece.org/media/press/372890> (accessed March 2024).
- [2] A. Nikolakopoulos *et al.*, "Reducing carbon emissions in cement production through solarization of the calcination process and thermochemical energy storage," *Computers & Chemical Engineering*, vol. 180, p. 108506, 2024/01/01/ 2024, doi: <https://doi.org/10.1016/j.compchemeng.2023.108506>.
- [3] L.A. Tokheim, A. Mathisen, L. E. Øi, C. Jayarathna, N. Eldrup, and T. Gautestad, "Combined calcination and CO₂ capture in cement clinker production by use of electrical energy," presented at the TCCS-10, Trondheim, Norway, 2019. [Online]. Available: https://www.researchgate.net/publication/338553982_Combined_calcination_and_CO2_capture_in_cement_clinker_production_by_use_of_electrical_energy.
- [4] N. A. Samani, C. K. Jayarathna, and L.-A. Tokheim, "CPFD simulation of enhanced cement raw meal fluidization through mixing with coarse, inert particles," presented at the SIMS 61, Linköping, 2020. [Online]. Available: https://www.researchgate.net/publication/346311848_CPFD_simulation_of_enhanced_cement_raw_meal_fluidization_through_mixing_with_coarse_inert_particles.
- [5] IEA, "Tracking Industry 2021," 2021: IEA Paris, France.
- [6] IEA., *Low-Carbon Transition in the Cement Industry*. IEA, 2018.
- [7] C. Dupont and S. Oberthür, "The European Union," *Research handbook on climate governance*, pp. 224-236, 2015.
- [8] M. G. Plaza, S. Martínez, and F. Rubiera, "CO₂ capture, use, and storage in the cement industry: State of the art and expectations," *Energies*, vol. 13, no. 21, p. 5692, 2020.
- [9] IEA, *International Energy Agency, Paris, France, 2020*. 2020.
- [10] M. Naranjo, D. T. Brownlow, and A. Garza, "CO₂ capture and sequestration in the cement industry," *Energy Procedia*, vol. 4, pp. 2716-2723, 2011/01/01/ 2011, doi: <https://doi.org/10.1016/j.egypro.2011.02.173>.
- [11] V. Hoenig, H. Hoppe, and B. Emberger, "Carbon capture technology-options and potentials for the cement industry," *PCA R&D Serial*, vol. 3022, p. 98, 2007.
- [12] T. Hills, D. Leeson, N. Florin, and P. Fennell, "Carbon Capture in the Cement Industry: Technologies, Progress, and Retrofitting," *Environmental Science & Technology*, vol. 50, no. 1, pp. 368-377, 2016/01/05 2016, doi: 10.1021/acs.est.5b03508.
- [13] B. R. Roger, "Process for separating acidic gases," United States, 1930. [Online]. Available: <https://patents.google.com/patent/US1783901A/en>
- [14] M. Wang, A. Lawal, P. Stephenson, J. Sidders, and C. Ramshaw, "Post-combustion CO₂ capture with chemical absorption: A state-of-the-art review," *Chemical*

- Engineering Research and Design*, vol. 89, no. 9, pp. 1609-1624, 2011/09/01/ 2011, doi: <https://doi.org/10.1016/j.cherd.2010.11.005>.
- [15] B. Dutcher, M. Fan, and A. G. Russell, "Amine-Based CO₂ Capture Technology Development from the Beginning of 2013—A Review," *ACS Applied Materials & Interfaces*, vol. 7, no. 4, pp. 2137-2148, 2015/02/04 2015, doi: 10.1021/am507465f.
- [16] J. N. Knudsen, O. M. Bade, I. Askestad, O. Gorset, and T. Mejdell, "Pilot Plant Demonstration of CO₂ Capture from Cement Plant with Advanced Amine Technology," *Energy Procedia*, vol. 63, pp. 6464-6475, 2014/01/01/ 2014, doi: <https://doi.org/10.1016/j.egypro.2014.11.682>.
- [17] F. Vega, F. M. Baena-Moreno, L. M. Gallego Fernández, E. Portillo, B. Navarrete, and Z. Zhang, "Current status of CO₂ chemical absorption research applied to CCS: Towards full deployment at industrial scale," *Applied Energy*, vol. 260, p. 114313, 2020/02/15/ 2020, doi: <https://doi.org/10.1016/j.apenergy.2019.114313>.
- [18] K. Koring *et al.*, "Deployment of CCS in the Cement Industry," *IEA Report 2013*, vol. 19, 2013.
- [19] L.M. Bjerge and P. Brevik, "CO₂ Capture in the Cement Industry, Norcem CO₂ Capture Project (Norway)," *Energy Procedia*, vol. 63, pp. 6455-6463, 2014/01/01/ 2014, doi: <https://doi.org/10.1016/j.egypro.2014.11.680>.
- [20] M. Voldsund *et al.*, "Comparison of Technologies for CO₂ Capture from Cement Production—Part 1: Technical Evaluation," *Energies*, vol. 12, no. 3, doi: 10.3390/en12030559.
- [21] E. D. Lena, M. Spinelli, and M. C. Romano, "CO₂ capture in cement plants by "Tail-End" Calcium Looping process," *Energy Procedia*, vol. 148, pp. 186-193, 2018/08/01/ 2018, doi: <https://doi.org/10.1016/j.egypro.2018.08.049>.
- [22] G. Cinti *et al.*, "Options for Calcium Looping for CO₂ Capture in the Cement Industry," in *Proceedings of the 2nd ECRA/CEMCAP Workshop: Carbon Capture Technologies in the Cement Industry, Dusseldorf, Germany*, 2017, pp. 6-7.
- [23] C. Dechsiri, "Particle Transport in Fluidized Beds (Experiments and Stochastic Models)," University Medical Centre Groningen, 2004.
- [24] D. Kunii, O. Levenspiel, and H. Brenner, *Fluidization Engineering*. Elsevier Science, 2013.
- [25] N. A. Samani, "Calcination in an electrically heated bubbling fluidized bed applied in calcium looping," Master, Faculty of Technology, Natural sciences and Maritime Sciences, University of South-Eastern Norway, 2020.
- [26] D. Kunii, "Octave Levenspiel. Fluidization Engineering," ed: Stoneham: Butterworth-Heinemann, 1991.
- [27] D. Geldart, "Types of gas fluidization," *Powder Technology*, vol. 7, no. 5, pp. 285-292, 1973/05/01/ 1973, doi: [https://doi.org/10.1016/0032-5910\(73\)80037-3](https://doi.org/10.1016/0032-5910(73)80037-3).
- [28] K. Kato, T. Takarada, N. Matsuo, T. Suto, and N. Nakagawa, "Residence time distribution of fine particles in a powder-particle fluidized bed," *Kagaku Kogaku*

- Ronbunshu*, vol. 17:5, pp. 970-975, Sep 1991. [Online]. Available: <https://www.osti.gov/etdeweb/biblio/5922008>.
- [29] T. Tashimo, T. Suto, J. Murota, and K. Kato, "Calcination of fine limestone particles by a powder-particle fluidized bed," *Journal of chemical engineering of Japan*, vol. 32, no. 3, pp. 374-378, 1999.
- [30] N. Nakagawa, R. Suzuki, K. Toda, and K. Kato, "Minimum fluidization velocity of binary particle mixtures with adhesive fine powder," *Journal of chemical engineering of Japan*, vol. 35, no. 7, pp. 595-603, 2002.
- [31] J. H. Kim, J. W. Bae, J. Nam, S. D. Kim, J.-H. Choi, and D. H. Lee, "Entrainment of Geldart C particles in fluidized beds with binary particles," *Korean Journal of Chemical Engineering*, vol. 31, no. 11, pp. 2094-2100, 2014/11/01 2014, doi: 10.1007/s11814-014-0113-4.
- [32] R. Jacob, B. Moldestad, and L.A. Tokheim, *Fluidization of Fine Calciner Raw Meal Particles by mixing with coarser Inert Particles – Experiments and CPFD Simulations*. 2022, pp. 333-340.
- [33] R. Jacob and L.A. Tokheim, "CPFD simulation of an electrically heated fluidized bed calciner with binary particles," *Energy Conversion and Management: X*, vol. 20, p. 100444, 2023/10/01/ 2023, doi: <https://doi.org/10.1016/j.ecmx.2023.100444>.
- [34] R. Jacob, "CO₂ capture through electrified calcination in cement clinker production," Ph.D dissertation, Faculty of Technology, Natural Sciences and Maritime Studies, University of South-Eastern Norway, Porsgrunn, 2023.
- [35] M. Reitz, M. Junk, J. Ströhle, and B. Epple, "Design and operation of a 300kWth indirectly heated carbonate looping pilot plant," *International Journal of Greenhouse Gas Control*, vol. 54, pp. 272-281, 2016/11/01/ 2016, doi: <https://doi.org/10.1016/j.ijggc.2016.09.016>.
- [36] D. M. Snider, "An Incompressible Three-Dimensional Multiphase Particle-in-Cell Model for Dense Particle Flows," *Journal of Computational Physics*, vol. 170, no. 2, pp. 523-549, 2001/07/01/ 2001, doi: <https://doi.org/10.1006/jcph.2001.6747>.
- [37] D. M. Snider, S. M. Clark, and P. J. O'Rourke, "Eulerian–Lagrangian method for three-dimensional thermal reacting flow with application to coal gasifiers," *Chemical Engineering Science*, vol. 66, no. 6, pp. 1285-1295, 2011/03/15/ 2011, doi: <https://doi.org/10.1016/j.ces.2010.12.042>.
- [38] *Barracuda Virtual Reactor version: 21.1.1 User Manual*. (2022).
- [39] H. Mikulčić *et al.*, "Numerical modelling of calcination reaction mechanism for cement production," *Chemical Engineering Science*, vol. 69, no. 1, pp. 607-615, 2012/02/13/ 2012, doi: <https://doi.org/10.1016/j.ces.2011.11.024>.
- [40] R. Borgwardt, "Calcination kinetics and surface area of dispersed limestone particles," *AIChE Journal*, vol. 31, no. 1, pp. 103-111, 1985.
- [41] A. Fenghour, W. A. Wakeham, and V. Vesovic, "The viscosity of carbon dioxide," *Journal of physical and chemical reference data*, vol. 27, no. 1, pp. 31-44, 1998.

- [42] K. Suksankraisorn, S. Patumsawad, and B. Fungtammasan, "Prediction of minimum fluidisation velocity from correlations: an observation," *Asian J Energy Environ*, vol. 2, no. 2, pp. 145-154, 2001.

Appendix A: Task Description

Title: Design of electrified calciner for direct capture of CO₂ from cement raw meal

USN supervisor: Lars-André Tokheim

External partner: Heidelberg Materials (Christoffer Moen)

Task background:

USN is one of the partners in the research project "*Combined calcination and CO₂ capture in cement clinker production by use of CO₂-neutral electrical energy*". The acronym ELSE¹ is used as a short name for the project. Phase 1 of the project was completed in April 2019, and Phase 2 was started in April 2020 and will be completed in January 2024. The current master's thesis project will be part of a follow-up project, in which the results from ELSE and ELSE 2 will be used in further process development.

The goal of the project is to utilize electricity (instead of carbon-containing fuels) to decarbonate the raw meal in the cement kiln process while at the same time capturing the CO₂ from decarbonation of the calcium carbonate in the calciner, see Figure 1. Such a concept may be less expensive than a regular post-combustion system applied to CO₂ capture from the cement plant. Moreover, as the fuel generated CO₂ will be eliminated, less CO₂ is produced in the calcination process.

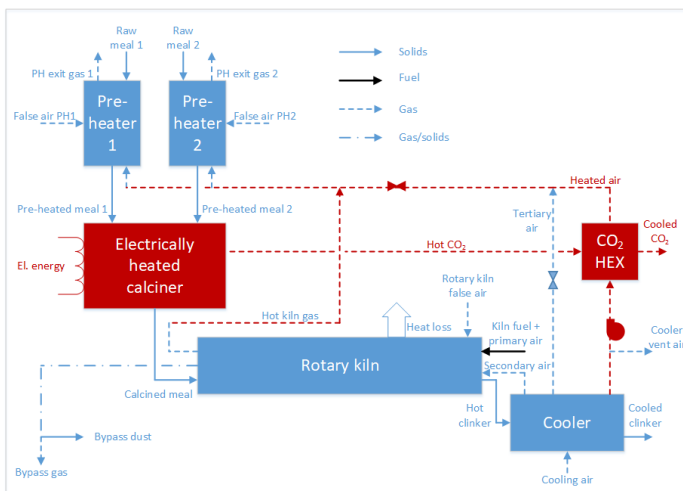


Figure 1: A modified cement kiln process applying electrical energy for calcination.

Different concepts to implement electrification of the calciner have been discussed in the project. One alternative is to use electricity (through resistance heating) to generate heat that is transferred to the calciner, where it is used to calcine the meal ($\text{CaCO}_3 \rightarrow \text{CaO} + \text{CO}_2$). Different

¹ ELSE is short for 'ELEktrifisert SEmentproduksjon' (Norwegian) meaning 'electrified cement production'.

reactor types may be used as a calciner, and have been assessed. A fluidized bed with immersed heating elements has been selected as the most promising concept.

As the meal particles are small (median $\sim 20\text{-}30\ \mu\text{m}$; i.e. Geldart C particles), they are difficult to fluidize. However, it is possible to improve the fluidization properties by mixing the small particles with coarser particles. In that case, the bed should be designed in such a way that the coarse particles remain in the bed, whereas the fine uncalcined particles are continuously fed close to the bottom of the bed and fine calcined particles are continuously discharged at top of the bed. In the ELSE 2 project, we have developed a reactor concept which will likely fulfill the requirements described above. However, as a preparation for lab-scale hot-flow experiments, the gas and particle behaviour in the bed needs to be investigated in more detail.

Task description:

The task may include some of the following sub-tasks (subject to change based on discussions between the student, the supervisor and the external partner):

- Describe the concept of electrified calcination in a fluidized bed
- Make a mass and energy balance of the system and calculate mass flow rates, temperatures, duties, etc.
- Explain operational constraints that must be taken into account when making the detailed design of the fluidized bed (gas velocity, bed thickness, reactor height are relevant examples in this connection)
- Suggest a reactor design which is suitable for lab-scale hot-flow experiments (expected power supply range 100-500 kW)
- Recommend settings for operation of the electrified calciner, both during startup and during steady state operation
- Carry out CFD simulations to support the design (requires CFD competence)
- Determine the required size of the BFB and other relevant equipment units

Student category: PT or EET (CFD competence is an advantage, but not a requirement)


Is the task suitable for online students (not present at the campus)?: Yes

Practical arrangements: Regular Teams/Zoom meetings with the external partner.

Supervision:

As a general rule, the student is entitled to 15-20 hours of supervision. This includes necessary time for the supervisor to prepare for supervision meetings (reading material to be discussed, etc.).

Signatures:

Supervisor (date and signature): 19 January 2024, 

Student (write clearly in all capitalized letters): LADAN SAMAEI

Student (date and signature): 19 January 2024, *Ladan Samaei*